Aspects of Irregular Punctures via Holography

Ibrahima Bah,^a Federico Bonetti,^b Emily Nardoni,^c and Thomas Waddleton^a

E-mail: iboubah@jhu.edu, federico.bonetti@maths.ox.ac.uk, emily.nardoni@ipmu.jp, twaddle1@jhu.edu

ABSTRACT: We present new families of AdS_5 solutions in M-theory preserving 4d $\mathcal{N}=2$ supersymmetry. We perform a systematic analysis of holographic observables for these solutions, providing evidence for an interpretation in terms of 4d superconformal field theories (SCFTs) of Argyres-Douglas type, realized in class \mathcal{S} via a sphere with one irregular, and one regular puncture. The gravity solutions exhibit internal M5-brane sources that correspond to the irregular puncture. For a family of solutions, we identify explicitly the class \mathcal{S} puncture data and perform a detailed match, including Higgs branch operators. For other families we comment on proposed field theory duals, based on irregular punctures labeled by nested Young tableaux.

^aDepartment of Physics and Astronomy, Johns Hopkins University, 3400 North Charles Street, Baltimore, MD 21218, USA

^bMathematical Institute, University of Oxford, Woodstock Road, Oxford, OX2 6GG, UK

^cKavli Institute for the Physics and Mathematics of the Universe (WPI), The University of Tokyo Institutes for Advanced Study, The University of Tokyo, Kashiwa, Chiba 277-8583, Japan

Co	ontents			
1	Introduction and summary 1.1 Holographic duals of Argyres-Douglas SCFTs	2		
	1.2 Summary of main results	2		
2	Supergravity solutions	6		
	2.1 Canonical form of AdS_5 solutions in 11d supergravity	(
	2.2 Toda equation and separation of variables	7		
3	Geometries, fluxes, and observables			
	3.1 Rectangular domains in the (t, u) plane	g		
	3.2 Flux quantization and holographic quantities	10		
	3.3 Examples of non-rectangular domains	18		
4	Electrostatic picture	21		
	4.1 Review of the Bäcklund transform	21		
	4.2 Electrostatic potential from Toda solutions	23		
	4.3 Electrostatic interpretation of Cases I and II	24		
	4.4 Electrostatic interpretation of Case III and beyond	27		
5	More monopoles			
	5.1 Charge density profile	28		
	5.2 Geometry of the solutions	30		
	5.3 Holographic central charge	32		
	5.4 't Hooft anomalies from inflow	35		
	5.5 Operators from wrapped M2-branes	35		
6	Comparison with field theory			
	6.1 Map to the Young tableaux	38		
	6.2 Checks of the holographic duality	40		
	6.3 Speculations on nested Young tableaux	47		
7	Discussion			
A	Further details on separable solutions			
В	Formulae for the electrostatic potential 5			
\mathbf{C}	Detailed analysis of generalized Case II 5			

1 Introduction and summary

1.1 Holographic duals of Argyres-Douglas SCFTs

Infinite families of non-trivial 4d superconformal field theories (SCFTs) can be realized by reducing a 6d (2,0) SCFT on a Riemann surface, implementing a partial topological twist to preserve supersymmetry. This idea dates back to the original class \mathcal{S} constructions of 4d $\mathcal{N}=2$ SCFTs [1, 2], as well as their generalizations to 4d $\mathcal{N}=1$ theories [3–7].

One of the key ingredients in the class S constructions is a rich spectrum of allowed punctures on the Riemann surface [1, 2]. This includes so-called irregular punctures, which can be used to realize 4d SCFTs of Argyres-Douglas type [8–10]. The latter exhibit remarkable features: they possess Coulomb branch operators of fractional dimensions; they are intrinsically strongly coupled; they can be regarded as describing the interactions of massless, mutually non-local BPS dyons, as in the original paper [11].

In this work, we investigate 4d $\mathcal{N}=2$ SCFTs that originate from the reduction of the 6d (2,0) SCFT of type A_{N-1} , which is realized on the worldvolume of a stack of N M5-branes. Working at large N, we may access non-trivial aspects of these 4d $\mathcal{N}=2$ SCFTs by studying the dual AdS_5 supersymmetric geometries in 11d supergravity. For the cases in which the Riemann surface has no punctures, or only regular punctures, the dual AdS_5 solutions have been known for quite some time [12, 13]. More recently, holographic duals for a family of class \mathcal{S} constructions with irregular punctures have been proposed [14–16].

Building on [15], in this paper we find new AdS_5 supersymmetric solutions in M-theory. Our analysis is based on a direct study of the BPS conditions in eleven dimensions (as opposed to uplift on S^4 from 7d gauged supergravity). The explicit, closed analytic forms of the new solutions allow us to compute exactly several holographic observables of interest. In particular, we identify a class of BPS M2-brane operators that have fractional conformal dimensions, together with the correct charges to be mapped to Coulomb branch operators on the field theory side: these prompt an interpretation in terms of putative dual SCFTs of Argyres-Douglas type.

Our geometries exhibit singularities that are interpreted in terms of internal M5-brane sources, along the lines of [15]. Previous results in the literature, see e.g. [17–24], show that internal sources in holography can be a powerful ingredient in the construction of non-trivial holographic pairs. This work makes further steps in the program of characterizing internal sources in gauge/gravity duality.

1.2 Summary of main results

We begin with an overview of the key steps in our analysis, and a summary of our findings.

The role of an additional U(1) isometry. Our starting point is the canonical form of AdS_5 solutions in 11d supergravity preserving 4d $\mathcal{N}=2$ supersymmetry [25]. The 11d metric

takes the form

$$ds_{11}^2 = \frac{e^{2\tilde{\lambda}}}{m^2} \left[ds_{AdS_5}^2 + \frac{y^2 e^{-6\tilde{\lambda}}}{4} ds_{S^2}^2 + \frac{D\chi^2}{1 - y \partial_y D} + \frac{-\partial_y D}{4 y} \left(dy^2 + e^D \left(dx_1^2 + dx_2^2 \right) \right) \right]. \quad (1.1)$$

In particular, the 6d internal space is an $S^2 \times S^1_{\chi}$ fibration over a 3d base space spanned by the coordinates x_1, x_2, y . A more complete review of this class of solutions, and the definition of all quantities entering (1.1), is given in section 2.1. For the purposes of this introduction, it suffices to recall that the warp factor $\tilde{\lambda}$ and all metric functions are determined in terms of a single function $D = D(x_1, x_2, y)$, satisfying the continual Toda equation

$$\partial_{x_1}^2 D + \partial_{x_2}^2 D + \partial_y^2 e^D = 0 . (1.2)$$

Our primary goal is to construct and analyze new solutions that may admit an interpretation in terms of a 4d SCFT of Argyres-Douglas type. The search for such solutions may be refined from the following considerations. In the geometric class S construction of the Argyres-Douglas type SCFTs, the Riemann surface is a sphere with an irregular puncture at one pole, and possibly a regular puncture at the opposite pole. In this setup, two U(1) symmetries play an important role. The first is the $U(1)_{\phi}$ symmetry that rotates the phase of the fiber in the cotangent bundle to the Riemann surface. The second is the $U(1)_z$ isometry of the Riemann surface (rotation along the axis connecting the two poles of the punctured sphere). In the absence of an irregular puncture, the superconformal $U(1)_r$ R-symmetry would simply be identified with $U(1)_{\phi}$. In the presence of the irregular puncture, however, the $U(1)_r$ symmetry is a linear combination of $U(1)_{\phi}$ and $U(1)_z$ [8–10],

$$\partial_{\chi} = \partial_{\phi} + \alpha \partial_z \ . \tag{1.3}$$

The mixing coefficient α depends on the specific Argyres-Douglas SCFT under consideration; for the cases relevant to this paper, $\alpha = \frac{N}{N+k}$, where N is the number of M5-branes wrapping the Riemann surface, and k is an integer determined by the choice of irregular puncture. As indicated on the LHS of (1.3), the superconformal R-symmetry is associated to the angle χ in (1.1).

In the search for new M-theory solutions, we would like the geometry to reflect the U(1) mixing in field theory recalled above. In order to see this manifestly, the line element (1.1) should admit a second U(1) isometry besides ∂_{χ} . We thus input an additional requirement in our construction: a U(1) isometry in the 3d base space spanned by x_1, x_2, y , which has to be compatible with the Toda equation (1.2). This leads to introduce polar coordinates

$$x_1 = r\cos\beta \,, \qquad x_2 = r\sin\beta \,, \tag{1.4}$$

and restricts the Toda potential D to be independent of the angular coordinate β . This

¹Another possible way to implement the additional U(1) isometry is to work with the x_1 , x_2 coordinates, demand that D be independent of x_2 , and periodically identify the x_2 coordinate. It may be verified, however, that this procedure is equivalent to the introduction of the polar coordinates (r, β) , up to a conformal scaling of $dx_1^2 + dx_2^2$ and a redefinition of D.

angular coordinate is associated to a linear combination of ∂_{ϕ} , ∂_z that is independent to the superconformal R-symmetry generator (1.3).

Before proceeding, it is worth clarifying an important physical point related to the ∂_{β} symmetry. Naïvely, the fact that the solution admits a ∂_{β} isometry seems to imply an additional global flavor U(1) symmetry in the 4d field theory. Crucially, however, this conclusion may be invalidated after a more careful analysis of the background 4-flux \overline{G}_4 . In the solutions of [14, 15], the Kaluza-Klein vector associated to ∂_{β} is massive by virtue of a Stückelberg coupling. This phenomenon originates from the fact that the background 4-flux \overline{G}_4 is invariant under ∂_{β} , but cannot be completed to an $U(1)_{\beta}$ -equivariant closed 4-form. We will observe the same phenomenon in all new solutions discussed in this work: even though ∂_{β} is a symmetry of the supergravity solution, the associated Kaluza-Klein vector is always massive via a Stückelberg mechanism of the same kind as in [14, 15].

Separable solutions to the Toda equation. At this stage, our task is to study solutions to the Toda equation that are invariant under β rotations. To keep the analysis tractable, at present we restrict our search to exact, analytic solutions. Building on previous experience in [15], we make a change of coordinates from r, y to a new pair of variables t, u, and impose the following separability condition,

$$y = tu$$
, $r = r_1(t)r_2(u)$. (1.5)

(1.5) is a technical assumption that results in a remarkable simplification: we achieve full separation of variables in the Toda equation, thus yielding new analytic solutions.²

The 11d geometries and flux configurations given by these new solutions to the Toda equation are studied in detail in section 3. Metric regularity and positivity dictate the allowed region for the coordinates t, u. The solutions can be grouped accordingly into two main classes. The first class consists of solutions in which we have a rectangular domain in the (t,u) plane. The second class consists instead of solutions with a non-rectangular domain. We perform a classification of solutions in the first class: three possibilities arise, as depicted in Figure 1, with Case II reducing to the solutions previously analyzed in [15]. We refrain from a classification of solutions in the second class, instead studying some representative examples, depicted in Figure 2.

The solutions of the first class (with rectangular domains) are singled out on physical grounds by the structure of singularities in the 11d metric and warp factor. Indeed, for all cases in Figure 1 we can furnish an interpretation of the singularities in the 11d solution in terms of smeared M5-brane sources of the same kind as in [15]. While the physical implications of these singularities are difficult to ascertain purely from a supergravity perspective, the analysis of [15] has demonstrated that they can be consistently utilized as ingredients in the construction of meaningful, non-trivial holographic pairs. This gives us confidence that the new solutions of this paper can also be interpreted as duals to some 4d SCFTs. We then proceed to compute

²The physics of the ansatz (1.5) is an interesting question which we reserve for the discussion section, since our comments rely on intuition gained from a closer analysis of the solutions.

various holographic observables: central charge; flavor central charges; dimensions of some BPS operators from wrapped M2-branes. A subclass of these BPS operators may be identified in the putative $\mathcal{N}=2$ field theory duals as Coulomb branch operators of fractional scaling dimension, reinforcing our classification of the dual SCFTs as of Argyres-Douglas type.

Map to an electrostatic problem: more geometries. The solutions to the axisymmetric Toda equation can be analyzed by means of the Bäcklund transformation, a functional transform that maps the Toda equation with rotational symmetry in the x_1x_2 plane to the Laplace equation in \mathbb{R}^3 with axial symmetry (see e.g. [13]). In this electrostatic picture, a solution is specified by a choice of charge density along the axis of cylindrical symmetry in \mathbb{R}^3 . From the perspective of this frame, our task is to identify those charge densities that correspond to solutions that have an interpretation in terms of 4d SCFTs of Argyres-Douglas type.

The next step in our analysis is to determine explicitly the Bäcklund transformation of the analytic Toda solutions found via the separation of variables (1.5). This task is addressed in section 4, where in particular, we identify the charge densities associated to our new Toda solutions. These charge densities are piecewise linear continuous functions, determined by a finite number of slope and intercept parameters. The latter are related in a non-trivial way to the flux quanta and geometry of the solutions in the Toda frame. Once the charge densities are identified, they can be generalized systematically, thereby furnishing solutions which do not necessarily originate from a separable Toda potential.

We apply this circle of ideas to the solutions first discussed in [15], corresponding to Case II in Figure 1. Upon identifying and generalizing the associated charge density in the electrostatic frame, we find solutions dual to class \mathcal{S} constructions with one irregular puncture, and one puncture labeled by an arbitrary Young diagram. Our analysis confirms and extends results first reported in [16].

Comparison with field theory: central charges and Higgs operators. In the final part of this paper, we perform a systematic comparison with 4d SCFTs of Argyres-Douglas type. More precisely, we consider class \mathcal{S} constructions in which the irregular puncture is of type $A_{N-1}^{(N)}[k]$ in the notation of [9, 10], while the regular puncture is specified by a partition of N, or equivalently a Young diagram Y. Building on previous results in the literature [9, 26–29] (see also [16]), we compute a closed-form expression for the large-N behavior of the central charge of the theory with labels $(A_{N-1}^{(N)}[k], Y)$, for arbitrary Young diagram Y. We similarly derive general expressions for the central charge of the flavor symmetry associated to the regular puncture, and for the Coulomb branch operators. All the solutions constructed here have Coulomb branch operators of fractional dimensions – one of the hallmarks of $\mathcal{N}=2$ SCFTs of Argyres-Douglas type. In the special case in which N/k is an integer, and the regular puncture is either maximal (full) or minimal (simple), a 4d $\mathcal{N}=1$ Lagrangian description is available [30, 31]. In these cases, the Lagrangian description is especially useful to access Higgs branch operators across the duality.

We identify the Case II solutions of Figure 1 with the Argyres-Douglas SCFTs with labels $(A_{N-1}^{(N)}[k], Y)$, for Y a regular puncture labeled by a general partition of N – these are the same solutions that were identified in [16], and that generalize the more restrictive class of regular puncture geometries described in [15]. The Case I solutions are a one parameter generalization of these SCFTs which include an additional smeared M5-brane source, leading to additional Higgs branch operators and larger flavor symmetry. A hypothesis for the field theory duals of the Case I solutions is that they correspond to Argyres-Douglas theory realized with one regular puncture and one irregular puncture which is labeled by more refined data compared to $A_{N-1}^{(N)}[k]$. We check that in a certain limit, this extra data is consistent with that of a nested Young tableaux structure of the irregular puncture, as in [9, 10]. The determination of the precise irregular puncture data and more refined tests of this proposal are left for future work.

Plan of the paper. The rest of this paper is organized as follows. Section 2 is devoted to the analysis of the Toda equation and its solutions obtained via separation of variables. In Section 3 we study the geometry and flux configurations of the M-theory solutions determined from the Toda solutions of Section 2. In Section 4 we perform the Bäcklund transform, while Section 5 is devoted to generalizations of the charge density profiles, and their implications on the M-theory solutions. In Section 6 we perform a detailed comparison with various large-N quantities for 4d SCFTs of Argyres-Douglas type. We conclude with a brief discussion. The appendices collect some derivations and technical material.

Reference [16] appeared while this work was being completed, which has some overlap with a class of solutions we present.

2 Supergravity solutions

In this section we briefly review the canonical form of AdS_5 solution of 11d supergravity preserving 4d $\mathcal{N}=2$ superconformal symmetry. These solutions are specified by a choice of Toda potential D satisfying (2.3) below. We proceed with a construction of analytic solutions to (2.3) based on a suitable separation of variables.

2.1 Canonical form of AdS_5 solutions in 11d supergravity

The most general AdS_5 solution of 11d supergravity preserving 4d $\mathcal{N}=2$ superconformal symmetry was characterized in Lin-Lunin-Maldacena (LLM) [25]. The 11d metric and flux are given as [13]

$$ds_{11}^{2} = \frac{e^{2\tilde{\lambda}}}{m^{2}} \left[ds^{2} (AdS_{5}) + \frac{y^{2} e^{-6\tilde{\lambda}}}{4} ds^{2} (S^{2}) + \frac{D\chi^{2}}{1 - y \partial_{y} D} + \frac{-\partial_{y} D}{4 y} \left(dy^{2} + e^{D} \left(dx_{1}^{2} + dx_{2}^{2} \right) \right) \right],$$

$$G_{4} = \frac{1}{4 m^{3}} \operatorname{vol}_{S^{2}} \wedge \left[D\chi \wedge d(y^{3} e^{-6\tilde{\lambda}}) + y \left(1 - y^{2} e^{-6\tilde{\lambda}} \right) dv - \frac{1}{2} \partial_{y} e^{D} dx_{1} \wedge dx_{2} \right]. \tag{2.1}$$

The line elements on AdS_5 and S^2 have unit radius. The quantity m is a mass scale. The warp factor $\tilde{\lambda}$ and the function D depend on y, x_1 , x_2 and are related by

$$e^{-6\tilde{\lambda}} = \frac{-\partial_y D}{y(1 - y\,\partial_y D)} \ . \tag{2.2}$$

The function D satisfies the Toda equation

$$\partial_{x_1}^2 D + \partial_{x_2}^2 D + \partial_y^2 e^D = 0 . (2.3)$$

The coordinate χ is an angular coordinate with period 2π . The 1-form $D\chi$ is defined as

$$D\chi = d\chi + v , \qquad v = -\frac{1}{2} \left(\partial_{x_1} D \, dx_2 - \partial_{x_2} D \, dx_1 \right) .$$
 (2.4)

The 2-form vol_{S^2} is the volume form on a unit-radius round S^2 . The Killing vector ∂_{χ} is dual to the $U(1)_r$ R-symmetry of the 4d $\mathcal{N}=2$ SCFT, while the isometries of S^2 are mapped to the $SU(2)_R$ R-symmetry.

It is convenient to introduce polar coordinates (r, β) in the (x_1, x_2) plane,

$$x_1 + i \, x_2 = r \, e^{i\beta} \ . \tag{2.5}$$

In particular, the angle β has period 2π . If the Toda potential D is independent of β , (2.3) can be rewritten as

$$\frac{1}{r}\partial_r(r\,\partial_r D) + \partial_y^2 e^D = 0 \ . \tag{2.6}$$

Convenient choice for the mass scale m. The value of the mass scale m is not physical. It can be set to any positive value by a rescaling of the x_1 , x_2 , y coordinates and the Toda potential, of the form $x_1 = a\hat{x}_1$, $x_2 = a\hat{x}_2$, $y = a\hat{y}$, $D(x_1, x_2, y) = \widehat{D}(\hat{x}_1, \hat{x}_2, \hat{y})$, where a > 0 is a constant. In later sections, we shall find it convenient to set

$$4\pi m^3 \ell_p^3 = 1 \ , \tag{2.7}$$

where ℓ_p denotes the 11d Planck length. In our conventions, G_4 -flux is quantized as

$$\int_{\mathcal{C}_4} \frac{G_4}{(2\pi\ell_p)^3} \in \mathbb{Z} , \qquad (2.8)$$

where C_4 is a 4-cycle in spacetime.

2.2 Toda equation and separation of variables

We can analyze the Toda equation (2.6) by taking the coordinates y and r to be separable functions. That is, we write

$$y = tu, \quad r = r_1(t)r_2(u) ,$$
 (2.9)

in terms of new coordinates t, u. Inserting (2.9) into the metric given in (2.1), we find a cross term of the form

$$ds_{11}^2 \supset -\frac{\partial_y D}{2y} \frac{e^{2\tilde{\lambda}}}{m^2} \left(tu + e^D r_1 r_1' r_2 r_2' \right) dt du$$
 (2.10)

Here and in the rest of this section, a prime on a function of one variable denotes differentiation with respect to that variable. Imposing that this cross term vanish, we obtain an expression for the Toda potential in terms of t, u, $r_1(t)$, $r_2(u)$,

$$e^D = -\frac{tu}{r_1 r_1' r_2 r_2'} \ . \tag{2.11}$$

Plugging this back into the Toda equation (2.6), we find a pair of decoupled ODEs for $r_1(t)$ and $r_2(u)$,

$$\frac{1}{t} \left(\frac{r_1 r_1''}{(r_1')^2} t^2 \right)' = \frac{1}{u} \left(\frac{r_2 r_2''}{(r_2')^2} u^2 \right)' \qquad \Rightarrow \qquad \frac{r_1'}{r_1} = -\frac{t}{K_1(t)} \;, \qquad \frac{r_2'}{r_2} = \frac{u}{K_2(u)} \;. \tag{2.12}$$

In the previous expression we have introduced the quadratic polynomials

$$K_1(t) = -\sigma(t - t_1)(t - t_2) , \qquad K_2(u) = \sigma(u - u_1)(u - u_2) ,$$
 (2.13)

where σ , t_1 , t_2 , u_1 , u_2 are constant parameters. In order to have real K_1 , K_2 , the parameter σ must be real. The roots t_1 , t_2 of K_1 are either both real, or both complex and complex conjugate of each other. Similar remarks apply to the roots u_1 , u_2 of K_2 .

Combining (2.11) and (2.12) we may write

$$e^D = \frac{K_1 K_2}{r_1^2 r_2^2} \ . {2.14}$$

If desired, the first order ODEs in (2.12) are readily integrated, yielding closed form expressions for $r_1(t)$ and $r_2(u)$, and hence for the Toda potential as a function of t, u. For the purposes of computing the 11d metric and flux, however, the explicit expressions for $r_1(t)$ and $r_2(u)$ are not needed: when r'_1 or r'_2 are encountered, they can be eliminated using the ODEs (2.12). In conclusion, we can express the metric and flux in terms of u, t, K_1 , and K_2 ,

$$ds_{11}^{2} = \frac{e^{2\tilde{\lambda}}}{m^{2}} \left[ds^{2} (AdS_{5}) + \frac{t^{2}u^{2}e^{-6\tilde{\lambda}}}{4} ds^{2} (S^{2}) + \frac{D\chi^{2}}{1 - tu\partial_{y}D} - \partial_{y}D \frac{K_{1}u^{2} + K_{2}t^{2}}{4tu} \left(\frac{dt^{2}}{K_{1}} + \frac{du^{2}}{K_{2}} + \frac{K_{1}K_{2}}{K_{1}u^{2} + K_{2}t^{2}} d\beta^{2} \right) \right],$$

$$G_{4} = \frac{1}{4m^{3}} \text{vol}_{S^{2}} \wedge d \left[-t^{3}u^{3}e^{-6\tilde{\lambda}}D\chi + tuv + \frac{1}{2}\mathcal{F}d\beta \right], \qquad (2.15)$$

where the quantities v, $-\partial_y D$, $e^{-6\tilde{\lambda}}$, and \mathcal{F} are given by

$$v \equiv v_{\beta}d\beta = -\frac{1}{2}r\partial_{r}Dd\beta = \left[1 - \frac{\sigma}{2} + \frac{\sigma}{2}\frac{u_{1}u_{2}K_{1} + t_{1}t_{2}K_{2}}{K_{1}u^{2} + K_{2}t^{2}}\right]d\beta$$

$$-\partial_{y}D = \frac{(u_{1} + u_{2})t - (t_{1} + t_{2})u}{K_{1}u^{2} + K_{2}t^{2}}\sigma$$

$$e^{-6\tilde{\lambda}} = \frac{(u_{1} + u_{2})t - (t_{1} + t_{2})u}{tu(u_{1}u_{2}t^{2} - t_{1}t_{2}u^{2})}$$

$$\mathcal{F} = 2(\sigma - 1)ut - \sigma(t_{1} + t_{2})u - \sigma(u_{1} + u_{2})t . \tag{2.16}$$

We observe that all quantities written above are real, even if we allow for complex roots of K_1 and/or K_2 .

Reflections in t and u. Let us consider a simultaneous flip in the signs of t, $t_{1,2}$, and the angular coordinates,

$$t \mapsto -t$$
, $t_{1,2} \mapsto -t_{1,2}$, $\chi \mapsto -\chi$, $\beta \mapsto -\beta$. (2.17)

The expressions (2.15) for the 11d metric and flux are invariant under these redefinitions. By a similar token, one verifies invariance under the sign flips

$$u \mapsto -u$$
, $u_{1,2} \mapsto -u_{1,2}$, $\chi \mapsto -\chi$, $\beta \mapsto -\beta$. (2.18)

From (2.15), (2.16) we see that the radius squared of the S^2 , given by $\frac{1}{4}t^2u^2e^{-6\tilde{\lambda}}$, changes sign as we cross t=0 or u=0. It follows that the allowed range for the (t,u) coordinates is necessarily contained in one of the four quadrants of the (t,u) plane. Performing the sign flips (2.17) or (2.18) if necessary, we can assume without loss of generality that the allowed region in the (t,u) plane lies in the first quadrant,

$$t \ge 0 , \qquad u \ge 0 . \tag{2.19}$$

Positivity of metric functions. From (2.14) we observe that K_1 and K_2 must either be both positive, or both negative. As a result, $K_1u^2 + K_2t^2$ is positive or negative, respectively. In either case, we see from (2.15) that the metric in the directions t, u, β is non-negative definite if and only if $tu(-\partial_y D) \geq 0$. This condition also automatically guarantees the nonnegativity of the coefficient of $D\chi^2$ in the line element.

Without loss of generality we can assume $\sigma < 0$. Indeed, $\sigma = 0$ would give $e^D \equiv 0$, and $\sigma > 0$ is equivalent up to exchanging the roles of t and u. Let us define

$$f_1(t,u) = t_1 t_2 u^2 - u_1 u_2 t^2$$
, $f_2(t,u) = (t_1 + t_2)u - (u_1 + u_2)t$. (2.20)

We proceed assuming (2.19). From the expressions of $(-\partial_y D)$ and $e^{-6\tilde{\lambda}}$, we infer that we have two possibilities to ensure non-negativity of the warp factor and metric functions,

$$\begin{array}{c|cccc}
 & \text{option (a)} & \text{option (b)} \\
\hline
 & t \ge 0, u \ge 0 & t \ge 0, u \ge 0 \\
 & (t - t_1)(t - t_2) \ge 0 & (t - t_1)(t - t_2) \le 0 \\
 & (u - u_1)(u - u_2) \le 0 & (u - u_1)(u - u_2) \ge 0 \\
 & f_1 \ge 0, f_2 \ge 0 & f_1 \le 0, f_2 \le 0
\end{array} \tag{2.21}$$

These two sets of inequalities are the starting point for a systematic discussion of the allowed domains in the (t, u) plane.

3 Geometries, fluxes, and observables

3.1 Rectangular domains in the (t, u) plane

Our next task is to identify possible choices for the parameters $t_{1,2}$, $u_{1,2}$ for which the inequalities (2.21) define a compact region in the (t, u) plane. In what follows, we focus on option (a) in (2.21), since option (b) gives analogous results with the roles of t and u exchanged.

Depending on the values of $u_{1,2}$, $t_{1,2}$, the allowed region in the (t,u) plane, if compact, is a polygon delimited by vertical, horizontal, and oblique lines. The latter (if present) originate from $f_1 \geq 0$ and/or $f_2 \geq 0$. In this subsection, we provide a complete classification of the choices of $u_{1,2}$, $t_{1,2}$ that yield rectangular domains in the (t,u) plane, as opposed to polygons admitting oblique sides. The physical motivation for this restriction on the shape of the allowed domain originates from the analysis of singularities in the supergravity solutions. For rectangular domains, all singularities that emerge can be interpreted in terms of smeared M5-branes sources of the same kind as in [15]. For non-rectangular domains, in contrast, novel singularities emerge, which are interpreted in terms of M5-brane sources that are smeared in more directions. While we refrain from a classification of non-rectangular domains, we discuss some examples in detail in section 3.3.

Inspection of the first column of (2.21) reveals that a necessary condition for having a rectangular, compact domain in the (t, u) plane is that all roots $t_{1,2}$, $u_{1,2}$ be real and such that $0 < t_1 \le t_2$, $u_1 < u_2$. As we vary $u_{1,2}$ we obtain different allowed regions. Restricting to rectangular domains, we find three cases, labeled I, II, III, and summarized in Figure 1.

3.2 Flux quantization and holographic quantities

While the geometries of Cases I, II, III are different, they share some common features. In particular, we observe that the β component v_{β} of the 1-form v in (2.15), (2.16) is piecewise constant along vertical and horizontal segments in the (t, u) plane of the form $t = t_i$ or $u = u_i$ (i = 1, 2). This implies that, along such segments, a constant linear combination of the Killing vectors ∂_{χ} , ∂_{β} has vanishing norm, with different linear combinations for each segment.

In order to elucidate the geometry in each case, we find it convenient to introduce new angular variables ϕ , z. They are related to the Toda angular variables β , χ by a change of coordinates of the form

$$\chi = \left(1 + \frac{1}{\mathcal{C}}\right)\phi - z , \qquad \beta = -\frac{1}{\mathcal{C}}\phi + z , \qquad (3.1)$$

where \mathcal{C} is a constant, which is given in terms of the value of the component v_{β} along the horizontal segment $u = u_2$, for each case in Figure 1. The new angular coordinates are engineered in such a way that, along the segment $u = u_2$, the Killing vector whose norm vanishes is simply ∂_{ϕ} .

In terms of the new variables ϕ , z, it is convenient to group the coordinates t, u, ϕ into a 3d base space, with the S^2 and the z circle being fibered on top. The 11d line element and flux take the form

$$ds_{11}^{2} = \frac{e^{2\tilde{\lambda}}}{m^{2}} \left[ds^{2} (AdS_{5}) + \frac{t^{2}u^{2}e^{-6\tilde{\lambda}}}{4} ds^{2} (S^{2}) + R_{z}^{2}Dz^{2} + R_{\phi}^{2}d\phi^{2} - \partial_{y}D \frac{K_{1}u^{2} + K_{2}t^{2}}{4tu} \left(\frac{dt^{2}}{K_{1}} + \frac{du^{2}}{K_{2}} \right) \right],$$

$$\overline{G}_{4} := -\frac{G_{4}}{(2\pi\ell_{p})^{3}} = \frac{\text{vol}_{S^{2}}}{4\pi} \wedge d \left[Y \frac{d\phi}{2\pi} - W \frac{Dz}{2\pi} \right], \qquad Dz = dz - Ld\phi.$$
(3.2)

In the previous expressions, the fibration of the z circle over the 3d base space is encoded in the 1-form Dz. We have introduced a rescaled version \overline{G}_4 of G_4 , which has the advantage of

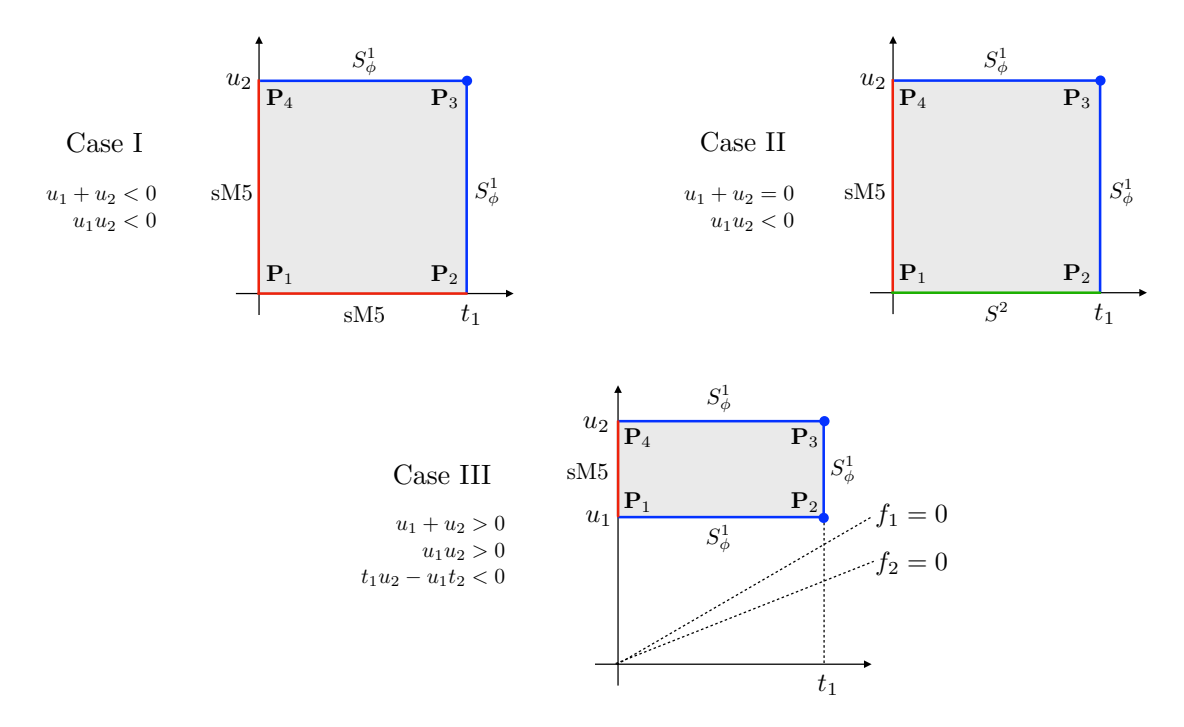


Figure 1: Cases that yield a rectangular domain in the (t, u) plane, as determined by the inequalities (2.21) option (a). In all cases, $0 < t_1 \le t_2$ and $u_1 < u_2$. The label S_{ϕ}^1 indicates that the ϕ circle in the base of the Dz fibration (3.2) shrinks smoothly along that component of the boundary of the allowed region. Similarly, the label S^2 indicates a smooth shrinking of the S^2 . The label sM5 stands for smeared M5-brane sources. Case III is understood to include the limiting case $t_1u_2 - u_1t_2 = 0$, in which the lines defined by f_1 and f_2 coincide, and touch the lower right corner of the shaded rectangle.

having integral periods, see (2.8) (the minus sign is for convenience). The quantities L, R_z , R_ϕ , Y, W are functions of t, u. We refer the reader to appendix A for further details on the change of coordinates (3.1) and for the expressions of C, L, R_z , R_ϕ , Y, W.

We now consider Cases I, II, III in turn. The results of the remainder of this subsection are summarized in Table 1.

3.2.1 Case I

Geometry. The allowed region in the (t, u) plane is $[0, t_1] \times [0, u_2]$ as depicted in Figure 1. We observe that, in this case, the inequalities $f_1 \geq 0$, $f_2 \geq 0$ are automatically satisfied once the other inequalities in (2.21) option (a) are satisfied. The radius R_{ϕ} of the ϕ circle in the 3d base space spanned by (t, u, ϕ) goes to zero along the segments $u = u_2$ and $t = t_1$. Along

	I	II	III
flux quanta	$ \begin{cases} q, K, M, N_{\text{W}}, N_{\text{S}} \\ N_{\text{eff}} := qM \end{cases} $	$\{q,K,M,N\}$	$ \begin{cases} q_1, q_2, K, M, N_{\mathbf{W}} \} \\ N_{\text{eff}} := q_1 \widetilde{M} + q_2 K, \widetilde{M} := M + K \end{cases} $
relations among fluxes	$N_{ m eff} = N_{ m W} - rac{MN_{ m S}}{K}$	N = qM	$N_{\text{eff}} = N_{\text{W}} - \frac{(q_1 + q_2)(\widetilde{M} + K)(q_2\widetilde{M} + q_1K)}{(q_1 - q_2)(\widetilde{M} - K)}$
$\partial_{\chi} = \partial_{\phi} + ()\partial_{z}$	$rac{N_{ ext{eff}}}{M+K}$	$\frac{N}{M+K}$	$rac{N_{ ext{eff}}}{\widetilde{M}+K}$
$c_{ m hol}$	$\frac{1}{12} \frac{K^2 N_{\text{eff}}^2}{M + K}$	$\frac{1}{12} \frac{K^2 N^2}{M + K}$	$\frac{1}{12} \frac{K^2 \left(N_{\text{eff}}^2 + q_2(q_1 + q_2)(\widetilde{M}^2 - K^2)\right)}{\widetilde{M} + K}$
$\left(\Delta(\mathcal{O}_1),\Delta(\mathcal{O}_2^i)\right)$	$(rac{KN_{ ext{eff}}}{M+K},K)$	$(\frac{KN}{M+K},K)$	$(rac{KN_{ ext{eff}}}{\widetilde{M}+K},K)$
other operators	$\Delta(\mathcal{O}_3^j) = M$	_	$\Delta(\mathcal{P}_1) = \frac{K(N_{\text{eff}} - (q_1 - q_2)(\widetilde{M} - K))}{\widetilde{M} + K}$ $\Delta(\mathcal{P}_2^j) = K$

Table 1: The flux quanta, $U(1)_r$ isometry generator, holographic c-central charge, and operator dimensions of the Case I, II, III holographic SCFTs, presented in variables most amenable to comparison. Note that Case II is recovered from the limit of Case I for which $N_S \to 0$, in which case $N_W \to N$. In section 5, the geometries with a monopole of charge q are generalized to monopole profiles corresponding to general Young tableaux.

these segments, the function L in the 1-form Dz is piecewise constant,

$$L(t, u_2) = 0,$$
 $L(t_1, u) = -\frac{2(t_2u_2 - t_1u_1)}{\sigma(t_2 - t_1)(u_2 - u_1)} \equiv q.$ (3.3)

The jump in L at the corner $(t, u) = (t_1, u_2)$ signals the presence of a monopole source for the Dz fibration over the 3d base space (t, u, ϕ) . The charge of the monopole source is the quantity q in (3.3), which is automatically positive for the ranges of the parameters that yield Case I. In order to have a well-defined geometry, the charge q must be an integer,

$$q \in \mathbb{N}$$
 . (3.4)

The radius R_z of the S_z^1 fiber over (t, u, ϕ) has an isolated zero at the location of the monopole point. Indeed, near the monopole the 4d geometry spanned by (t, u, ϕ, z) is locally $\mathbb{R}^4/\mathbb{Z}_q$. Thus, for $q \geq 2$, the space develops an orbifold singularity.

Along the segment $\mathbf{P}_1\mathbf{P}_2$, the warp factor goes to zero. In terms of the Toda angular variables χ , β , in the limit $u \to 0$, the line element takes the form

$$ds_{11}^{2} \approx \frac{u^{1/3}}{m^{2}} \left[\frac{u_{1}u_{2}t^{2/3}}{(u_{1} + u_{2})^{1/3}} ds^{2} (AdS_{5}) + \frac{u_{1}u_{2}t^{2/3}}{(u_{1} + u_{2})^{1/3}} D\chi^{2} \right]$$

$$+ \frac{u^{-2/3}}{m^{2}} \left[\frac{(u_{1} + u_{2})^{2/3}}{4} \left(du^{2} + u^{2} ds^{2} (S^{2}) \right) - \frac{u_{1}u_{2}(u_{1} + u_{2})^{2/3}}{4(t - t_{1})(t - t_{2})} \left(dt^{2} + \frac{K_{1}^{2}}{t^{2}} d\beta^{2} \right) \right].$$

$$(3.5)$$

Thus, we have M5-brane sources smeared along the t and β directions, with harmonic function $H \propto 1/u$. More precisely, the M5-branes are extended along the AdS_5 and χ directions, while the are smeared in two directions, t and β . The geometry near the segment $\mathbf{P}_4\mathbf{P}_1$ is completely analogous, with a harmonic function $H \propto 1/t$. These smeared M5-branes sources are denoted with the label sM5 in Figure 1. They are the same sort of sources considered in [15].

Flux quantization. The geometry of Case I admits non-trivial 4-cycles, constructed as follows. The 4-cycle $\mathcal{A}_{4,N}$ is obtained combining the segment $\mathbf{P}_3\mathbf{P}_4$ with the S^2 and the Dz fiber. Notice that the S^2 shrinks at \mathbf{P}_4 , while the Dz fiber shrinks at the monopole point \mathbf{P}_3 . By a similar token, we define the 4-cycle $\mathcal{A}_{4,E}$ by combining the segment $\mathbf{P}_2\mathbf{P}_3$ with the S^2 and the Dz fiber. The periods of \overline{G}_4 over $\mathcal{A}_{4,N}$, $\mathcal{A}_{4,E}$ are determined by the values of W in (3.2) at the points $\mathbf{P}_{2,3,4}$. With the expressions recorded in appendix A, we find

$$\int_{\mathcal{A}_{4,N}} \overline{G}_4 = -\frac{\sigma}{2} (u_2 - u_1) t_1 \equiv K \in \mathbb{N} , \qquad \int_{\mathcal{A}_{4,E}} \overline{G}_4 = -\frac{\sigma}{2} (t_2 - t_1) u_2 \equiv M \in \mathbb{N} . \tag{3.6}$$

In these expressions we have fixed the mass scale m as in (2.7).

We also have 4-cycles that measure the charges of the smeared M5-brane loci, in the spirit of a "Gaussian pillbox" from electrostatics. We take two 4-cycles³, $\mathcal{A}_{4,S}$ and $\mathcal{A}_{4,W}$, to measure the charges of the brane stacks along the South and West edges respectively. These are comprised of the relevant interval, the S^2 , and the ϕ circle. The associated periods of \overline{G}_4 are determined by the values of Y in (3.2) at $\mathbf{P}_{2,3,4}$. The result reads

$$\int_{\mathcal{A}_{4,W}} \overline{G}_4 = \frac{(t_1 + t_2)u_2^2}{u_2 - u_1} \equiv N_W \in \mathbb{N} , \qquad \int_{\mathcal{A}_{4,S}} \overline{G}_4 = \frac{(u_1 + u_2)t_1^2}{t_2 - t_1} \equiv N_S \in \mathbb{N} . \tag{3.7}$$

The expressions of the flux quanta K, M, $N_{\rm W}$, $N_{\rm S}$ and the monopole charge q imply

$$M = \frac{N_{\rm W}}{q + \frac{N_{\rm S}}{K}} \ . \tag{3.8}$$

In particular, integrality of M imposes a constraint on the possible values for $N_{\rm W}$, $N_{\rm S}$, K, q: $Kq + N_{\rm S}$ must divide $KN_{\rm W}$. An analogous constraint was found in the solutions of [15].

With the flux quanta computed above, the χ Killing vector can be written as

$$\partial_{\chi} = \partial_{\phi} + \frac{qM}{K+M} \partial_z = \partial_{\phi} + \frac{N_{\text{eff}}}{K+M} \partial_z , \qquad N_{\text{eff}} := qM .$$
 (3.9)

In the second step, we have defined an "effective brane charge" $N_{\rm eff}$, which will prove to be useful in discussing the dual field theory interpretation of these solutions.

 $^{^{3}}$ To be proper, we construct these using intervals away from the edge, then consider the limit as we take either t or u to zero.

Central charge. For an AdS_5 solution in 11d supergravity of the form

$$ds_{11}^2 = \frac{e^{2\tilde{\lambda}}}{m^2} \left[ds^2 (AdS_5) + ds^2 (M_6) \right] , \qquad (3.10)$$

the holographic central charge is computed via the relation [32]

$$c = \frac{1}{2^7 \pi^6 (m\ell_p)^9} \int_{M_6} e^{9\tilde{\lambda}} \operatorname{vol}_{M_6}.$$
 (3.11)

Using our metric in (2.15), for values of the parameters yielding Case I, we can compute c as

$$c_{\rm I} = \frac{-\sigma(t_1 u_2)^2 (t_2 u_2 - t_1 u_1)}{2^9 3\pi^3 (m\ell_p)^9} = \frac{1}{12} \frac{(qKM)^2}{K + M} = \frac{1}{12} \frac{qK^2 N_{\rm eff}^2}{qK + N_{\rm eff}} \ . \tag{3.12}$$

In the second step, we have fixed m according to (2.7) and we have expressed the result in terms of the monopole charge q in (3.3) and the flux quanta defined in (3.6), (3.9).

M2-brane operators. An M2-brane wrapping a calibrated 2d submanifold C_2 in the internal space yields a BPS operator. The calibration condition reads

$$Y'|_{\mathcal{C}_2} = \operatorname{vol}_{M_6}(\mathcal{C}_2) , \qquad (3.13)$$

where the right hand side is the induced volume form from M_6 . The calibration 2-form Y' is a bilinear in the Killing spinors [32]. For a solution in canonical LLM form (2.1), it reads [15]

$$Y' = \frac{1}{4}y^{3}e^{-9\tilde{\lambda}}\operatorname{vol}_{S^{2}} + \frac{1}{2}ye^{-3\tilde{\lambda}}(1 - y^{2}e^{-6\tilde{\lambda}})d\tau \wedge D\chi$$
$$-\frac{1}{2}\tau e^{-3\tilde{\lambda}}D\chi \wedge dy - \frac{1}{4}\frac{ye^{-9\tilde{\lambda}}\tau e^{D}}{1 - y^{2}e^{-6\tilde{\lambda}}}dx^{1} \wedge dx^{2}. \tag{3.14}$$

In the previous expression, the quantity τ is a coordinate on the S^2 , which is parametrized as

$$ds^{2}(S^{2}) = \frac{d\tau^{2}}{1 - \tau^{2}} + (1 - \tau^{2})d\varphi^{2}.$$
(3.15)

The explicit expression of Y' for the metric in (3.2) is reported in appendix A.

Let us take C_2 to be the S^2 on top of the monopole point \mathbf{P}_3 (at which both ∂_{ϕ} and ∂_z shrink). The calibration 2-form restricted on C_2 reads

$$Y'|_{\mathcal{C}_2} = \frac{1}{4} (t_1 u_2)^3 \left(\frac{(t_1 + t_2)u_2 - (u_1 + u_2)t_1}{(t_1 u_2)(t_1 t_2 u_2^2 - u_1 u_2 t_1^2)} \right)^{3/2} \text{vol}_{S^2} = \frac{1}{4} \text{vol}_{S^2} . \tag{3.16}$$

On the other hand, the induced volume form on C_2 is

$$ds^{2}(\mathcal{C}_{2}) = \frac{1}{4} \frac{t_{1}^{2} u_{2}^{2}}{t_{1}^{2} u_{2}^{2}} ds^{2}(S^{2}) = \frac{1}{4} ds^{2}(S^{2}) . \tag{3.17}$$

The calibration condition (3.13) is then satisfied. We can compute the conformal dimension of an M2-brane operator \mathcal{O} via [32]

$$\Delta(\mathcal{O}) = \frac{1}{4\pi^2 (m\ell_p)^3} \int_{\mathcal{C}_2} e^{3\tilde{\lambda}} \operatorname{vol}_{M_6}(\mathcal{C}_2). \tag{3.18}$$

If \mathcal{O}_1 denotes the BPS operator associated to \mathcal{C}_2 as above, we find

$$\Delta(\mathcal{O}_1) = t_1 u_2 = \frac{qKM}{M+K} = \frac{qKN_{\text{eff}}}{qK+N_{\text{eff}}}.$$
(3.19)

We can define another submanifold \mathcal{B}_2 by considering the interval $\mathbf{P}_3\mathbf{P}_4$ and the linear combination of the z and ϕ circles that does not vanish along this interval. That is, we choose the Dz fiber. This 2-manifold sits at a single point on the S^2 . We notice that \mathcal{B}_2 is not a 2-cycle, but rather describes an open M2-brane ending on a smeared M5-brane source. The form Y' can be computed as

$$Y'|_{\mathcal{B}_2} = \frac{\tau_*(2+\lambda)(u_1-u_2)}{8} \sqrt{\frac{u_1t + u_2(t-t_1-t_2)}{u_2^2t(u_1t^2 - t_1t_2u_2)}} dt \wedge Dz , \qquad (3.20)$$

while the induced metric is

$$ds^{2}(\mathcal{B}_{2}) = R_{z}^{2}(t, u_{2})Dz^{2} + \frac{(t_{1} + t_{2})u_{2} - (u_{1} + u_{2})t}{4tu_{2}(t - t_{1})(t - t_{2})}dt^{2}.$$
(3.21)

One can readily check that the calibration condition is satisfied, provided we choose $\tau_* = 1$. Let \mathcal{O}_2 denote the operator associated to \mathcal{B}_2 . Since \mathcal{B}_2 is an open M2-brane, we expect \mathcal{O}_2 to admit a degeneracy due to possible choice of boundary conditions for the M2-brane ending on the M5-branes. The dimension of \mathcal{O}_2 is

$$\Delta(\mathcal{O}_2^i) = -\frac{\sigma}{2}t_1(u_2 - u_1) = K \ . \tag{3.22}$$

We can construct yet another submanifold \mathcal{D}_2 using the interval $\mathbf{P}_3\mathbf{P}_2$ and the Dz fiber. We find that Y' takes the form

$$Y'|_{\mathcal{D}_2} = \frac{\tau_* \sigma(t_2 - t_1)}{4} \sqrt{\frac{t_2 u + t_1 (u - u_1 - u_2)}{t_1^2 u (t_2 u^2 - t_1 u_1 u_2)}} du \wedge Dz , \qquad (3.23)$$

and the induced metric becomes

$$ds^{2}(\mathcal{D}_{2}) = R_{z}^{2}(t_{1}, u)Dz^{2} - \frac{(t_{1} + t_{2})u - (u_{1} + u_{2})t_{1}}{4t_{1}u(u - u_{1})(u - u_{2})}dt^{2}.$$
(3.24)

The calibration condition is satisfied provided $\tau_* = 1$, and we again have a collection of BPS operators, denoted collectively \mathcal{O}_3 , with conformal dimension

$$\Delta(\mathcal{O}_3^j) = -\frac{\sigma}{2}u_2(t_2 - t_1) = M = \frac{N_{\text{eff}}}{q} . \tag{3.25}$$

3.2.2 Case II

The allowed domain in Case II is $[0, t_1] \times [0, u_2]$, the same as in Case I, see Figure 1. Case II can be regarded as a limiting case of Case I, in which $u_1 + u_2 > 0$ is sent to zero. The salient new feature of Case II is the behavior of the metric near the segment $\mathbf{P}_1\mathbf{P}_2$. One can verify that in this case the S^2 shrinks smoothly, while the warp factor remains finite. Compared with Case I, we still have a monopole source for Dz at \mathbf{P}_3 , and a smeared M5-branes source along $\mathbf{P}_4\mathbf{P}_1$.

The solutions of Case II are the same as the solutions discussed in [15]. We refer the reader to appendix A for the explicit change of coordinates that makes the correspondence manifest. Since these solutions have already been studied in detail in [15], we will be brief.

Flux quanta K, M can be defined for Case II, in complete analogy with (3.6). We also have the analog of the flux quantum $N_{\rm W}$, while $N_{\rm S}$ is absent, since we no longer have a smeared M5-brane source along $\mathbf{P}_1\mathbf{P}_2$. The flux quanta K, M, $N_{\rm W}$ satisfy the same constraint as (3.8) with $N_{\rm S}$ set to zero.

The expression of the holographic central charge is

$$c_{\text{II}} = \frac{1}{12} \frac{qK^2N^2}{qK+N} , \qquad N := qM .$$
 (3.26)

We have the direct analogs of the \mathcal{O}_1 operators associated to M2-branes wrapping the S^2 on top of the monopole point, as well as analogs of the operators \mathcal{O}_2 associated to open M2-branes ending on the M5-brane source along $\mathbf{P}_1\mathbf{P}_4$. We do not have, however, the analog of the \mathcal{O}_3 operators, because we only have one set of smeared M5-branes. The dimensions of \mathcal{O}_1 , \mathcal{O}_2 are

$$\Delta(\mathcal{O}_1) = \frac{qKN}{qK+N} , \qquad \Delta(\mathcal{O}_2^i) = K . \tag{3.27}$$

3.2.3 Case III

Geometry. The allowed domain in Case III is the rectangle $[0, t_1] \times [u_1, u_2]$, see Figure 1. In this case, we find that the ϕ circle in the 3d base spanned by (t, u, ϕ) shrinks along the three segments $\mathbf{P}_1\mathbf{P}_2$, $\mathbf{P}_2\mathbf{P}_3$, and $\mathbf{P}_3\mathbf{P}_4$. The function L is piecewise constant along these segments,

$$L(t, u_2) = 0,$$
 $L(t_1, u) = -\frac{2(t_2u_2 - t_1u_1)}{\sigma(t_2 - t_1)(u_2 - u_1)},$ $L(t, u_1) = -\frac{2(u_2 + u_1)}{\sigma(u_2 - u_1)}.$ (3.28)

We see that L jumps both at \mathbf{P}_2 and at \mathbf{P}_3 . It follows that the Dz fibration has two monopole sources, located at \mathbf{P}_3 , \mathbf{P}_2 , with charges q_1 , q_2 respectively,

at
$$\mathbf{P}_3$$
: $q_1 = -\frac{2(t_2u_2 - t_1u_1)}{\sigma(t_2 - t_1)(u_2 - u_1)} \in \mathbb{N}$, at \mathbf{P}_2 : $q_2 = -\frac{2(t_2u_1 - t_1u_2)}{\sigma(t_2 - t_1)(u_2 - u_1)} \in \mathbb{N}$. (3.29)

Along the segment $\mathbf{P}_4\mathbf{P}_1$ we have a smeared M5-brane source of the same kind as explained in Case I.

Flux quantization. A first class of 4-cycles is associated to the three components along the boundary of the allowed region, in which the ϕ circle in the base shrinks. Let us define

 $\mathcal{B}_{4,\mathrm{N}}$: segment $\mathbf{P}_3\mathbf{P}_4$ combined with the Dz fiber and the S^2 , $\mathcal{B}_{4,\mathrm{E}}$: segment $\mathbf{P}_2\mathbf{P}_3$ combined with the Dz fiber and the S^2 , (3.30) $\mathcal{B}_{4,\mathrm{S}}$: segment $\mathbf{P}_1\mathbf{P}_2$ combined with the Dz fiber and the S^2 .

As before, we can compute the flux through these cycles in terms of the values of the function W at $\mathbf{P}_{1,2,3,4}$. The result reads

$$\int_{\mathcal{B}_{4,N}} \overline{G}_4 = \int_{\mathcal{B}_{4,S}} \overline{G}_4 = -\frac{\sigma}{2} t_1(u_2 - u_1) \equiv K \in \mathbb{N} ,$$

$$\int_{\mathcal{B}_{4,E}} \overline{G}_4 = -\frac{\sigma}{2} (t_2 - t_1)(u_2 - u_1) \equiv M \in \mathbb{N} .$$
(3.31)

Interestingly we find that the fluxes through $\mathcal{B}_{4,N}$ and $\mathcal{B}_{4,S}$ are equal.

Next, we can construct a 4-cycle to measure the flux from the M5-branes source along $\mathbf{P}_4\mathbf{P}_1$. To this end, we consider the S^2 combined with the u interval and the ϕ circle, yielding a 4-cycle denoted $\mathcal{A}_{4,\mathrm{W}}$. The associated flux quantum is

$$\int_{\mathcal{A}_{4,W}} \overline{G_4} = \frac{(t_1 + t_2)(u_2^2 + u_1^2)}{u_2 - u_1} \equiv N_W \in \mathbb{N}.$$

We find it convenient to define

$$\widetilde{M} = M + K$$
, $N_{\text{eff}} = q_1 \widetilde{M} + q_2 K$. (3.32)

We may then write

$$\partial_{\chi} = \partial_{\phi} + \frac{Mq_1 + K(q_1 + q_2)}{M + 2K} \partial_z = \partial_{\phi} + \frac{N_{\text{eff}}}{\widetilde{M} + K} \partial_z . \tag{3.33}$$

The quanta found above satisfy the relation

$$N_W = \frac{M^2(q_1^2 + q_2^2) + 2K(K + M)(q_1 + q_2)^2}{M(q_1 - q_2)},$$
(3.34)

which in terms of $N_{\rm eff}$ and \widetilde{M} can be written

$$N_{\text{eff}} = N_W - \frac{(q_1 + q_2)(\widetilde{M} + K)}{(q_1 - q_2)(\widetilde{M} - K)} (q_1 K + q_2 \widetilde{M}). \tag{3.35}$$

Central charge. Applying formula (3.11), we arrive at

$$c_{\text{III}} = \frac{-\sigma}{2^9 3\pi^3 (m\ell_p)^9} t_1^2 \left(t_1 u_1 u_2 (u_1 - u_2) + t_2 (u_2^3 - u_1^3) \right)$$

$$= \frac{1}{12} \frac{K^2 \left((K+M)^2 (q_1 + q_2)^2 - M^2 q_1 q_2 \right)}{M + 2K}$$

$$= \frac{1}{12} \frac{K^2 (\widetilde{M}^2 (q_1 + q_2)^2 - (\widetilde{M} - K)^2 q_1 q_2)}{\widetilde{M} + K}$$
(3.36)

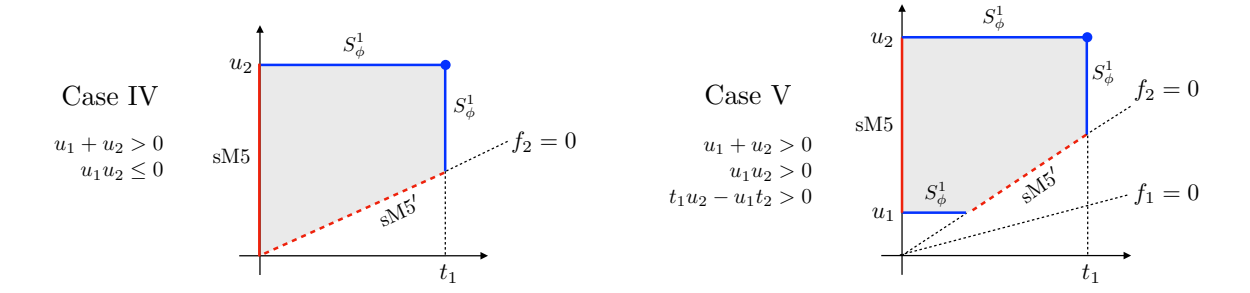


Figure 2: Non-rectangular domains arising from the inequalities (2.21) option (a), under the assumptions $0 < t_1 \le t_2$ and $u_1 < u_2$. The label S^1_{ϕ} indicates that the ϕ circle in the base of the Dz fibration (3.2) shrinks smoothly along that component of the boundary of the allowed region. The labels sM5 and sM5' stand for two different kinds of smeared M5-brane sources.

M2-brane operators. We still have the direct analogs of the calibrated submanifolds C_2 and \mathcal{B}_2 constructed in Case I, associated to operators \mathcal{O}_1 , \mathcal{O}_2 , respectively. In the case at hand, their dimensions are

$$\Delta(\mathcal{O}_1) = \frac{K}{M+2K} \left(Mq_1 + K(q_1 + q_2) \right) = \frac{KN_{\text{eff}}}{\widetilde{M} + K} , \qquad \Delta(\mathcal{O}_2^i) = K . \tag{3.37}$$

We also have a new calibrated 2-cycle, analogous to C_2 , given by the S^2 on top of the new monopole point \mathbf{P}_2 . If we denote the corresponding operator as \mathcal{P}_1 , we find

$$\Delta(\mathcal{P}_1) = t_1 u_1 = \frac{K}{M + 2K} \left(M q_2 + K (q_1 + q_2) \right) = \frac{K N_{\text{eff}}}{\widetilde{M} + K} - \frac{\widetilde{M} - K}{\widetilde{M} + K} (q_1 - q_2) K . \tag{3.38}$$

Moreover, we also have a new open calibrated submanifold, analogous to \mathcal{B}_2 , constructed using $\mathbf{P}_1\mathbf{P}_2$ and the Dz fiber. We thus obtain a family of BPS operators, denoted collectively \mathcal{P}_2^j , with dimension

$$\Delta(\mathcal{P}_2^j) = -\frac{\sigma}{2} t_1(u_2 - u_1) = K. \tag{3.39}$$

Finally, we can combine the $\mathbf{P}_2\mathbf{P}_3$ segment connecting the two monopoles and the Dz fiber to obtain a closed calibrated submanifold. We denote the associated BPS operator as \mathcal{Q} and we compute its dimension to be

$$\Delta(Q) = -\frac{\sigma}{2}(t_2 - t_1)(u_2 - u_1) = M .$$
(3.40)

3.3 Examples of non-rectangular domains

In the previous section, we have assumed $0 < t_1 \le t_2$, $u_1 < u_2$, as these are necessary conditions for having a rectangular domain. These conditions, however, are not sufficient. Indeed, if we let $u_{1,2}$ vary, we obtain two more cases, with non-rectangular domains, denoted IV and V and summarized in Figure 2.

Let us remark that Cases IV and V do not provide a full classification of all non-rectangular, compact domains. Further domains (including triangular domains) can be obtained by relaxing some of the assumptions $t_{1,2} \in \mathbb{R}$, $0 < t_1 \le t_2$, $u_1 < u_2$. In this section, we provide some details on Cases IV and V as representative examples of non-rectangular domains, but we refrain from a full classification.

Cases IV and V are conveniently described in terms of the same angular coordinates ϕ , z introduced above in (3.1) and entering (3.2).

3.3.1 Case IV

Geometry. The main novel feature of Case IV is the presence of a boundary component with positive slope, which is determined by the inequality $f_2 \geq 0$, see Figure 2. Near the vertical and horizontal segments along the boundary of the allowed region, we have similar features as the Cases I, II, III.

Let us look closer at the geometry along the diagonal line defined by $f_2 = 0$. For convenience, and in analogy with (3.5), we work with the Toda angular variables χ , β . We rearrange the coordinates (t, u) into linear combinations x_{\parallel} , x_{\perp} , where x_{\parallel} runs longitudinally to the diagonal line, and x_{\perp} runs transversally. More precisely, we can set

$$t = \bar{t}x_{\parallel} - \bar{u}x_{\perp} , \qquad u = \bar{u}x_{\parallel} + \bar{t}x_{\perp} , \qquad \bar{t} := t_1 + t_2 , \qquad \bar{u} := u_1 + u_2 .$$
 (3.41)

In the limit $x_{\perp} \to 0$, the line element takes the form

$$ds_{11}^{2} \approx \frac{x_{\perp}^{-1/3}}{m^{2}} \left[x_{\parallel}^{4/3} \left(\frac{\bar{t}\bar{u} \left(t_{1}t_{2}\bar{u}^{2} - u_{1}u_{2}\bar{t}^{2} \right)}{(\bar{t}^{2} + \bar{u}^{2})^{2}} \right)^{1/3} \left(ds^{2} (AdS_{5}) + D\chi^{2} \right) \right]$$

$$+ \frac{x_{\perp}^{2/3}}{m^{2}} \left[\frac{1}{4} \left(\frac{\left(t_{1}t_{2}\bar{u}^{2} - u_{1}u_{2}\bar{t}^{2} \right)}{(\bar{t}\bar{u}x_{\parallel})^{2} (\bar{t}^{2} + \bar{u}^{2})^{2}} \right)^{1/3} \left(\frac{(\bar{t}\bar{u}x_{\parallel})^{2}}{(t_{1}t_{2}\bar{u}^{2} - u_{1}u_{2}\bar{t}^{2})} ds^{2} (S^{2}) + (\bar{t}^{2} + \bar{u}^{2})^{2} ds^{2} (M_{3}) \right) \right].$$

$$(3.42)$$

Here $ds^2(M_3)$ denotes the metric on the space described by $(x_{\perp}, x_{\parallel}, \beta)$, whose explicit expression is omitted for brevity. We interpret (3.42) in terms of a smeared M5-brane source with harmonic function $H \propto x_{\perp}$. The linear behavior of H is indicative of a smearing to effective codimension 1. Indeed, the M5-branes are now smeared over more directions, compared to (3.5). More precisely, they are extended along AdS_5 and χ , and smeared in all other directions, except x_{\perp} . In Figure 2 we use the label sM5' to signal this new kind of source.

Flux quantization. The analysis of G_4 -flux quantization is closely analogous to Case I. The role of the segment $\mathbf{P}_1\mathbf{P}_2$ of Case I is now played by the diagonal line determined by $f_2 = 0$. We can define the analog of the flux quanta M, K, $N_{\rm S}$, and $N_{\rm W}$ and verify that they satisfy the same relation as in Case I.

Central charge. Application of (3.11) yields the result

$$c_{\text{IV}} = -\frac{\sigma}{15} \frac{1}{2^9 \pi^3 (m\ell_p)^9} t_1^2 \left(5u_2^2 (t_2 u_2 - t_1 u_1) + \frac{t_1^3 (u_1 + u_2)^3}{(t_1 + t_2)^2} \right)$$

$$= \frac{1}{120} \frac{qKM}{M + K} \left(5qKM + \frac{N_S^3 M^3}{N_W^2 K^2} \right) . \tag{3.43}$$

3.3.2 Case V

The salient features of the geometry of Case V are a combination of the ingredients already introduced above, as can be seen from Figure 2. The charge of the monopole at (t_1, u_2) is

$$q = \frac{2(t_1u_1 - t_2u_2)}{\sigma(t_1 - t_2)(u_1 - u_2)} \ . \tag{3.44}$$

We can define the analog of the flux quanta K and M, given by differences of the values of W at the points (t_1, u_2) and $(0, u_2)$, $(t_1, (u_1 + u_2)t_1/(t_1 + t_2))$,

$$K = -\frac{\sigma}{2}t_1(u_2 - u_1) , \qquad M = -\frac{\sigma}{2}u_2(t_2 - t_1) .$$
 (3.45)

We observe that the analogous flux constructed with the horizontal segment at $u=u_1$ is vanishing. We can also define the analog of the flux $N_{\rm W}$, which measures the charge of the sM5 smeared source, and a new flux $N_{\rm d}$ which measures the sM5' charge along the diagonal component of the boundary of the allowed region. These fluxes are determined by the values of Y, and are given by

$$N_{\rm W} = -\frac{(t_1 + t_2)(u_1^2 + u_2^2)}{u_1 - u_2} , \qquad N_{\rm d} = \frac{u_1^2(t_1 + t_2)}{u_1 - u_2} - \frac{t_1^2(u_1 + u_2)}{t_1 - t_2} . \tag{3.46}$$

The flux quanta and the monopole charge satisfy the following identity,

$$0 = 2q(N_{\rm d} + N_{\rm W}) \left(K^2 N_{\rm W} - KM(N_{\rm d} + N_{\rm W}) + M^2 (2N_{\rm d} + N_{\rm W}) \right) - 2KMq^3 \left(K^2 + M^2 \right) + q^2 (K - M)^2 (KN_{\rm W} - M(2N_{\rm d} + N_{\rm W})) + (N_{\rm d} + N_{\rm W})^2 (KN_{\rm W} - M(2N_{\rm d} + N_{\rm W})) .$$

$$(3.47)$$

Let us define

$$\widetilde{N} = N_{\rm d} + N_{\rm W} \ . \tag{3.48}$$

We can use (3.47) to express $N_{\rm W}$ in terms of q, K, M, \widetilde{N}

$$N_{W} = \frac{2M(Kq + \tilde{N})\left(q^{2}\left(K^{2} + M^{2}\right) - 2M\tilde{N}q + \tilde{N}^{2}\right)}{(K + M)(q(K - M) + \tilde{N})^{2}}.$$
(3.49)

The expression of the central charge in terms of the parameters σ , $t_{1,2}$, $u_{1,2}$ is

$$c_{V} = -\frac{\sigma}{15} \frac{1}{2^{9} \pi^{3} (m\ell_{p})^{9}} \left(\frac{t_{1}^{5} (u_{1} + u_{2})^{3}}{(t_{1} + t_{2})^{2}} - \frac{u_{1}^{5} (t_{1} + t_{2})^{3}}{(u_{1} + u_{2})^{2}} + 5t_{1}^{2} u_{2}^{2} (t_{2}u_{2} - t_{1}u_{1}) \right) . \tag{3.50}$$

We may also express this quantity in terms of the flux quanta and monopole charge,

$$c_{V} = \frac{K^{2}M^{2}q^{2}}{60(K+M)^{2}(Kq+\tilde{N})^{2}(\tilde{N}-Mq)^{2}(q(K-M)+\tilde{N})^{5}} \times \left[5K^{7}q^{6} \left(19M^{2}\tilde{N}q^{2} - 2M^{3}q^{3} - 22M\tilde{N}^{2}q + 7\tilde{N}^{3} \right) \right. \\ \left. \times \left[5K^{7}q^{6} \left(19M^{2}\tilde{N}q^{2} - 2M^{3}q^{3} - 22M\tilde{N}^{2}q + 7\tilde{N}^{3} \right) \right. \\ \left. + 5K^{6}q^{5} \left(68M^{2}\tilde{N}^{2}q^{2} - 27M^{3}\tilde{N}q^{3} + 6M^{4}q^{4} - 69M\tilde{N}^{3}q + 23\tilde{N}^{4} \right) \right. \\ \left. + K^{5}\tilde{N}q^{4} \left(765M^{2}\tilde{N}^{2}q^{2} - 470M^{3}\tilde{N}q^{3} + 125M^{4}q^{4} - 595M\tilde{N}^{3}q + 176\tilde{N}^{4} \right) \right. \\ \left. + 5K^{4}q^{3}(\tilde{N}-Mq) \left(104M^{2}\tilde{N}^{3}q^{2} - 31M^{3}\tilde{N}^{2}q^{3} - 11M^{4}\tilde{N}q^{4} + 4M^{5}q^{5} - 101M\tilde{N}^{4}q + 34\tilde{N}^{5} \right) \right. \\ \left. + 5K^{3}q^{2}(\tilde{N}-Mq)^{2} \left(24M^{2}\tilde{N}^{3}q^{2} + 22M^{3}\tilde{N}^{2}q^{3} - 15M^{4}\tilde{N}q^{4} + 2M^{5}q^{5} - 54M\tilde{N}^{4}q + 23\tilde{N}^{5} \right) \right. \\ \left. + 5K^{2}q(Mq-\tilde{N})^{3}(Mq+\tilde{N}) \left(-14M^{2}\tilde{N}^{2}q^{2} + M^{3}\tilde{N}q^{3} + M^{4}q^{4} + 23M\tilde{N}^{3}q - 10\tilde{N}^{4} \right) \right. \\ \left. + 5K^{8}Mq^{8}(3Mq-\tilde{N}) + 5K^{9}Mq^{9} + K^{10}q^{9} \right. \\ \left. + 5K(\tilde{N}-Mq)^{4} \left(-3M^{2}\tilde{N}^{3}q^{2} + 3M^{4}\tilde{N}q^{4} - M^{5}q^{5} + 2\tilde{N}^{5} \right) \right. \\ \left. + M^{3}q^{2}(Mq-\tilde{N})^{5} \left(M^{2}q^{2} - 5M\tilde{N}q + 5\tilde{N}^{2} \right) \right] .$$
 (3.51)

4 Electrostatic picture

In this section we review the map from the axisymmetric Toda system to an electrostatic problem, and we describe the electrostatic interpretation of the solutions discussed in section 3.

4.1 Review of the Bäcklund transform

In this work, we study solutions for which the Toda function D is independent of the angular coordinate β in the x^1 , x^2 plane. For such solutions, it is possible to perform a Bäcklund transform, which furnishes an electrostatic interpretation for the BPS conditions [13].

The Bäcklund transform takes the coordinates (r, y) and the function D(r, y) of the canonical LLM form to new coordinates (ρ, η) and a new function $V(\rho, \eta)$. The Bäcklund transform is defined implicitly by the relations

$$\rho^2 = r^2 e^D , \qquad y = \rho \, \partial_\rho V , \qquad \log r = \partial_\eta V . \tag{4.1}$$

The 11d metric and flux can be written as

$$ds_{11}^{2} = \frac{1}{m^{2}} \left[\frac{\dot{V} \widetilde{\Delta}}{2 V''} \right]^{1/3} \left[ds_{AdS_{5}}^{2} + \frac{V'' \dot{V}}{2 \widetilde{\Delta}} ds_{S^{2}}^{2} + \frac{V''}{2 \dot{V}} \left(d\rho^{2} + d\eta^{2} + \frac{2 \dot{V}}{2 \dot{V} - \ddot{V}} \rho^{2} d\chi_{B}^{2} \right) + \frac{\dot{V} - \ddot{V}}{2 \dot{V} \widetilde{\Delta}} \left(d\beta - \frac{2 \dot{V} \dot{V}'}{2 \dot{V} - \ddot{V}} d\chi_{B} \right)^{2} \right],$$

$$G_{4} = \frac{1}{4 m^{3}} \operatorname{vol}_{S^{2}} \wedge d \left[-\frac{2 \dot{V}^{2} V''}{\widetilde{\Delta}} d\chi_{B} + \left(\eta - \frac{\dot{V} \dot{V}'}{\widetilde{\Delta}} \right) d\beta \right], \tag{4.2}$$

where we used the notation $\dot{V} = \rho \, \partial_{\rho} V$, $V' = \partial_{\eta} V$, and so on, and we introduced

$$\widetilde{\Delta} = (2\,\dot{V} - \ddot{V})\,V'' + (\dot{V}')^2 \,. \tag{4.3}$$

The angle χ_B after the Bäcklund transform is related to the angle χ in the canonical LLM form as [33]

$$\chi_{\rm B} = \chi + \beta \ . \tag{4.4}$$

The function V obeys the 3d Laplace equation in cylindrical coordinates: away from sources,

$$\partial_{\eta}^{2}V + \frac{1}{\rho}\partial_{\rho}(\rho\,\partial_{\rho}V) = 0. \tag{4.5}$$

This equation motivates the interpretation of V as an electrostatic potential in three dimensions. We allow for electric charges localized along the η axis, with a charge density $\lambda(\eta)$. The charge density can be extracted from the potential V via

$$\lambda(\eta) = \lim_{\rho \to 0^+} \rho \,\partial_\rho \,V \ . \tag{4.6}$$

Some redundancies in the parametrization. We have already observed that the mass scale m can be fixed according to (2.7) without loss of generality. We also notice that the 11d metric and flux depend on V'', \dot{V} , \dot{V} , \dot{V} , \dot{V} , but not on V'. It follows that a replacement of the form

$$V(\rho, \eta) \mapsto V(\rho, \eta) + k \eta$$
, (4.7)

where k is an arbitrary constant, has no effect on the 11d metric and flux.

Line element and flux in terms of V, z, ϕ . In what follows, it will be convenient to rewrite the metric and flux in (4.2) by trading the angular variables $\chi_{\rm B}$, β with the angular variables z, ϕ first introduced in section 3.2 and discussed in greater detail in appendix A. The change of coordinates that related the Toda angular variables χ , β to the new variables $\chi_{\rm B}$, β is of the form

$$\chi = \left(1 + \frac{1}{\mathcal{C}}\right)\phi - z , \qquad \beta = -\frac{1}{\mathcal{C}}\phi + z , \qquad (4.8)$$

where \mathcal{C} is a positive constant. Below, we demonstrate that \mathcal{C} can be identified with a ratio of G_4 -flux quanta. Combining (4.4) and (4.8), we can recast (4.2) in the following form

$$ds_{11}^{2} = (4\pi)^{2/3} \ell_{p}^{2} \left[\frac{\dot{V} \widetilde{\Delta}}{2 V''} \right]^{1/3} \left[ds_{AdS_{5}}^{2} + \frac{V'' \dot{V}}{2 \widetilde{\Delta}} ds_{S^{2}}^{2} + \frac{V''}{2 \dot{V}} (d\rho^{2} + d\eta^{2}) + R_{\phi}^{2} d\phi^{2} + R_{z}^{2} Dz^{2} \right],$$

$$\overline{G}_{4} := -\frac{G_{4}}{(2\pi \ell_{p})^{3}} = \frac{\text{vol}_{S^{2}}}{4\pi} \wedge d \left[Y \frac{d\phi}{2\pi} - W \frac{Dz}{2\pi} \right],$$
(4.9)

where we have introduced

$$R_{\phi}^{2} = \frac{V''}{2\dot{V} - \ddot{V}} \rho^{2} , \qquad \qquad R_{z}^{2} = \frac{2\dot{V} - \ddot{V}}{2\dot{V} \widetilde{\Delta}} ,$$

$$Dz = dz - L d\phi , \qquad \qquad L = \frac{1}{\mathcal{C}} + \frac{2\dot{V}\dot{V}'}{2\dot{V} - \ddot{V}} ,$$

$$W = \eta - \frac{\dot{V}\dot{V}'}{\widetilde{\Delta}} , \qquad \qquad Y = \frac{2\dot{V}(\dot{V} - \dot{V}'\eta)}{2\dot{V} - \ddot{V}} . \qquad (4.10)$$

Notice that we have fixed the mass scale m according to (2.7).

4.2 Electrostatic potential from Toda solutions

Let us study the Bäcklund transform reviewed above in the cases discussed in Section 3. The expressions in this subsection apply to all cases.

From (2.11) and (4.1), we can immediately find the expression for $\rho(t, u)$,

$$\rho = \sqrt{K_1 K_2} = \sqrt{-\sigma^2(t - t_1)(t - t_2)(u - u_1)(u - u_2)} . \tag{4.11}$$

The function $\eta(t, u)$ can be found in the following way. Let us treat $V_{\rm T}$ as function of t and u, where we have included the subscript 'T' to remind ourselves that this is the electrostatic potential as inferred from the Toda coordinates via the Backlünd transformation. We can use the chain rule, equation (4.1), and the unspecified $\eta(t, u)$ to write

$$\partial_t V_{\rm T} = \partial_t \eta \left(\log r_1 + \log r_2 \right) + \frac{tu}{2K_1} \partial_t K_1 ,$$

$$\partial_u V_{\rm T} = \partial_u \eta \left(\log r_1 + \log r_2 \right) + \frac{tu}{2K_2} \partial_u K_2 .$$

$$(4.12)$$

Imposing the integrability condition $\partial_t \partial_u V_T = \partial_u \partial_t V_T$ yields

$$K_2 t \partial_t K_1 - K_1 u \partial_u K_2 = 2 \left(K_2 t \partial_u \eta + K_1 u \partial_t \eta \right) , \qquad (4.13)$$

while the condition that $V_{\rm T}$ is a solution to Laplace's equation gives

$$\frac{1}{\rho}(\rho\partial_{\rho}V_{\mathrm{T}}) + \partial_{\eta}^{2}V_{\mathrm{T}} = 0 \quad \Rightarrow \quad 2\left(u\partial_{u}\eta - t\partial_{t}\eta\right) - \left(t\partial_{u}K_{2} + u\partial_{t}K_{1}\right) = 0 \ . \tag{4.14}$$

By combining (4.13) and (4.14), we can solve for $\partial_t \eta$, $\partial_u \eta$ and find the simple relations

$$\partial_t \eta = \frac{1}{2} \frac{\partial K_2}{\partial u}$$
 and $\partial_u \eta = -\frac{1}{2} \frac{\partial K_1}{\partial t}$. (4.15)

We can use these to solve for the total $\eta(t, u)$ as

$$\eta(t,u) = \sigma\left(tu - \frac{(u_1 + u_2)t + (t_1 + t_2)u}{2}\right) + A. \tag{4.16}$$

where A is an integration constant.

Now that we have expressions for both ρ and η in the (t, u) coordinates, we can use (4.12) to find an expression for the potential in (t, u) coordinates. After rearranging we find

$$V_{\rm T}(t,u) = (\eta - A)\log(r_1 r_2) + t\left(\frac{u_1 + u_2}{2}\right) + u\left(\frac{t_1 + t_2}{2}\right)$$

$$-\frac{1}{2}\left(\frac{u_1 + u_2}{t_2 - t_1}\left(t_1^2\log(t_1 - t) - t_2^2\log(t_2 - t)\right)\right)$$

$$+\frac{t_1 + t_2}{u_2 - u_1}\left(u_1^2\log(u - u_1) - u_2^2\log(u_2 - u)\right) + V_0,$$

$$(4.17)$$

where V_0 is another integration constant. We have used the fact that, for all Cases I through V, in the interior of the allowed region in the (t, u) plane we have we have $0 < t < t_1 < t_2$ and $u_1 < u < u_2$.

Having determined the explicit change of coordinates from (ρ, η) to (t, u), for each Case I through V we can map the allowed region in the (t, u) plane to the allowed region in the (ρ, η) plane, up to a constant shift in η related to the integration constant A, see Figure 4. In particular, we observe that, in each case, the components of the boundary in the (t, u) plane where the ϕ circle in the base shrinks are mapped to segments along the η axis.

4.3 Electrostatic interpretation of Cases I and II

We now analyze the electrostatic interpretation of Case I. The interpretation for Case II follows by taking the limit $u_2 \to -u_1$, or equivalently $N_S \to 0$.

Charge density profile. The electrostatic potential $V_{\rm T}$ satisfies the Laplace equation for any $\rho > 0$, but there are localized electric sources on the η axis. We can find their charge density using the formula

$$\lambda_{\rm T} = \lim_{\rho \to 0} \rho \partial_{\rho} V_{\rm T}. \tag{4.18}$$

Firstly, we have the segments on the η axis that correspond to the edges $\mathbf{P}_3\mathbf{P}_4$ and $\mathbf{P}_2\mathbf{P}_3$ in Figure 1. For these segments we find

$$\lambda_{\mathrm{T}}(t) = u_2 t \; , \qquad \lambda_{\mathrm{T}}(u) = t_1 u \; , \tag{4.19}$$

respectively. The charge density is piecewise linear. At the monopole the charge density takes the form

$$\lambda_1 := \lambda_{\rm T}(\mathbf{P_4}) = t_1 u_2 = \frac{qKM}{K+M} \ .$$
 (4.20)

Using this and the expression (4.16) for η , we can write the charge density as a piecewise linear function in η ,

$$\lambda_{\mathrm{T}}(\eta) = \begin{cases} \frac{t_1}{t_2 - t_1} \left(-\frac{2}{\sigma} (\eta - A) - t_1 (u_1 + u_2) \right), & \tilde{\eta}_{\min} \leq (\eta - A) < \tilde{\eta}_1, \\ -\frac{u_2}{u_2 - u_1} \left(-\frac{2}{\sigma} (\eta - A) - u_2 (t_1 + t_2) \right), & \tilde{\eta}_1 \leq (\eta - A) < \tilde{\eta}_2. \end{cases}$$
(4.21)

We have defined the special η positions as

$$\tilde{\eta}_{\min} = -\frac{\sigma}{2}t_1(u_1 + u_2), \qquad \tilde{\eta}_1 = -\frac{\sigma}{2}(t_2u_2 + t_1u_1), \qquad \tilde{\eta}_2 = -\frac{\sigma}{2}u_2(t_1 + t_2).$$
 (4.22)

We find it convenient to fix the integration constant A to the value $A = -\tilde{\eta}_{\min}$, that is

$$A = -\frac{\sigma}{2}t_1(u_1 + u_2) \ . \tag{4.23}$$

With this choice, the linear charge density takes the form

$$\lambda_{\mathrm{T}}(\eta) = \begin{cases} \frac{\lambda_{1}}{\eta_{1}} \eta, & 0 \leq \eta < \eta_{1} ,\\ -\frac{\lambda_{1}}{\eta_{2} - \eta_{1}} (\eta - \eta_{2}) , & \eta_{1} \leq \eta < \eta_{2} , \end{cases}$$
(4.24)

where we have defined

$$\eta_1 = -\frac{\sigma}{2}u_2(t_2 - t_1) = M, \qquad \eta_2 = -\frac{\sigma}{2}(t_2u_2 - t_1u_1) = (K + M).$$
(4.25)

This charge density $\lambda(\eta)$ is depicted as a solid line in Figure 3.

Improved Form for V. The expression for $V_{\rm T}$ in (4.17) suffers from some drawbacks: it is not a closed form expression in the (ρ, η) coordinates, and it is only determined within the region in the (ρ, η) plane that corresponds to the allowed region in the (t, u) plane. The charge density profile $\lambda_{\rm T}(\eta)$ is thus similarly confined.

To fix these issues, we replace $V_{\rm T}$ with a new electrostatic potential V, defined throughout the entire (ρ, η) plane. We observe that V and $V_{\rm T}$ need not be identical: if they differ by a transformation of the form (4.7), they yield the same 11d metric and flux.

We write the new electrostatic potential V using the standard Green's function for the Laplace operator in \mathbb{R}^3 ,

$$V(\rho, \eta) = -\frac{1}{2} \int_{-\infty}^{+\infty} \frac{\lambda(\eta')}{\sqrt{\rho^2 + (\eta - \eta')^2}} d\eta' . \tag{4.26}$$

Notice that the charge density profile is now extended to be a function on the whole η axis. The new $\lambda(\eta)$ must necessarily agree with $\lambda_{\rm T}(\eta)$ computed above for values of η within the allowed region. Outside this region, we need an educated guess for the form of $\lambda(\eta)$.

With the benefit of hindsight, we choose $\lambda(t)$ to be the piecewise linear function

$$\lambda(\eta) = \begin{cases} -\frac{\lambda_2}{\eta_{-2} - \eta_{-1}} \left(\eta + \eta_{-2} \right), & -\eta_{-2} \leq \eta < -\eta_{-1}, \\ \frac{\lambda_1 + \lambda_2}{\eta_1 + \eta_{-1}} \left(\eta - \eta_1 + \frac{\eta_1 + \eta_{-1}}{\lambda_1 + \lambda_2} \lambda_1 \right), & -\eta_{-1} \leq \eta < \eta_1, \\ -\frac{\lambda_1}{\eta_2 - \eta_1} \left(\eta - \eta_2 \right), & \eta_1 \leq \eta < \eta_2. \end{cases}$$
(4.27)

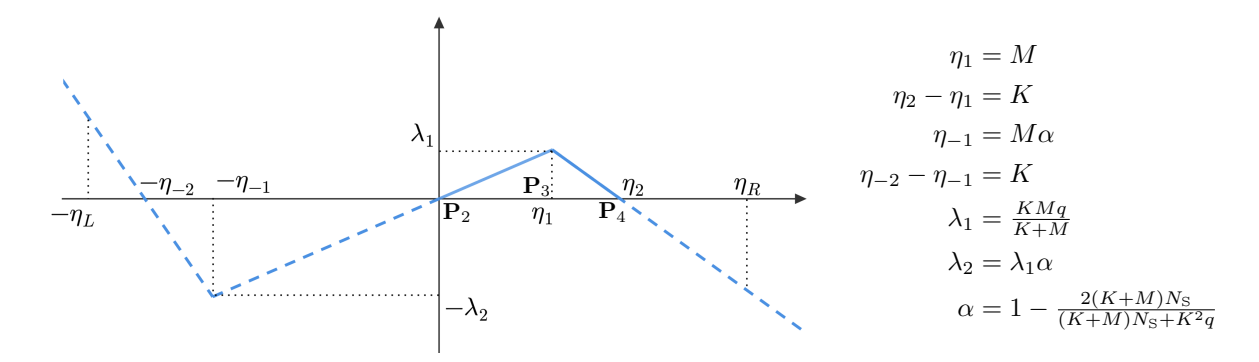


Figure 3: The extended charge density profile $\lambda(\eta)$ for Case I, featuring a "mirror monopole" located at $-\eta_{-1}$ paired with the known monopole located at η_1 . The labels $\mathbf{P}_2, \ldots, \mathbf{P}_4$ refer to Figure 1. The extended charge density for Case II can be obtained by considering the limit $N_{\rm S} \to 0$, which implies $\eta_{-1,-2} = \eta_{1,2}$, $\lambda_2 = \lambda_1$ and gives an odd function of η .

This charge density profile is depicted in Figure 3. It agrees with $\lambda_{\rm T}$ in (4.24) for $0 \le \eta \le \eta_2$. It extends $\lambda_{\rm T}$ including a second monopole, *i.e.* a location on the η axis where the slope changes. The extension is governed by the parameters η_{-2} , η_{-1} , λ_2 , which will be fixed below.

We may now insert $\lambda(\eta)$ from (4.27) into (4.26) to compute the improved electrostatic potential V. Due to the linear growth of λ as $\eta \to +\infty$ and $\eta \to -\infty$, the η' integral in (4.26) is divergent. We treat it by regularization and "minimal subtraction". More explicitly, we write

$$V = \lim_{\substack{\eta_L \to \infty \\ \eta_R \to \infty}} \left[\widehat{V}(\eta_L, \eta_R) + \frac{\lambda_2 [\eta_L - (\eta + \eta_{-2}) \log(2\eta_L)]}{2(\eta_{-2} - \eta_{-1})} - \frac{\lambda_1 [\eta_R + (\eta - \eta_2) \log(2\eta_R)]}{2(\eta_2 - \eta_1)} \right] . \quad (4.28)$$

In the previous expression, $\widehat{V}(\eta_L, \eta_R)$ is the same as V in (4.26), but with region of integration $[-\eta_L, \eta_R]$. We add two "counterterms" to $\widehat{V}(\eta_L, \eta_R)$ to remove all divergences. Notice that the counterterms are independent of ρ and at most linear in η , of the same form as the transformation (4.7).

Allowed regions. Now that we have an expression for $V(\rho, \eta)$ coming from our ansatz for the linear charge density $\lambda(\eta)$, we can look at the regularity conditions coming from the metric and find our allowed regions in the (ρ, η) plane. Looking at the 11d line element, we see that we must satisfy

$$\rho \ge 0 , \qquad \partial_{\rho} V \ge 0 , \qquad \partial_{\eta}^{2} V \ge 0.$$
(4.29)

These inequalities determine a region in the (ρ, η) plane, which depends on the unfixed parameters η_{-1} , η_{-2} , λ_2 in the extended charge density profile (4.27). On the other hand, we know what the allowed region in the (ρ, η) plane must be, since it can be deduced from the allowed region in the (t, u) plane using (4.11), (C.6). By comparison, we determine the unfixed

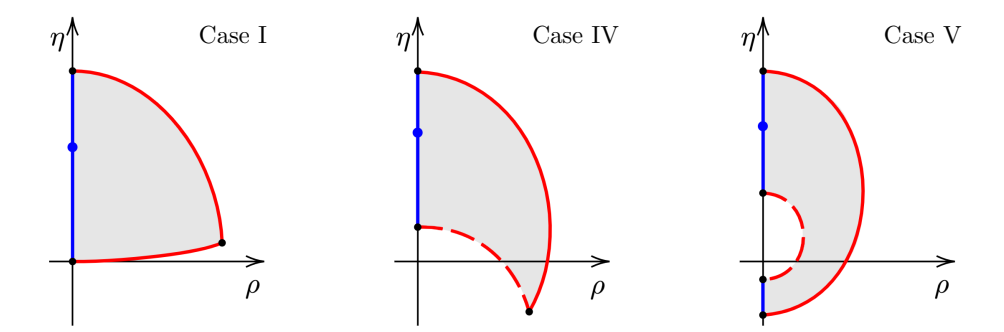


Figure 4: The allowed regions in the (ρ, η) plane for Cases I, IV, and V respectively. The solid red arcs signify the loci where $\partial_{\rho}V=0$, while the dashed red lines represent the loci where $\partial_{\eta}^2 V = 0$. The similarity with Figures 1, 2 is intentional, as the solid and dashed lines in each figure correspond to one another. As the combination $t_1u_2 - u_1t_2$ goes from positive to negative, we transition from Case V to Case III. The red dashed arc of Case V shrinks and is replaced by the second monopole present in Case III.

parameters to be

$$\eta_{-1} = \frac{\sigma}{2} u_1(t_2 - t_1) , \qquad \eta_{-2} = \frac{\sigma}{2} (t_2 u_1 - t_1 u_2) , \qquad \lambda_2 = -t_1 u_1 ,$$
(4.30)

The allowed region can be seen in Figure 4.

Electrostatic interpretation of Case III and beyond

Case III. Case III can be studied in an analogous way. Compared to Case I, we also have the edge $\mathbf{P}_1\mathbf{P}_2$ with charge density

$$\lambda_{\mathrm{T}}(t) = u_1 t,\tag{4.31}$$

with another monopole at P_2 such that

$$\lambda_2 := \lambda_{\mathrm{T}}(\mathbf{P}_2) = t_1 u_1 = \frac{K(Mq_2 + K(q_1 + q_2))}{M + 2K}.$$
 (4.32)

The charge density, after fixing A as in (4.23), reads

$$\lambda_{\rm T}(\eta) = \begin{cases}
\frac{\lambda_2}{\eta_0 - \eta_{\rm min}} (\eta - \eta_{\rm min}), & \eta_{\rm min} \leq \eta < \eta_0, \\
\frac{\lambda_1}{\eta_1} \eta, & \eta_0 \leq \eta < \eta_1, \\
-\frac{\lambda_1}{\eta_2 - \eta_1} (\eta - \eta_2), & \eta_1 \leq \eta < \eta_2,
\end{cases} (4.33)$$

where the η_i are given as

$$\eta_{\min} = \frac{q_2(M+2K)}{q_1 - q_2} , \qquad \eta_0 = \frac{Mq_2 + K(q_1 + q_2)}{q_1 - q_2} , \qquad (4.34)$$

$$\eta_1 = \frac{Mq_1 + K(q_1 + q_2)}{q_1 - q_2} , \qquad \eta_2 = \frac{q_1(M+2K)}{q_1 - q_2} . \qquad (4.35)$$

$$\eta_1 = \frac{Mq_1 + K(q_1 + q_2)}{q_1 - q_2}, \qquad \eta_2 = \frac{q_1(M + 2K)}{q_1 - q_2}.$$
(4.35)

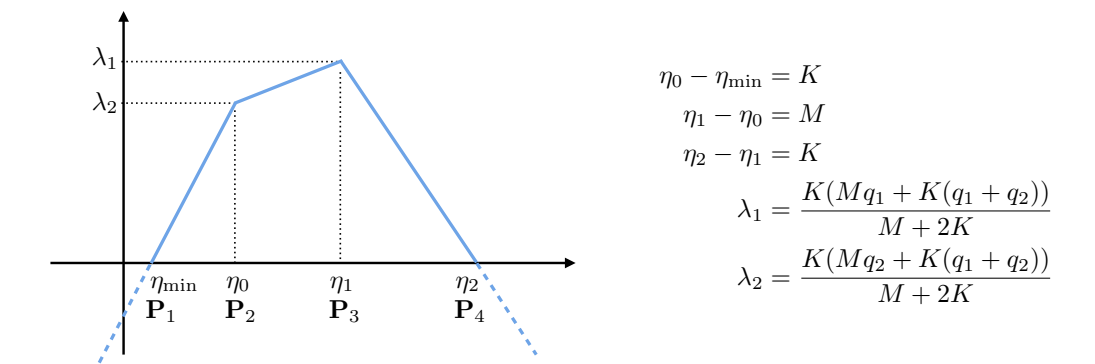


Figure 5: The extended charge density profile $\lambda(\eta)$ for Case III. We notice the absence of "mirror monopoles": the charge density outside the interval $[\eta_{\min}, \eta_2]$ is obtained by prolonging the outermost segments in a trivial way. The labels $\mathbf{P}_1, \ldots, \mathbf{P}_4$ refer to Figure 1.

The profile $\lambda_{\rm T}$ is depicted in Figure 5 as a solid line.

As before, we seek an extension of $\lambda_{\rm T}$ to the entire η axis, in such a way as to reproduce the allowed region in the (ρ, η) plane as determined via the Bäcklund transform. The outcome of this analysis is that, in contrast with Case I, the extended charge density profile in Case III does not feature any "mirror monopole": the profile $\lambda_{\rm T}$ is extended to the whole η axis by simply extending the outermost linear pieces with constant slopes.

Cases IV and V. These cases can be studied in a similar fashion. Overall, we observe that for all Cases I through V the extended charge density profile has exactly two monopoles. We refrain from giving explicit expressions for Cases IV and V, but we depict the allowed regions in the (ρ, η) plane in Figure 4.

5 More monopoles

In the previous section, we have identified the extended charge density profiles associated to Cases I through V. This allows us to consider natural generalizations of these solutions, obtained by decorating the extended charge density profiles with additional monopoles. The explicit expression for the electrostatic potentials sourced by these multi-monopole charge densities are reported in appendix B.

In this section we study in detail generalizations of Case II, for which the charge density profile is an odd function of η . The solutions discussed here will be identified in section 6 as gravity duals of class \mathcal{S} constructions with one irregular puncture, and one regular puncture associated to a Young diagram of arbitrary shape.

5.1 Charge density profile

The sought-for generalizations of Case II solutions are all of the form (4.9). They are specified by a choice of the positive constant C, and a choice of electrostatic potential V. The latter

can in turn be written in terms of the standard Green's function on \mathbb{R}^3 and a charge density profile $\lambda(\eta)$ along the η axis, see (4.26), repeated here for convenience,

$$V(\rho, \eta) = -\frac{1}{2} \int_{-\infty}^{+\infty} \frac{\lambda(\eta')}{\sqrt{\rho^2 + (\eta - \eta')^2}} d\eta' . \tag{5.1}$$

Notice that the charge density $\lambda(\eta)$ is defined along the entire η axis. The actual physical range of the coordinate η is determined by the regularity and positivity of the metric functions.

The total charge density profile λ that enters in (5.1) is conveniently written as the sum of two contributions, see Figure 6,

$$\lambda(\eta) = \lambda_{\text{reg}}^{Y}(\eta) + \lambda_{\text{irreg}}^{(N,k)}(\eta) . \tag{5.2}$$

In the first term, Y denotes the Young diagram associated to the partition

$$N = \sum_{a=1}^{p} k_a w_a , (5.3)$$

in which $p \ge 1$ is an integer, $\{w_a\}_{a=1}^p$ is an increasing sequence of positive integers, and k_a are positive integers. The function $\lambda_{\text{reg}}^Y(\eta)$ is continuous and piecewise linear. It is also assumed to be odd in η ,

$$\lambda_{\text{reg}}^{Y}(-\eta) = -\lambda_{\text{reg}}^{Y}(\eta) . \tag{5.4}$$

It is sufficient to specify $\lambda_{\text{reg}}^{Y}(\eta)$ for $\eta \geq 0$: it is given as

$$\lambda_{\text{reg}}^{Y}(\eta) = \begin{cases}
\eta \sum_{b=1}^{p} k_{b} & \text{for } 0 \leq \eta < w_{1}, \\
\eta \sum_{b=a+1}^{p} k_{b} + \sum_{b=1}^{a} w_{b} k_{b} & \text{for } w_{a} \leq \eta < w_{a+1}, \quad a = 1, 2, \dots, p-1, \\
N & \text{for } \eta \geq w_{p}.
\end{cases} (5.5)$$

The profile $\lambda_{\text{reg}}^{Y}(\eta)$ is exactly the same charge density profile that enters the AdS_5 solutions that describe the local geometry near a regular puncture [13], hence the label "reg".

The second term $\lambda_{\text{irreg}}^{(N,k)}(\eta)$ in (5.2) is determined by two integer parameters N and k, where N is the same as in the partition (5.3), and k satisfies

$$k > w_p - N (5.6)$$

The quantity $\lambda_{\mathrm{irreg}}^{(N,k)}(\eta)$ is a simple linear function of $\eta,$

$$\lambda_{\text{irreg}}^{(N,k)}(\eta) = -\frac{N}{k+N} \eta . \tag{5.7}$$

The label "irreg" is motivated by the analysis of section 6, which shows that $\lambda_{\text{irreg}}^{(N,k)}(\eta)$ is naturally associated to the irregular puncture in the dual class S field theory construction.

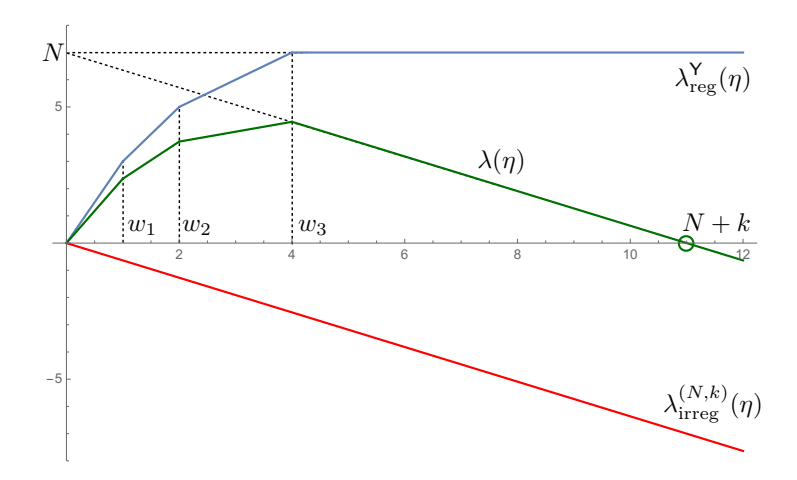


Figure 6: The total charge density $\lambda(\eta)$ can be written as the sum of the contributions $\lambda_{\text{reg}}^{Y}(\eta)$ and $\lambda_{\text{irreg}}^{(N,k)}(\eta)$. Both $\lambda_{\text{reg}}^{Y}(\eta)$ and $\lambda_{\text{irreg}}^{(N,k)}(\eta)$ are odd functions of η . The plot depicts $\lambda(\eta)$, $\lambda_{\text{reg}}^{Y}(\eta)$, and $\lambda_{\text{irreg}}^{(N,k)}(\eta)$ on the semiaxis $\eta \geq 0$ in the case N=7, p=3, $w_1=1$, $w_2=2$, $w_3=4$, $k_1=k_2=k_3=1$, N+k=11.

Notice that, due to the linear growth of $\lambda_{\text{irreg}}^{(N,k)}(\eta)$ as $|\eta| \to \infty$, the formula (5.1) for the electrostatic potential V is formally divergent. These divergences are treated by regularizing the η' integral with a cutoff λ_{max} , and performing a "minimal subtraction" of divergent terms. We refer the reader to appendix B for further details, and for the explicit expression for V.

Finally, the positive constant C is also determined by the parameters N, k,

$$C = \frac{N+k}{N} \ . \tag{5.8}$$

Having prescribed C and $\lambda(\eta)$, we have fully specified the solution. For p=1 we recover precisely the electrostatic description of the solutions in Case II.

Notice that we have not justified the form (5.2) of the charge density or the value of C. We refer the reader to appendix C for a detailed analysis of the problem, which demonstrates that (5.2) and (5.8) can be inferred from metric regularity and flux quantization.

5.2 Geometry of the solutions

Allowed region in the (ρ, η) plane. Since we have chosen an odd profile for $\lambda(\eta)$, the electrostatic potential satisfies

$$V(\rho, -\eta) = -V(\rho, \eta) . \tag{5.9}$$

In particular $V(\rho, 0) = 0$, signaling the presence of a conducting plane at $\eta = 0$. The radius of the S^2 shrinks there. As a result, we restrict to $\eta \ge 0$.

Using the explicit expressions of the metric functions that can be obtained using (4.10), we verify that all positivity requirements are satisfied, provided that we consider the region

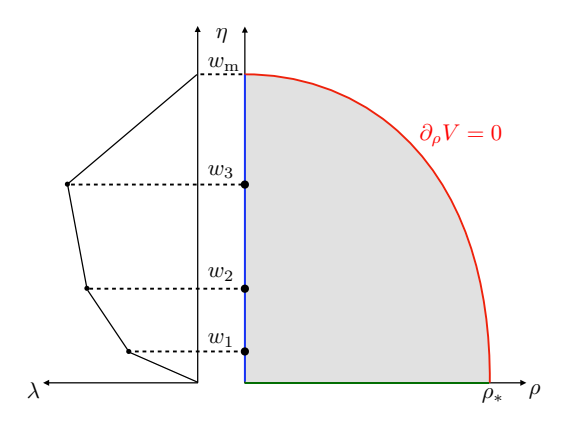


Figure 7: A schematic depiction of the allowed region in the (ρ, η) plane, for a case with p = 3 monopoles along the η axis. The arc connecting $w_{\rm m}$ and ρ_* corresponds to $\partial_{\rho}V = 0$ and is defined by the equation (5.11). On the right, we also include the plot of the charge density $\lambda(\eta)$ on the interval $[0, w_{\rm m}]$.

in the (ρ, η) plane determined by the conditions

$$\rho \ge 0 , \qquad \eta \ge 0 , \qquad \partial_{\rho} V \ge 0 .$$
(5.10)

This domain is depicted in Figure 7. The curve $\partial_{\rho}V = 0$ is given more explicitly as

$$-\frac{2\eta}{\mathcal{C}} + \sum_{a=1}^{p} k_a \left(\sqrt{(\eta + w_a)^2 + \rho^2} - \sqrt{(\eta - w_a)^2 + \rho^2} \right) = 0.$$
 (5.11)

One can verify that this curve intersects the η axis at

$$w_{\rm m} = N + k \tag{5.12}$$

which is precisely the location of the positive zero of the function $\lambda(\eta)$, see Figure 6. The curve (5.11) intersects the ρ axis at a point ρ_* , where ρ_* is the positive solution to the equation

$$\sum_{a=1}^{p} \frac{k_a w_a}{\sqrt{\rho_*^2 + w_a^2}} = \frac{1}{\mathcal{C}} . \tag{5.13}$$

We also observe that, in the case p=1, the equation (5.11) can be equivalently written as

$$\frac{\rho^2}{w_1^2 (k_1^2 \mathcal{C}^2 - 1)} + \frac{\eta^2}{k_1^2 w_1^2 \mathcal{C}^2} = 1 , \qquad (5.14)$$

which describes an ellipse in the (ρ, η) plane. For $p \geq 2$, this is no longer the case, but the locus $\partial_{\rho}V = 0$ has the same qualitative shape as for p = 1.

Geometry of the internal space. The internal space M_6 can be regarded as an $S^2 \times S_z^1$ fibration over the 3d space spanned by ρ , η , ϕ . The radius of the ϕ circle in the 3d base goes to zero smoothly along the η axis.

The size of the S^2 depends on ρ , η , but it is not twisted over the 3d base. In contrast, the z circle is twisted over the ϕ circle, as prescribed by the metric function L in (4.10). In particular, L is piecewise constant along the η axis, with jumps at the locations $\eta = w_a$ where the slope of the charge density λ changes. It follows that the points (ρ, w_a) are monopole sources for the Dz fibration over (ρ, η, ϕ) . Notice that the radius of Dz goes to zero at the monopole points.

Behavior near the boundary of the allowed region. The boundary of the allowed region depicted in Figure 7 consists of several components, which we discuss in turn.

As mentioned above, along the segment $[0, \rho_*]$ on ρ axis the S^2 shrinks smoothly, and caps off the internal space. This is the green horizontal line in Figure 7.

Let us now consider the segment $[w_a, w_{a+1}]$ (a = 0, 1, ..., p-1) along the η axis. Here a combination of the S_z^1 and S_ϕ^1 circles shrinks smoothly. More precisely, the following linear combination of ∂_z , ∂_ϕ ,

$$\partial_{\phi} + \sum_{b=a+1}^{p} k_b \, \partial_z \,\,, \tag{5.15}$$

has vanishing norm as we approach the $[w_a, w_{a+1}]$ segment. By a similar token, it is the Killing vector ∂_{ϕ} that has vanishing norm along the $[w_p, w_{\rm m}]$ segment. We have thus accounted for the whole vertical blue line in Figure 7.

Finally, we have to discuss the arc $\partial_{\rho}V=0$, depicted in red in Figure 7. As shown in appendix C, this locus corresponds to an M5-brane source, of total charge N, which is extended along AdS_5 and z, smeared along ϕ and the $\partial_{\rho}V=0$ arc in the (ρ,η) plane, and localized in the remaining directions.

5.3 Holographic central charge

The general formula (3.11) is easily specialized to solutions of the form (4.9). It reads

$$c = \frac{1}{128 (\pi m^3 \ell_p^3)^3} \int_{\mathcal{B}_2} \rho \, \dot{V} \, V'' \, d\rho \, d\eta \,\,, \tag{5.16}$$

where we have reinstated the mass scale m and \mathcal{B}_2 denotes the allowed region for the ρ , η coordinates, determined by the conditions (5.10). To proceed, we observe that

$$\rho \dot{V} V'' = \partial_{\rho} \left[-\frac{1}{2} \rho^{2} (\partial_{\rho} V)^{2} \right] + \rho \left(\rho \partial_{\rho} V \right) \left[\partial_{\eta}^{2} V + \frac{1}{\rho} \partial_{\rho} (\rho \partial_{\rho} V) \right]. \tag{5.17}$$

We argue that the second term can be dropped. We know that the combination $\partial_{\eta}^2 V + \frac{1}{\rho} \partial_{\rho} (\rho \partial_{\rho} V)$ is zero, except for terms localized on the η axis. The quantity $\rho \partial_{\rho} V$ is finite as we approach the η axis: it is given by the charge density $\lambda(\eta)$. Because of the extra ρ factor in front, we conclude that this term drops away in the limit ρ going to zero.

The quantity of interest can then be cast as

$$\int_{\mathcal{B}_2} \partial_{\rho} \left[-\frac{1}{2} \rho^2 (\partial_{\rho} V)^2 \right] d\rho \, d\eta = \int_{\mathcal{B}_2} d \left[-\frac{1}{2} \rho^2 (\partial_{\rho} V)^2 \, d\eta \right] = \int_{\partial \mathcal{B}_2} \left[-\frac{1}{2} (\rho \, \partial_{\rho} V)^2 \, d\eta \right]. \tag{5.18}$$

Recall that $\partial \mathcal{B}_2$ consists of three components: the segment $[0, \rho_*]$ along the ρ axis, the arc defined by the equation $\partial_{\rho}V = 0$, and the segment $[0, w_{\rm m}]$ along the η axis. The 1-form $-\frac{1}{2} (\rho \partial_{\rho} V)^2 d\eta$ vanishes along the ρ axis (because it only has a leg along η), and it also vanishes along the arc where $\partial_{\rho}V = 0$. It follows that the only non-trivial contribution originates from the integral over the segment $[0, w_{\rm m}]$ along the η axis. Along this segment, we can make the replacement $\rho \partial_{\rho}V \to \lambda$. In conclusion, collecting all factors, the holographic central charge can be written as

$$c = \frac{1}{256 (\pi m^3 \ell_p^3)^3} \int_0^{w_{\rm m}} \lambda(\eta)^2 d\eta = \frac{1}{4} \int_0^{w_{\rm m}} \lambda(\eta)^2 d\eta .$$
 (5.19)

In the second step we have fixed the value of the mass scale m according to (2.7).

The integral in (5.19) is readily evaluated making use of the expression (5.2) for the charge density. Let us introduce the notation

$$y_a = \sum_{b=1}^{a} w_b k_b$$
, $m_a = -\frac{N}{N+k} + \sum_{b=a+1}^{p} k_b$, $a = 0, 1, \dots, p$. (5.20)

For a = p, the sum in the second expression is understood to be zero. We also use the convention $w_0 := 0$. We may then write

$$c = \frac{1}{4} \sum_{a=0}^{p} \left[\frac{1}{3} m_a^2 (w_{a+1}^3 - w_a^3) + m_a y_a (w_{a+1}^2 - w_a^2) + y_a^2 (w_{a+1} - w_a) \right].$$
 (5.21)

We can also write c directly in terms of k and the partition $N = \sum_{a=1}^{p} k_a w_a$,

$$c = \frac{1}{12}(N+k)N^2 + \frac{1}{12}\frac{N}{N+k}\sum_{a=1}^{p}k_a w_a^3 - \frac{1}{6}\sum_{a=1}^{p}k_a^2 w_a^3 - \frac{1}{12}\sum_{a=1}^{p}\sum_{b=a+1}^{p}(w_a^3 + 3w_a w_b^2)k_a k_b.$$
(5.22)

5.4 't Hooft anomalies from inflow

The inflow methods of [34] (based on [35, 36]) provide a systematic way of extracting 't Hooft anomalies from a holographic solution in 11d supergravity. The key ingredient in this approach is the construction of the 4-form E_4 , which is the closed equivariant completion of the background flux \overline{G}_4 in (4.9). We refer the reader to appendix C for a discussion of E_4 and the derivation of the inflow anomaly polynomial. The results of our analysis are as follows.

Symmetries from isometries. Even though the geometry possesses two U(1) isometries, generated by ∂_z and ∂_{ϕ} , only one linear combination of these Killing vectors yields a massless U(1) gauge field in the 5d low-energy effective theory that describes 11d supergravity reduced on M_6 . The other linear combination of putative massless U(1) gauge fields gets massive by a Stückelberg mechanism: it "eats" an axionic scalar, which comes from the expansion of the M-theory 3-form onto a cohomologically non-trivial closed 3-form in M_6 . In terms of the angular variables χ , β in the canonical LLM form, the linear combination of Killing vectors that yields a massless U(1) gauge field is simply ∂_{χ} . This is to be expected, since this isometry corresponds to the superconformal $U(1)_r$ symmetry. Using (4.8), we can also write

$$\partial_{\chi} = \partial_{\phi} + \frac{1}{\mathcal{C}} \, \partial_{z} = \partial_{\phi} + \frac{N}{N+k} \, \partial_{z} \, . \tag{5.23}$$

To summarize, the relevant isometries on M_6 that correspond to massless 5d gauge fields are $U(1)_{\chi}$, and the SO(3) isometry of the S^2 . Let $c_1(U(1)_{\chi})$, $p_1(SO(3))$ denote the first Chern class and the first Pontryagin class constructed in terms of these massless gauge fields. These quantities are identified on the field theory side with the Chern classes $c_1^r := c_1(U(1)_r)$ and $c_2^R := c_2(SU(2)_R)$ constructed with the background fields for the $U(1)_r \times SU(2)_R$ R-symmetry. More precisely, we have the relations

$$c_1(U(1)_{\chi}) = -2c_1^r, \qquad p_1(SO(3)) = -4c_2^R.$$
 (5.24)

Orbifold points and flavor symmetries. From the expressions recorded in (4.9), (4.10), we verify that the monopole locations $(\rho, \eta) = (0, w_a)$, $a = 1, \ldots, p$ are orbifold points for the internal space geometry M_6 , More precisely, near the ath monopole location $(\rho, \eta) = (0, w_a)$, the internal space M_6 is locally given as $S^2 \times (\mathbb{R}^4/\mathbb{Z}_{k_a})$, where $k_a \in \mathbb{Z}_{>0}$ is the charge of the ath monopole. Following the same logic as in [13], we conclude that these orbifold points correspond holographically to non-Abelian summands $\mathfrak{su}(k_a)$ in the global 0-form symmetry algebra. Accordingly, in our inflow analysis we introduce background gauge fields for these symmetries. We use $c_2(SU(k_a))$ for the second Chern class constructed with these background fields.

Inflow anomaly polynomial. The anomaly inflow analysis in appendix C yields the following expression for the leading terms in the inflow anomaly polynomial at large N,

$$-I_6^{\text{inflow}} = \mathcal{A}_{r,R} c_1^r c_2^R + \sum_{a=1}^p k_{SU(k_a)} c_1^r c_2(SU(k_a)) . \tag{5.25}$$

The 't Hooft anomaly coefficient $A_{r,R}$ is given as

$$\mathcal{A}_{r,R} = \sum_{a=0}^{p} \left[\frac{2}{3} m_a^2 (w_{a+1}^3 - w_a^3) + m_a y_a (w_{a+1}^2 - w_a^2) \right], \qquad (5.26)$$

where m_a , y_a are as in (5.20). One can verify that

$$\mathcal{A}_{r,R} = -4c , \qquad (5.27)$$

where c is given by (5.22). This identification is the expected 4d $\mathcal{N}=2$ SCFT relation that holds at large N between the central charges a=c and the mixed $U(1)_r SU(2)_R$ anomaly. It provides a consistency check of the result (5.22) for the holographic central charge.

More interestingly, the inflow analysis provides the following values for the flavor central charges of the $SU(k_a)$ symmetries,

$$k_{SU(k_a)} = 2(y_a + m_a w_a), (5.28)$$

with m_a , y_a defined in (5.20).

5.5 Operators from wrapped M2-branes

The expression of the calibration 2-form Y' in terms of the electrostatic potential V is

$$Y' = 2 \left[\frac{V'' \dot{V}}{2 \widetilde{\Delta}} \right]^{3/2} \operatorname{vol}_{S^{2}} + \sqrt{\frac{V''}{2 \dot{V} \widetilde{\Delta}}} \frac{(\dot{V}')^{2} + \rho^{2} (V'')^{2}}{(\dot{V}')^{2} - \ddot{V} V''} \tau Dz d\eta$$

$$+ \sqrt{\frac{V''}{2 \dot{V} \widetilde{\Delta}}} \frac{(\Delta V) \dot{V}' \rho}{(\dot{V}')^{2} - \ddot{V} V''} \tau Dz d\rho + \sqrt{\frac{V''}{2 \dot{V} \widetilde{\Delta}}} \frac{\dot{V} \dot{V}'}{\widetilde{\Delta}} Dz d\tau - \sqrt{\frac{V''}{2 \dot{V} \widetilde{\Delta}}} \frac{\dot{V} \ddot{V}}{2 \dot{V} - \ddot{V}} d\tau d\phi$$

$$- \sqrt{\frac{V''}{2 \dot{V} \widetilde{\Delta}}} \frac{\dot{V}' (\ddot{V} \widetilde{\Delta} + 2 \rho^{2} \dot{V} (V'')^{2})}{(2 \dot{V} - \ddot{V}) ((\dot{V}')^{2} - \ddot{V} V'')} \tau d\eta d\phi - \sqrt{\frac{V''}{2 \dot{V} \widetilde{\Delta}}} \frac{\ddot{V}^{2} \widetilde{\Delta} + 2 \dot{V} (\dot{V}')^{2} V'' \rho^{2}}{(2 \dot{V} - \ddot{V}) ((\dot{V}')^{2} - \ddot{V} V'')} \rho^{2} \tau d\rho d\phi .$$
(5.29)

In the previous expression, we have used the shorthand notation

$$\Delta V = V'' + \frac{1}{\rho^2} \ddot{V} , \qquad (5.30)$$

and we have used the coordinates τ , φ on S^2 as in (3.15).

M2-branes located at monopoles. Let us consider an M2-brane wrapping the S^2 and located at one of the monopole points, $\rho = 0$, $\eta = w_a$. The relevant terms in the calibration 2-form Y' and the 6d line element are

$$Y' \supset 2 \left[\frac{V'' \dot{V}}{2 \, \widetilde{\Delta}} \right]^{3/2} \text{vol}_{S^2} , \qquad ds^2(M_6) \supset \frac{V'' \dot{V}}{2 \, \widetilde{\Delta}} ds_{S^2}^2 .$$
 (5.31)

In order to verify the calibration condition, we have to evaluate the limit of the quantity $\frac{V''\dot{V}}{2\tilde{\Delta}}$ as we approach the monopole location. This can be done by setting

$$\rho = R\sqrt{1 - t^2} \;, \qquad \eta = w_a + Rt \;, \tag{5.32}$$

and considering the limit $R \to 0$ at fixed t. With this prescription, we find that

$$\dot{V} = \sum_{b=1}^{a-1} k_b w_b + w_a \sum_{b=a}^{p} k_b - \frac{N}{N+k} w_a + \mathcal{O}(R) ,$$

$$\ddot{V} = 0 + \mathcal{O}(R) , \quad V'' = \mathcal{O}(1/R) ,$$

$$\dot{V}' = \text{finite but } t\text{-dependent quantity} + \mathcal{O}(R) .$$
(5.33)

Because of the 1/R pole in V'', near the ath monopole we can write

$$\frac{V''\dot{V}}{2\tilde{\Delta}} = \frac{V''\dot{V}}{2(2\dot{V} - \ddot{V})V'' + 2(\dot{V}')^2} = \frac{1}{4} + \mathcal{O}(R) . \tag{5.34}$$

Notice how the finite value of \dot{V} drops from the result. The calibration condition is then satisfied by virtue of $2\left(\frac{1}{4}\right)^{3/2} = \frac{1}{4}$. Let us denote the BPS operator associated to an M2-brane located at $\eta = w_a$ as \mathcal{O}_a .

The dimension of wrapped M2-brane operators is computed with the formula (3.18), which in the present context takes the form (temporarily reinstating the mass scale m)

$$\Delta = \frac{1}{\pi \left(4\pi m^3 \ell_p^3\right)} \int_{\mathcal{C}_2} \left[\frac{\dot{V} \,\widetilde{\Delta}}{2 \, V''}\right]^{1/2} \operatorname{vol}_{\mathcal{C}_2} . \tag{5.35}$$

Let us specialize to the operators \mathcal{O}_a defined above. We have

$$\operatorname{vol}_{\mathcal{C}_2} = \frac{V''\dot{V}}{2\widetilde{\Delta}} \bigg|_{(\rho,\eta)=(0,\eta_a)} \operatorname{vol}_{S^2} . \tag{5.36}$$

The dimension of the operator \mathcal{O}_a is then given by $(\text{vol}_{S^2} \text{ gives a factor } 4\pi)$

$$\Delta(\mathcal{O}_a) = \frac{1}{(4\pi m^3 \ell_p^3)} \cdot 4 \left[\frac{\dot{V} \widetilde{\Delta}}{2 V''} \right]^{1/2} \frac{V'' \dot{V}}{2 \widetilde{\Delta}} \bigg|_{(\rho,\eta)=(0,\eta_a)} . \tag{5.37}$$

We have already observed that $\frac{V''\dot{V}}{2\tilde{\Delta}}$ approaches 1/4, for all monopoles. Near the ath monopole, we also have

$$\frac{\dot{V}\,\widetilde{\Delta}}{2\,V''} = \frac{\dot{V}\,(2\,\dot{V} - \ddot{V})\,V'' + \dot{V}\,(\dot{V}')^2}{2\,V''} = \dot{V}^2 + \mathcal{O}(R) \ . \tag{5.38}$$

In conclusion, making use of (5.33) for the value of \dot{V} , we arrive at

$$\Delta(\mathcal{O}_a) = \sum_{b=1}^{a-1} k_b \, w_b + w_a \sum_{b=a}^{p} k_b - \frac{N}{N+k} \, w_a \ . \tag{5.39}$$

M2-branes stretching along the interval $[w_p, w_m]$. These M2-branes wrap the 2d submanifold obtained by considering the final segment $[w_p, w_m]$ combined with the Dz circle. Notice that this 2d submanifold is not closed: we are considering open M2-branes, which end on the smeared M5-brane source. The relevant terms in Y' are

$$Y' \supset \sqrt{\frac{V''}{2 \dot{V} \widetilde{\Delta}}} \frac{(\dot{V}')^2 + \rho^2 (V'')^2}{(\dot{V}')^2 - \ddot{V} V''} \tau Dz d\eta . \tag{5.40}$$

This quantity has to be evaluated in the limit $\rho \to 0$, for a generic η with $w_p < \eta < w_{\rm m}$. In this limit, \dot{V} is finite (it is given by the charge density), $\dot{V}' \to -N/(N+k)$ (independent of $w_p < \eta < w_{\rm m}$), \ddot{V} goes to zero, V'' is finite. It follows that

$$\frac{(\dot{V}')^2 + \rho^2 (V'')^2}{(\dot{V}')^2 - \ddot{V} V''} \to 1 . \tag{5.41}$$

The relevant parts of the M_6 line element are

$$ds^{2}(M_{6}) \supset \frac{V''}{2\dot{V}} d\eta^{2} + \frac{2\dot{V} - \ddot{V}}{2\dot{V}\tilde{\Delta}} Dz^{2},$$
 (5.42)

which implies

$$\operatorname{vol}_{\mathcal{B}_{2}} = \frac{1}{2\dot{V}} \sqrt{\frac{V''(2\dot{V} - \ddot{V})}{\widetilde{\Delta}}} \, d\eta \, Dz = \sqrt{\frac{V''}{2\dot{V}\,\widetilde{\Delta}}} \, d\eta \, Dz \,, \tag{5.43}$$

where in the second step we used the fact that \ddot{V} vanishes as ρ goes to zero. Comparing with Y', we see that the calibration condition is satisfied for $\tau = -1$. We denote the BPS operators associated to these wrapped M2-branes as $\mathcal{O}_{[w_p,w_{\rm m}]}$.

The dimension of these operators is computed from (5.35), The result reads

$$\Delta(\mathcal{O}_{[w_p, w_{\rm m}]}) = \frac{1}{\pi (4\pi m^3 \ell_p^3)} \int_{\mathcal{B}_2} \frac{1}{2} d\eta \, Dz = \frac{1}{(4\pi m^3 \ell_p^3)} \int_{[w_p, w_{\rm m}]} d\eta = N + k - w_p \; . \tag{5.44}$$

M2-branes stretching along the intervals $[w_a, w_{a+1}]$. The discussion above generalizes directly to M2-branes that wrap an interval $[w_a, w_{a+1}]$ combined with the Dz circle on that interval. In this case, this 2d submanifold is closed. The calibration condition holds for the same reason as in the $[w_p, w_{\rm m}]$ case: \ddot{V} goes to zero, with finite \dot{V} , \dot{V}' , V''. The dimensions of these operators are again computed from (5.35), with the result

$$\Delta(\mathcal{O}_{[w_a, w_{a+1}]}) = w_{a+1} - w_a . (5.45)$$

6 Comparison with field theory

In this section, we present evidence that the supergravity solutions presented in section 5 are dual to the four-dimensional $\mathcal{N}=2$ Argyres-Douglas SCFTs that arise from wrapping N M5-branes on a sphere with one irregular puncture labeled by k, and one regular puncture labeled by a partition of N. In particular, we identify Case II with the generalized monopole profiles constructed in section 5 with the Argyres-Douglas SCFTs labeled by an irregular puncture $A_{N-1}^{(N)}[k]$, for integer k > -N, and one regular puncture labeled by a partition of N. This proposal is checked in detail in the remainder of this section. It also matches the proposal of [16].

It is natural to propose that Cases I and III also correspond to SCFTs of this type, with an irregular puncture with possibly more finely-grained structure, and one regular puncture labeled by a partition of N. Indeed, the three solutions share key features, as we briefly summarize below. In order to simplify this discussion, let us temporarily restrict the regular puncture to be labeled by a single monopole of charge q. By inspection of Table 1, we then observe the following:

• In all cases, an integer N_{eff} may be identified which plays the role of an effective number of M5-branes; and an integer \widetilde{M} may be identified which plays a similar role to the integer M in the Case II solution.

- In terms of N_{eff} , \widetilde{M} , and the other fluxes, we observe that the R-symmetry twist, dimension of the Coulomb branch operator \mathcal{O}_1 , and dimensions of the Higgs branch operators \mathcal{O}_2^i are identical between the three cases.
- Case I and Case II share more features. Case I represents a one-parameter generalization of the Case II solution labeled by the flux quantum $N_{\rm S}$, and which reproduces the Case II geometry when $N_{\rm S} \to 0$. In terms of the effective number of branes $N_{\rm eff}$, the holographic central charge is identical in these two cases. The difference lies in the additional stack of smeared M5-branes labeled by $N_{\rm S}$, and additional associated Higgs branch operators \mathcal{O}_3^j . At the end of this section, we speculate on a possible field theory interpretation of these features.
- By contrast, Case III is evidently not continuously connected to the other two by tuning flux quanta. At present we refrain from further speculation as to the specific field theory dual of Case III, but point out some intriguing features. The central charge differs from that of Cases I and II by a term proportional to the new monopole charge q_2 , and there are new operators in the spectrum. Furthermore, the two monopole charges $q_{1,2}$ are mixed by the relation $N_{\text{eff}} = q_1 \widetilde{M} + q_2 K$. It would be interesting to understand the mapping of these features to the field theory dual.

We now return to the proposed Case II duality, beginning with a summary of the partition of N labeling the regular puncture is mapped to the electrostatic charge profile.

6.1 Map to the Young tableaux

As discussed in section 5, the geometry of the blue sides of the square depicted in Figure 1 is specified by a charge density profile $\lambda(\eta)$. We now summarize the relationship between the profile $\lambda(\eta)$ and the data of a Young tableaux specifying a regular puncture in this region of the geometry. Our notation for this mapping closely follows the discussion in [33].

There are p monopoles located on the η axis at locations $\eta_{a=1,\dots,p}$, with positive integer charges k_a given by

$$k_a = \ell_a - \ell_{a+1} , \qquad \ell_a = \sum_{b=a}^p k_b , \qquad \ell_{p+1} = 0 .$$
 (6.1)

The configuration is labeled by a partition of N,

$$N = \sum_{a=1}^{p} k_a w_a , (6.2)$$

where w_a are an increasing series of positive integers. (We remind the reader that k without a subscript labels the irregular puncture, and is not to be confused with the monopole charges k_a !) This data is related to the data of a Young tableaux as follows. Rewriting the partition

of N as

$$N = \sum_{a=1}^{p} (w_a - w_{a-1})\ell_a , \qquad w_0 = 0 , \qquad (6.3)$$

we identify a corresponding Young tableaux with distinct row lengths ℓ_a with multiplicities $(w_a - w_{a-1})$. Changing variables, the lengths of all rows *including* repetitions are given by the quantities

$$\tilde{\ell}_i = \ell_a \quad \text{for all } i = w_{a-1} + 1, \dots, w_a$$

$$\tag{6.4}$$

with $\tilde{p} = w_p$ the total number of rows. This reformulates the partition as $N = \sum_{i=1}^{\tilde{p}} \tilde{\ell}_i$. We furthermore define the quantities $\tilde{k}_i = \tilde{\ell}_i - \tilde{\ell}_{i+1}$ (equivalently, $\tilde{\ell}_i = \sum_{j=i}^{\tilde{p}} \tilde{k}_j$) such that

$$\tilde{k}_i = k_a$$
 if $i = w_a$, otherwise $\tilde{k}_{i \neq w_a} = 0$. (6.5)

The flavor symmetry of the associated regular puncture is given in terms of the monopole charges as

$$G_F = S\left[\prod_{a=1}^p U(k_a)\right] = S\left[\prod_{i=1}^{\tilde{p}} U(\tilde{k}_i)\right], \qquad (6.6)$$

where the product over i is understood to not include the cases $\tilde{k}_i = 0$.

Other useful quantities related to the Young tableaux are as follows. We introduce the notation

$$N_a = \sum_{b=1}^{a} (w_b - w_{b-1})\ell_b = \sum_{b=1}^{a-1} w_b k_b + w_a \ell_a , \quad N_p = N .$$
 (6.7)

The corresponding variables \tilde{N}_i in terms of the Young tableaux data are

$$\tilde{N}_{i} = \sum_{j=1}^{i} \tilde{\ell}_{j} = \sum_{j=1}^{i-1} j\tilde{k}_{j} + i \sum_{j=i}^{\tilde{p}} \tilde{k}_{j} , \quad \tilde{N}_{\tilde{p}} = \tilde{N}_{\tilde{p}+1} = N ,$$
(6.8)

which satisfy $\tilde{\ell}_i = \tilde{N}_i - \tilde{N}_{i-1}$. We also will utilize the pole structure, a set of N integers $p_i = i$ – (height of i'th box) labeling the i'th box in the diagram, starting with i = 1 and $p_1 = 0$ in the bottom left corner and increasing from left to right across a row (in a convention in which row lengths decrease from bottom to top). The p_i are related to the \tilde{N}_i by

$$\sum_{i=1}^{N} (2i-1)p_i = \frac{1}{6} \left(4N^3 - 3N^2 - N \right) - \sum_{i=1}^{\tilde{p}} (N^2 - \tilde{N}_i^2) . \tag{6.9}$$

For reference, these data for some special cases are as follows:

Rectangular box puncture, with N/ℓ rows of length ℓ , and flavor symmetry $G_F = SU(\ell)$. The case $\ell = N$ corresponds to the maximal puncture, while $\ell = 1$ corresponds to the "non-puncture".

tableaux data:
$$\tilde{p} = N/\ell$$
; $\tilde{\ell}_{1,...,\tilde{p}} = \ell$; $\tilde{k}_{\tilde{p}} = \ell$, $\tilde{k}_{1,...,\tilde{p}-1} = 0$; $\tilde{N}_{i} = i\ell$
geometric data: $p = 1$; $\ell_{1} = \ell$; $k_{1} = \ell$; $N_{1} = N$; $w_{1} = N/\ell$ (6.10)
pole structure: $p_{i=1+(m-1)\ell,...,m\ell} = i - m$, $m = 1,...,N/\ell$

Minimal puncture, with one row of length 2 and N-2 rows of length 1, and flavor symmetry $G_F = U(1)$.

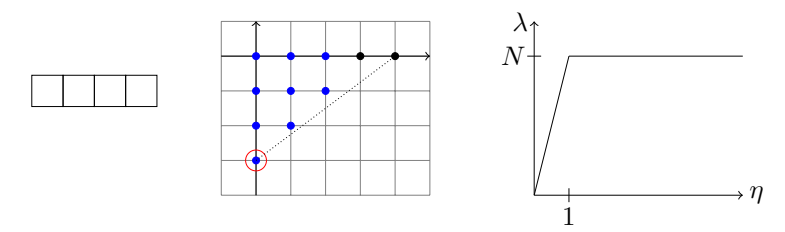
tableaux data:
$$\tilde{p} = N-1$$
; $\tilde{\ell}_1 = 2$, $\tilde{\ell}_{2,\dots,N-1} = 1$; $\tilde{k}_1 = \tilde{k}_{N-1} = 1$, $\tilde{k}_{2,\dots,N-2} = 0$; $\tilde{N}_i = i+1$ geometric data: $p=2$; $\ell_1 = 2$, $\ell_2 = 1$; $k_1 = k_2 = 1$; $k_1 = k_2 = 1$; $k_1 = 2$, $k_2 = 1$; pole structure: $k_1 = 2$, $k_2 = 2$; $k_3 = 2$; $k_4 = 2$; $k_5 = 2$; $k_6 = 2$; $k_7 = 2$; $k_8 =$

These are drawn for the case N=4 in Figure 8.

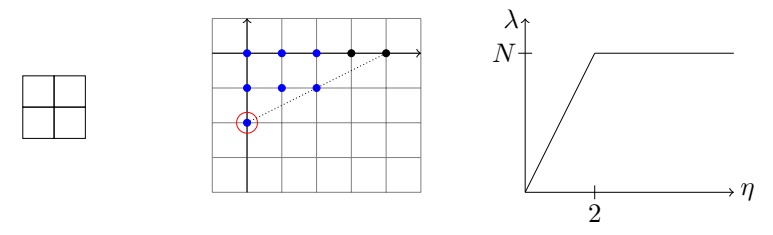
6.2 Checks of the holographic duality

We now review some properties of the field theories $(A_{N-1}^{(N)}[k],Y)$ which participate in the proposed duality, and match these properties with those of the supergravity solutions presented above. The $(A_{N-1}^{(N)}[k],Y)$ field theories are 4d $\mathcal{N}=2$ SCFTs of Argyres-Douglas type, engineered by wrapping N M5-branes on a sphere with one irregular puncture labeled by the integer k denoted $A_{N-1}^{(N)}[k]$ [9, 10], and one regular puncture labeled by the Young tableaux Y which is a partition of N. Since [15] includes a review of the classification of irregular singularities, as well as a detailed review of the properties of the $(A_{N-1}^{(N)}[k],Y)$ SCFTs when Y is a Young tableaux of rectangular box type (including the trivial case with no regular puncture on the sphere), in this section we focus primarily on how the data of the general Young tableaux enters the checks between properties of the SCFTs and the holographic solutions⁴.

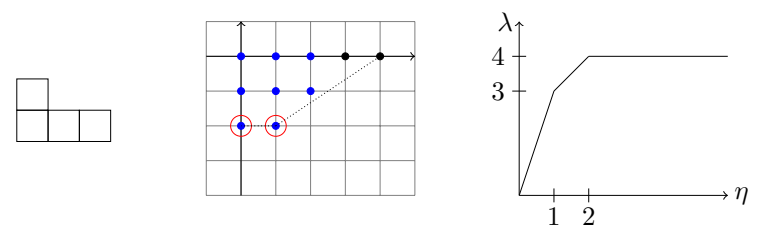
 $^{^4}$ We note that most of the checks performed in this section are not sensitive to differences between the irregular singularities $A_{N-1}^{(b)}[k]$ with b=N (Type I) versus b=N-1 (Type II), although we explicitly perform checks for the former case. In particular, the central charges, R-symmetry twist, maximum Coulomb-branch operator dimension, and rank of the flavor symmetry are all unchanged at leading order in N between the Type I and Type II theories, differing only at subleading order. The Case II identification of the holographic parameter K with the field theory parameter k would have an additional order 1 term in matching to the Type II singularity, but this difference does not affect the leading order duality checks. One difference is that we do not have access to a check of Higgs branch operator dimensions for the Type II singularities, since these cases do not have a known quiver Lagrangian description.



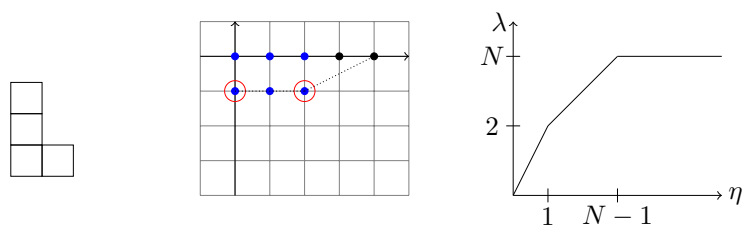
(a) The maximal puncture with $G_F = SU(N)$, corresponding to the box diagram Y_ℓ with $\ell = N$. Here, $p_\ell = \ell - 1$, such that $p_\ell = \{0, 1, 2, 3\}$ in the above diagram (allowing $\ell = 1, \ldots, N$).



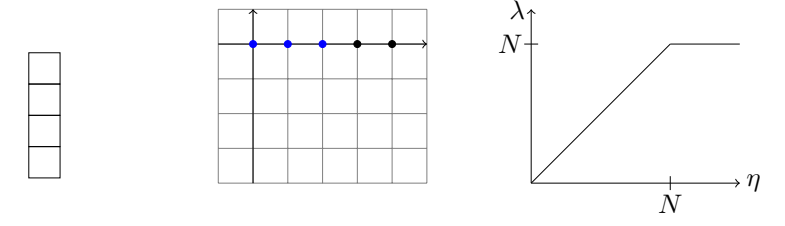
(b) The puncture with $G_F = SU(N/2)$, corresponding to the box diagram Y_ℓ with $\ell = N/2$. Here, $p_{\ell=1,\ldots,N/2} = \ell - 1$ and $p_{\ell=N/2+1,\ldots,N} = \ell - 2$, such that in the diagram shown $p_\ell = \{0,1,1,2\}$.



(c) The puncture with $G_F = S(U(2) \times U(1))$. Here, $p_{\ell} = \{0, 1, 2, 2\}$.



(d) The minimal puncture with $G_F = U(1)$, corresponding to the tableaux with one row of length 2 and N-2 rows of length 1. Here, $p_\ell = \{0, 1, \dots, 1\}$.



(e) The non-puncture, corresponding to the box diagram Y_{ℓ} with $\ell = 1$. Here, $p_{\ell} = 0$ for all ℓ .

Figure 8: The Young tableaux, Newton polygons, and charge density profiles λ_{reg} of the possible regular punctures for N=4. The blue dots represent deformation parameters of the Seiberg-Witten curve. The red circled dots are the Coulomb branch operators \mathcal{O}_a identified in (6.31).

6.2.1 R-symmetry

The $U(1)_r$ superconformal R-symmetry of these $\mathcal{N}=2$ SCFTs is independent of the details of the regular puncture. It is given by a linear combination of the global $U(1)_z$ isometry of the sphere and the would-be $U(1)_{\phi}$ R-symmetry that would be preserved in the absence of an irregular defect, as

$$r = R_{\phi} + \frac{N}{k+N}R_z \ . \tag{6.12}$$

This matches the R-symmetry identified in (5.23).

6.2.2 Central charge

The central charge of the $(A_{N-1}^{(N)}[k], Y)$ theories may be decomposed as the sum of the central charge $c_{(A_{N-1}, A_{k-1})}$ for the SCFTs without the regular puncture, plus the additional contribution Δc ,⁵

$$c = c_{(A_{N-1}, A_{k-1})} + \Delta c . (6.13)$$

The quantity $c_{(A_{N-1},A_{k-1})}$ is given by [9]

$$c_{(A_{N-1},A_{k-1})} = \frac{k^2(N^2 - 1) - (k+N)(N-2 + GCD(k,N))}{12(k+N)}$$
(6.14)

$$\stackrel{N \to \infty}{=} \frac{N^2(M-N)^2}{12M} , \quad M = k+N$$
 (6.15)

where for later reference we also evaluated the large N limit of large N, k at fixed k/N, and are using M = k + N. Δc depends on the details of the Young tableaux Y, and can be derived by partial closure of the maximal puncture to an arbitrary regular puncture [29],

$$\Delta c = \frac{1}{12} \left(n_h(Y) + 2n_v(Y) + 2N^3 - N - 1 + \frac{N}{(k+N)} \left(6I_{\rho_Y} - N^3 + N \right) \right) . \tag{6.16}$$

This is given in terms of the quantities $n_v(Y)$ and $n_h(Y)$ which represent the effective number of vector multiplets and hypermultiplets respectively contributed by the regular puncture labeled by Y,

$$n_v(Y) = -\sum_{i=1}^{\tilde{p}} (N^2 - \tilde{N}_i^2) - \frac{1}{2}N^2 + \frac{1}{2} , \qquad (6.17)$$

$$n_h(Y) = n_v(Y) + \frac{1}{2} \sum_{i=1}^{\tilde{p}} \tilde{N}_i \tilde{k}_i - \frac{1}{2} , \qquad (6.18)$$

⁵Since we are interested in checks at large N where a=c, here we focus only on the c central charge.

as well as the embedding index I_{ρ_Y} of $\mathfrak{su}(2)$ into $\mathfrak{su}(N)$ labeling the partial closure of the full puncture,

$$I_{\rho_Y} = \frac{1}{6} \sum_{i=1}^{\tilde{p}} i(i^2 - 1)\tilde{k}_i . \tag{6.19}$$

These are given in terms of the Young tableaux data $(\tilde{N}_i, \tilde{k}_i, \tilde{p})$ defined in section 6.1. For example, using (6.10) one can verify that for the box diagram labeled by ℓ , these evaluate to $I_{\rho_{Y_\ell}} = \frac{1}{6}N(\frac{N^2}{\ell^2} - 1)$, $n_h(Y_\ell) = \frac{2N}{3\ell}(\ell^2 - N^2)$, and $n_v(Y_\ell) = \frac{1}{6}(3 + \ell N - \frac{4N^3}{\ell})$, which upon substituting into (6.16) and (6.13) yield the c central charge evaluated in [14, 15]. One can similarly verify that using (6.11) for the case of the minimal puncture, the resulting central charge matches the result obtained in [27].

The field theory central charge (6.13) can be compared with the holographic central charge, computed above in (5.22) as

$$c_{\text{hol}} = \frac{1}{12} \left(MN^2 + \sum_{a=1}^{p} \left(\frac{N}{M} k_a w_a^3 - 2k_a^2 w_a^3 - \sum_{b=a+1}^{p} (w_a^3 + 3w_a w_b^2) k_a k_b \right) \right) . \tag{6.20}$$

In order to check that these two quantities match at large N, we need to evaluate the large-N limit of (6.16). First we change from Young tableaux variables $(\tilde{N}_i, \tilde{k}_i, \ldots, i = 1, ..., \tilde{p})$ to variables $(N_a, k_a, \ldots, a = 1, ..., p)$. Since \tilde{k}_i is only nonzero at the location of a monopole $i = w_a$, at which point $\tilde{k}_i = k_a$ and $\tilde{N}_i = N_a$, we can replace $\sum_i \tilde{N}_i \tilde{k}_i$ with $\sum_a N_a k_a$ in $n_h(Y)$, as well as $\sum_i i(i^2 - 1)\tilde{k}_i$ with $\sum_a w_a(w_a^2 - 1)k_a$ in I_{ρ_Y} . We also make use of the following identity (e.g. [33]),

$$\sum_{i=1}^{\tilde{p}} (N^2 - \tilde{N}_i^2) = \sum_{a=1}^{p} \left(\frac{2\ell_a^2}{3} (w_a^3 - w_{a-1}^3) + \ell_a (N_a - w_a \ell_a) (w_a^2 - w_{a-1}^2) - \frac{N_a k_a}{6} \right) - \frac{N^2}{2} + \frac{1}{2} .$$
(6.21)

Terms of $\mathcal{O}(N^2)$ and less are subleading in the large N limit and can be dropped. These include the sum $\sum_a N_a k_a$, as well as the -1 part of the sum $\sum_a w_a (w_a^2 - 1) k_a$. Putting all this together, and adding Δc to the large N limit of $c_{(A_{N-1},A_{k-1})}$ given in (6.15), we evaluate

$$c \stackrel{N \to \infty}{=} \frac{1}{12} \left(MN^2 + \sum_{a=1}^p \left(\frac{Nw_a^3 k_a}{M} - 2\ell_a^2 (w_a^3 - w_{a-1}^3) - 3\ell_a (N_a - w_a \ell_a) (w_a^2 - w_{a-1}^2) \right) \right) . \tag{6.22}$$

Substituting for N_a and ℓ_a from (6.1) and (6.7), we evaluate

$$c \stackrel{N \to \infty}{=} \frac{1}{12} \left[MN^2 + \sum_{a=1}^p \frac{N}{M} w_a^3 k_a - \sum_{a=1}^p \left(2 \left(\sum_{b=a}^p k_b \right)^2 (w_a^3 - w_{a-1}^3) + 3 \left(\sum_{b=a}^p k_b \right) \left(\sum_{b=1}^{a-1} w_b k_b \right) (w_a^2 - w_{a-1}^2) \right) \right]$$

$$= \frac{1}{12} \left[MN^2 + \sum_{a=1}^p \left(\frac{N}{M} k_a w_a^3 - 2k_a^2 w_a^3 - \sum_{b=a+1}^p w_a^3 k_a k_b - 3 \sum_{b=1}^{a-1} w_a^2 w_b k_a k_b \right) \right] , \qquad (6.24)$$

where in the second equality we converted the sums over w_{a-1} to sums over w_a , and then expanded the remaining sums in order to cancel some terms. The final sum in (6.24) can be recast as

$$\sum_{a=1}^{p} \sum_{b=1}^{a-1} w_a^2 w_b k_a k_b = \sum_{a=1}^{p} \sum_{b=a+1}^{p} w_a w_b^2 k_a k_b . \tag{6.25}$$

Substituting into (6.24) and comparing with the holographic central charge (6.20), we find agreement.

6.2.3 Coulomb branch operators

The Seiberg-Witten curve of the SCFT takes the form

$$y^{2} = x^{N} + z^{k} + \dots + u_{ab}x^{a}z^{b} + \dots$$
 (6.26)

where u_{ab} are deformations of the curve with scaling dimension

$$\Delta(u_{ab}) = \frac{kN - ak - bN}{k + N} \ . \tag{6.27}$$

The regular puncture with associated Young tableaux Y contributes terms

$$y^2 \supset \sum_{l=2}^{N} \sum_{n=1}^{p_l} v_{l,n} z^{-n} x^{N-l} , \qquad \Delta(v_{l,n}) = \frac{l(M-N) + nN}{M} ,$$
 (6.28)

where p_l is the pole structure defined above (6.9).

Coulomb branch operators are scalar primaries of protected $\mathcal{N}=2$ chiral multiplets with superconformal $SU(2)_R \times U(1)_r$ R-charges satisfying $r=2\Delta, R=0$. These correspond to deformation parameters u_{ab} with $\Delta(u_{ab}) > 1$. These deformations are nicely encoded in a Newton polygon, by plotting the (a,b) coordinates associated to operators u_{ab} on a grid. In particular, the operators $v_{l,n}$ associated contributed by the addition of the regular puncture on the sphere will correspond to points below the horizontal axis of this grid, since the associated powers of x and z in (6.28) are negative. Examples of the quadrants of the Newton polygon associated to the regular puncture deformations are shown in Figure 8.

In (5.33), we identified Coulomb branch type operators associated to wrapping an M2-brane on the S^2 at each of the $a=1,\ldots,p$ monopole locations, and computed their scaling dimensions

$$\Delta(\mathcal{O}_a) = \sum_{b=1}^{a-1} k_b w_b + w_a \sum_{b=a}^{p} k_b - \frac{Nw_a}{M} = N_a - \frac{Nw_a}{M}.$$
 (6.29)

In the second equality we used the definition of N_a from (6.7). We can match these onto operators in the SCFT as follows. Firstly we note that these operators correspond to some value of l and $n = p_l$ in (6.28), since at a given value of l we are interested in the largest dimension Coulomb branch operator (which has $n = p_l$). In the Newton polygon, these are points bounding the lower edge of the triangle.

Since the \mathcal{O}_a are associated with fluxes through the S^2 surrounding the monopole locations, we restrict attention to these points. The locations of the monopoles η_a coincide with changes in the slope of the density profile $\lambda(\eta)$, and correspondingly with changes in the lengths between subsequent rows of the associated Young tableaux (or equivalently, changes in the slope of the Newton polygon). Since the distinct lengths of rows of the Young tableaux are given by the ℓ_a , with multiplicities $(w_a - w_{a-1})$, evidently these changes in slope occur at box numbers $l_a = \sum_{b=1}^a (w_b - w_{b-1})\ell_b$, which is none other than N_a . Thus, we identify the operators \mathcal{O}_a with the $v_{l,n}$ for $l = N_a$ and $n = p_{N_a}$, with dimensions

$$\Delta(v_{l=N_a,n=p_{N_a}}) = N_a - \frac{N}{M} (N_a - p_{N_a}) . {(6.30)}$$

Finally, we evaluate $p_{N_a} = N_a$ —(height of N_a 'th box) by again appealing to the partition of N. Since there are $(w_a - w_{a-1})$ rows of length ℓ_a in the tableaux, the height of the N_a 'th box is equal to the number of rows that have already been surpassed, namely $\sum_{b=1}^{a} (w_b - w_{b-1}) = w_a$. Therefore,

$$\Delta(v_{l=N_a,n=p_{N_a}}) = N_a - \frac{Nw_a}{M} , \qquad (6.31)$$

which exactly matches the dimensions of the holographic operators (6.29). These operators are circled in red in the example Newton polygons drawn in Figure 8.

6.2.4 Flavor central charge

The flavor central charges associated to the $SU(k_a)$ flavor symmetries at the monopole locations were computed in (5.28) as

$$k_{SU(k_a)} = 2(y_a + m_a w_a) (6.32)$$

Using $m_a = \ell_{a+1} - \frac{N}{M}$, $\ell_a = \sum_{b=a}^p k_b$ (with $\ell_{p+1} = 0$), $y_a = \sum_{b=1}^a w_b k_b$, this can be rewritten

$$k_{SU(k_a)} = 2\left(\sum_{b=1}^{a} k_b w_b + w_a \sum_{b=a+1}^{p} k_b - \frac{N}{M} w_a\right) = 2\Delta(\mathcal{O}_a) , \qquad (6.33)$$

where $\Delta(\mathcal{O}_a)$ are the scaling dimensions given in (6.29), which we showed in that section match the maximal-dimension Coulomb branch operators associated to the *a*'th monopole. This confirms the conjecture that the flavor symmetry central charge of the associated Argyres-Douglas SCFT is equal to twice the scaling dimension of the Coulomb branch operator of maximal dimension [27].

6.2.5 Higgs branch operators for the minimal puncture

In the special case that Y corresponds to either a maximal puncture or a minimal puncture, a Lagrangian quiver description of the Argyres-Douglas SCFT is known. In [15], a class of Higgs branch operators are matched in the case of the maximal puncture between baryonic operators in the quiver, and a class of M2-brane probes in the holographic solution. With the generalized holographic solutions for any regular puncture, we can now perform a similar check for the minimal puncture case.

The Lagrangian description for the theories with a simple puncture in addition to the irregular puncture is known for the case that k=mN is an integer multiple of N. The UV quiver and IR quiver are depicted in Figure 9. They consists of N-1 gauge nodes $SU(m\ell+1)$, $\ell=1,\ldots,N-1$. Bifundamental hypermultiplets (Q_ℓ,\tilde{Q}_ℓ) connect the ℓ 'th node to the $\ell+1$ 'th node. There is one fundamental hypermultiplet (q_1,\tilde{q}_1) at the first node, and one $(q_{N-1},\tilde{q}_{N-1})$ at the last node. There are adjoints ϕ_ℓ for each of the gauge nodes. There are also singlets $M_j,\ j=1,\ldots,m(N-1)\ (j=\hat{j}-m\ \text{for}\ \hat{j}\ \text{the index in}\ [30])$. The $\mathcal{N}=1$ R-charges of the quarks and adjoints are

$$R_{\mathcal{N}=1}(Q_{\ell}) = R_{\mathcal{N}=1}(q_1) = \frac{3m+2}{3(m+1)} , \qquad R_{\mathcal{N}=1}(q_{N-1}) = \frac{3m+2-mN}{3(m+1)} ,$$

$$R_{\mathcal{N}=1}(\phi_{\ell}) = \frac{2}{3(m+1)} , \qquad (6.34)$$

from which the dimensions can be computed $\Delta = \frac{3}{2}R_{\mathcal{N}=1}$.

From the quivers, we can evidently construct sets of baryonic operators of the form

$$B_1 = \epsilon_{i_1 \dots i_{(N-1)m+1}} (q_{N-1})^{i_1} (q_{N-1}\phi)^{i_2} \dots (q_{N-1}\phi^{(N-1)m})^{i_{(N-1)m+1}} ,$$

$$B_2 = q_1 Q_1 \dots Q_{N-2} q_{N-1} ,$$

$$(6.35)$$

with dimensions

$$\Delta(B_1) = k - \frac{k}{N} + 1 , \qquad \Delta(B_2) = N .$$
 (6.36)

On the gravity side, we computed the dimensions of M2-brane probes corresponding to Higgs branch operators in (5.44) and (5.45). For the minimal puncture with data summarized in (6.11), these correspond to operators with dimensions

$$\Delta(\mathcal{O}_{[w_p, w_m]}) = k + \mathcal{O}(1) , \qquad \Delta(\mathcal{O}_{[w_1, w_2]}) = N + \mathcal{O}(1) .$$
 (6.37)

At large N, these operator dimensions match (6.36). We thus identify the M2-brane probes $\mathcal{O}_{[w_p,w_{\mathrm{m}}]}$ and $\mathcal{O}_{[w_1,w_2]}$ in the minimal puncture geometry with the baryons B_1 and B_2 in the Lagrangian quiver of the proposed dual SCFT.

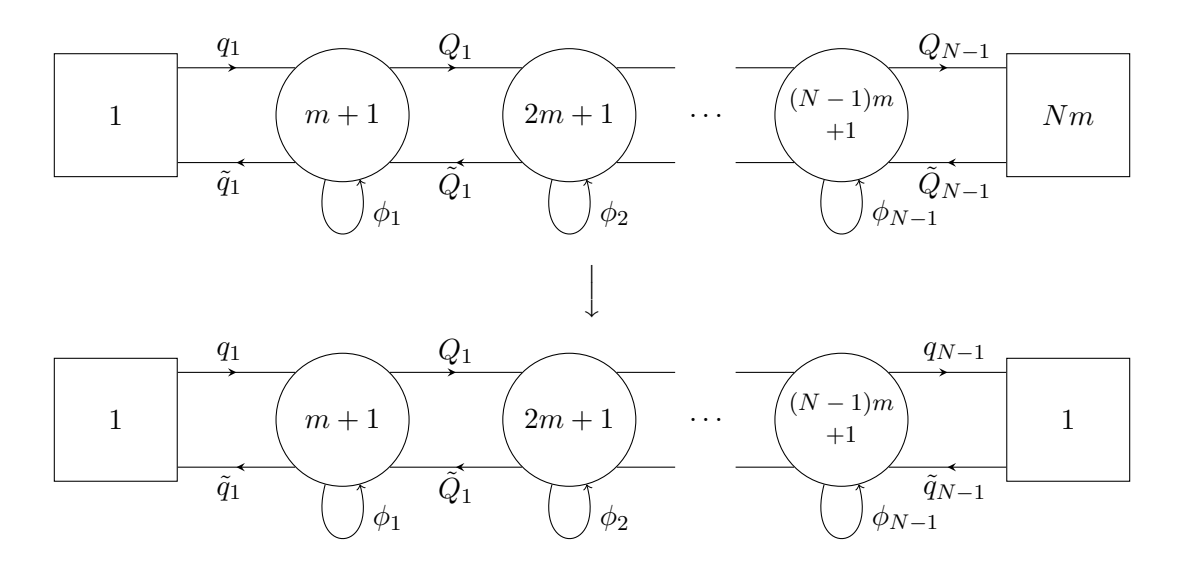


Figure 9: The upper figure is the UV quiver and the lower figure the IR quiver for the flow to the $(A_{N-1}^{(N)}[k=mN], S)$ SCFTs.

6.3 Speculations on nested Young tableaux

We end this section with some comments on another Argyres-Douglas SCFT, which we speculate might be dual to the Case I geometries constructed in this work.

One generalization of the $(A_{N-1}^{(\bar{N})}[k], Y)$ Argyres-Douglas SCFTs takes the Higgs field in the Hitchin system to be specified by a series $T_1 \subseteq T_2 \subseteq \cdots \subseteq T_{2+\frac{k}{N}}$ of semisimple elements of $\mathfrak{su}(N)$ that are not necessarily regular (e.g. see [9, 10]). Then, the data of the irregular puncture is refined to depend on a sequence of Young tableaux $Y_n \subseteq Y_{n-1} \cdots \subseteq Y_1$, $n = \frac{k}{N} + 2$. The Young tableaux encode the degeneracies of the eigenvalues of the matrices T_i . The "maximal" irregular singularity $A_{N-1}^{(N)}[k]$ is recovered in the limit that there is no degeneration of the eigenvalues, so that all matrices are of maximal type.

In this case, the Seiberg-Witten curve has additional parameters,

$$x^{N} + \sum_{i=2}^{N} \left(\dots + \sum_{j=1}^{m_{i}} u_{j}^{(i)} z^{m_{i}-j} \right) x^{N-i} = 0 , \quad m_{i} = \sum_{l} p_{i}^{(l)} - 2i + 1 .$$
 (6.38)

Here $p_i^{(l)}$ is the pole structure of the *i*'th box in the *l*'th Young tableaux of the sequence. The independent Coulomb branch operators thus have dimensions

$$\Delta(u_j^{(i)}) = \frac{ik - (m_i - j)N}{k + N} \ . \tag{6.39}$$

Suggestive example: $\{Y_Q, \ldots, Y_Q\}$. Let us illustrate such a scenario with a suggestive example. Suppose there is just one type of tableaux labeled by Q, which occurs with multiplicity $n = \frac{k}{N} + 2$,

$$\rho = \{Y_Q, \dots, Y_Q\} \ , \tag{6.40}$$

where we assume that k is an integer multiple of N. The limit Q = N reduces to the "maximal" irregular puncture without the additional nested structure. For simplicity let us take the regular puncture on the other pole of the sphere to be trivial, *i.e.* q = 1. Then, the pole structure parameters are given by,

$$p_i^{(l)} = i - m \;, \quad i = 1 + (m - 1)Q, \dots, mQ \;, \quad m = 1, \dots, N/Q \;,$$
 (6.41)

$$m_i = \left(\frac{k}{N} + 2\right) p_i - 2i + 1 \ .$$
 (6.42)

For $Q \sim \mathcal{O}(1)$, the quantities m_i are negative, and we cannot use this description (6.38) to enumerate the Coulomb branch operators. However for $Q \sim \mathcal{O}(N)$, one may verify that the m_i are positive. In this case, we check that the Coulomb branch operator $u_{m_N}^{(N)}$ has dimension of order N, given by

$$\Delta(u_{m_N}^{(N)}) = \frac{Nk}{k+N} \ , \tag{6.43}$$

and that the rank of the Coulomb branch is given by⁶

$$rank(CB) = \frac{kN}{2} - \frac{N}{2Q}(k+2N) + 1.$$
 (6.44)

We may compute the central charge at large N by summing over the Coulomb branch operator dimensions [26], yielding

$$2a - c = \frac{1}{4} \sum_{i} (2\Delta(u_i) - 1) = \frac{1}{2} \sum_{i=2}^{N} \sum_{j=1}^{m_i} \frac{ik - (m_i - j)N}{k + N} - \frac{1}{4} \text{rank}(CB)$$
$$= \frac{k^2 N^2}{12(k + N)} + \mathcal{O}(N^2) . \tag{6.45}$$

In particular, we note that at leading order for large N, these data – the large-N central charge, maximal dimension Coulomb branch operator, and rank of the Coulomb branch – are indistinguishable from the "maximal" irregular puncture theory, (A_{N-1}, A_{k-1}) . This is not surprising, since this singularity labeled by $Q \sim \mathcal{O}(N)$ is quite similar to the maximal irregular puncture case. However, even for $Q \sim \mathcal{O}(N)$ there is additional data contributed by the nested structure: the flavor symmetry of the field theory is enhanced. The number of mass parameters is equal to the number of distinguished eigenvalues of T_1 [10], which in this example contributes $\operatorname{rank}_{\rho}(F)$ to the rank of the flavor symmetry as,

$$\operatorname{rank}_{\rho}(F) = \frac{N}{Q} - 1 , \qquad \operatorname{rank}(F) = \operatorname{rank}_{\rho}(F) + \operatorname{rank}_{\rho}(SU(N)) . \tag{6.46}$$

⁶One check on this formula is that it satisfies the expected relation rank(CB) = $\dim_{\rho}(CB) - \dim(SU(N))$, where $\dim_{\rho}(CB)$ is equal to one half times the sum over the dimensions of the nilpotent orbits of $\mathfrak{su}(N)$ that appear in the sequence ρ .

Now, return to the Case I holographic solutions, again for simplicity taking q=1 such that there is no regular puncture on the sphere. Their data is summarized in Table 1, where since q=1 we may replace $M=N_{\rm eff}$. If we identify the number of M5-branes N and the irregular puncture parameter k with the holographic fluxes $N_{\rm eff}$ and K in a way identical to the Case II dictionary,

$$N = N_{\text{eff}} , \qquad k = K + M - N = K ,$$
 (6.47)

then evidently the R-symmetry, central charges, and dimensions of the operators \mathcal{O}_1 match both data of the Argyres-Douglas SCFT labeled by "maximal" regular puncture $A_{N-1}^{(N)}[k]$, and the Argyres-Douglas SCFT labeled by the nested Young tableaux $\rho = \{Y_Q, \dots, Y_Q\}$ with $Q \sim \mathcal{O}(N)$.

In addition, both Case I and the $\rho = \{Y_Q, \dots, Y_Q\}$ irregular puncture theory possess enhanced flavor symmetry. Naively, we expect a flavor symmetry coming from the two stacks of N_W and N_S smeared M5-branes in the geometry, where (again, naively) we might expect that the maximal rank of this flavor symmetry is identified with the maximal possible rank of the sources, equaling $N_W + N_S - 1$. This identification would provide a proposed map between the flux quantum N_S on the gravity side, and the field theory parameters N, k, and q.

While a proposed duality along these lines seems promising, more precise checks would be required to put it on firmer footing. In particular, a more precise understanding of the flavor symmetry of the smeared M5-brane geometry would be necessary. We leave this direction to future work. At present, we view this discussion as a hint that the dual to the Case I geometry is consistent with Argyres-Douglas SCFT whose irregular puncture has refined structure.

7 Discussion

The results of this work suggest several interesting directions for future research, some of which are discussed below.

Exploring the geometry of irregular singularities. The separable Toda solutions of Case I and II studied in this paper exhibit an interesting qualitative feature that sets them apart from the Maldacena-Nuñez [12] and Gaiotto-Maldacena [13] solutions. Recall that the latter describe the holographic duals of class \mathcal{S} setups without punctures, and with regular punctures, respectively.

To elucidate the novel features of the solutions of Case I and II, let us examine in closer detail the locus y=0 in the standard form of the line element (2.1). Recall that the internal space M_6 can be regarded as an $S^2 \times S^1_{\chi}$ fibration over a 3d base space B_3 , with coordinates x_1, x_2, y . The line element (2.1) reveals that the locus y=0 in B_3 has an intrinsic geometric meaning, because it corresponds to the region where the S^2 shrinks. Both in the Maldacena-Nuñez and in the Gaiotto-Maldacena solutions, the locus y=0 consists of a single component, at which the S^2 shrinks smoothly, while the warp factor remains non-singular. This should be contrasted with the solutions of Case I and II, in which the locus y=0 splits

into two components, meeting transversally at a point. This structure is made manifest by the introduction of the t, u coordinates, see (2.9). In particular, the relation y = tu can be regarded as a way of parametrizing the split of the locus y = 0 into two components, t = 0 and u = 0, intersecting transversally at u = t = 0. In Case II, the splitting of the y = 0 locus is particularly important for the structure of the internal geometry, because the behavior of the warp factor and line element along the two components u = 0 and t = 0 exhibits clear qualitative differences: along the component u = 0, the S^2 shrinks but the warp factor remains non-singular, while along the component t = 0 we find a smeared M5-brane source, see Figure 1.

The considerations of the previous paragraphs suggest a more physical way of thinking about the change of coordinates y = tu: it describes setups in which the y = 0 locus has a non-trivial sub-structure. From this point of view, it is natural to wonder whether the locus y = 0 might admit richer structures than those studied in this paper. For example, one might ask whether y = 0 could split into three components, C_1 , C_2 , C_3 say, with C_1 and C_2 meeting at a point, and similarly for C_2 and C_3 . It is not clear whether such more complicated setups would still allow for a separation of variables in the Toda equation; this might pose a technical challenge to exploring such possibilities analytically in the Toda frame.

A possible strategy to study a multi-component y = 0 locus might be inspired by the methods of [37]. This reference studies the most general AdS_5 M-theory solution preserving $4d \mathcal{N} = 1$ supersymmetry in which the internal space is a fibration of a compact 4-manifold over a (punctured) Riemann surface. The internal geometry is assumed to preserve at least a $U(1)^2$ isometry. The 4-dimensional fiber over the Riemann surface can be described as a $U(1)^2$ fibration over a 2d base space. The latter is a region in \mathbb{R}^2 with a boundary consisting of several segments, where on each segment, a different linear combination of the two U(1) Killing vectors shrinks to zero size. These setups bear some formal analogies to the multi-component y = 0 locus we would like to explore.

Alternatively, one might work in the electrostatic picture after the Bäcklund transform. In this frame, the task is to identify those charge densities that give rise to a multi-component y = 0 locus, and to study them systematically.

Connections with Painlevé equations and integrable systems. In the Introduction, we have motivated our assumption that the internal geometry admits an additional Killing vector ∂_{β} , in addition to the Killing vector ∂_{χ} dual to the superconformal $U(1)_r$ symmetry. We have also noticed, however, how this ∂_{β} isometry does not give rise to a continuous U(1) flavor symmetry on the field theory side. It is natural to wonder whether we could relax the assumption of having the additional isometry ∂_{β} , and search for solutions that can be interpreted in terms of irregular punctures. In particular, one may wonder whether, upon relaxing the ∂_{β} isometry, non-singular (or less singular) solutions could be found in which the smeared M5-brane sources encountered in this work are resolved.

The study of the Toda equation (1.2) in non-axisymmetric setups is particularly challenging. A possible inroad into this problem is furnished by the analysis in [38]. The main idea is

to consider a coordinate change from x_1, x_2, y to a new set of coordinates τ, ϑ, φ , of the form

$$x_1 = e^{a\tau}\Omega_1(\tau)\sin\theta\cos\varphi$$
, $x_2 = e^{a\tau}\Omega_2(\tau)\sin\theta\sin\varphi$, $y = \Omega_2(\tau)\cos\theta$, (7.1)

where a is a constant parameter, $\Omega_{1,2}$ are functions of τ , $0 \le \vartheta \le \pi$, and φ is an angle of period 2π . In the generic case in which $\Omega_1(\tau)$ is not identically equal to $\Omega_2(\tau)$, this ansatz describes a non-axisymmetric configuration. Nonetheless, one retains analytic control as follows. If we introduce a new coordinate s via $as = e^{-a\tau}$, and we set the Toda potential D to be $e^D = a^2s^2$, we can verify that the Toda equation reduces to an ODE for a single function w = w(s). The ODE is of Painlevé III type,

$$w'' = \frac{(w')^2}{w} - \frac{w'}{s} + \gamma w^3 + \frac{\delta}{w} , \qquad (7.2)$$

where γ , δ are constant parameters.

Relating the search of M-theory solutions dual to irregular punctures to a Painlevé equation is particularly tantalizing, given that Painlevé equations have natural links to the Hitchin integrable system on punctured Riemann surfaces, see e.g. [39]. A functional transform from the Toda equation to the Painlevé III equation might thus be a way to establish a precise correspondence between the holographic description of the class \mathcal{S} model, and its description in terms of the Higgs field entering the Hitchin system. We plan to investigate this direction further in the future.

Holographic realizations of renormalization group flows. Another interesting direction is to understand the holographic analogues of known renormalization group flows between Argyres-Douglas SCFTs. For example, there is an RG flow between the $(A_{N-1}^{(N)}[k], Y_{\text{max}})$ theory with a regular maximal puncture on the sphere, and the (A_{N-1}, A_{k+N-1}) theory with no regular puncture, via nilpotent Higgsing [40]. This flow can furthermore be understood purely from the Lagrangian perspective. It would be quite interesting to reproduce such an RG flow holographically, using the proposed holographic duals that we have now identified.

Acknowledgments

We are grateful to Davide Gaiotto, Enoch Leung, Kazunobu Maruyoshi, and Peter Weck for interesting conversations. The work of IB and TW is supported in part by NSF grant PHY-2112699. The work of IB and TW is also supported in part by the Simons Collaboration on Global Categorical Symmetries. FB is supported by STFC Consolidated Grant ST/T000864/1. The research of EN is supported by World Premier International Research Center Initiative (WPI), MEXT, Japan. Part of this work was completed while IB was visiting the Institute for Advanced Study. We also acknowledge Perimeter Institute, where part of this work was completed. Research at Perimeter Institute is supported in part by the Government of Canada through the Department of Innovation, Science and Economic Development Canada and by the Province of Ontario through the Ministry of Colleges and Universities.

A Further details on separable solutions

A.1 Angular coordinates ϕ , z

As anticipated in the main text, it is convenient to perform a change of coordinates from the Toda angles χ , β to a new pair of angles ϕ , z. The change of coordinates is engineered in such a way that, along the segment $\mathbf{P}_3\mathbf{P}_4$ in each case in Figure 1, the linear combination of Killing vectors ∂_{χ} , ∂_{β} that has vanishing norm is simply ∂_{ϕ} . This can be achieved by setting

$$\chi = \frac{\tilde{v}}{\tilde{v} - 1}\phi - z, \qquad \beta = -\frac{1}{\tilde{v} - 1}\phi + z, \tag{A.1}$$

where $\tilde{v} \equiv v_{\beta}(t, u_2)$ is the constant value attained by v_{β} along the $\mathbf{P}_3\mathbf{P}_4$ segment,

$$\tilde{v} = 1 - \frac{\sigma}{2} \left(1 - \frac{u_1}{u_2} \right) \qquad \Rightarrow \qquad \mathcal{C} = \tilde{v} - 1 = -\frac{\sigma}{2} \left(1 - \frac{u_1}{u_2} \right) , \tag{A.2}$$

where we have also given the value of the constant C that enters the parametrization (3.1) used in the main text. In terms of the Killing vectors and differential forms, we can write

$$\begin{pmatrix} \partial_{\chi} \\ \partial_{\beta} \end{pmatrix} = \begin{pmatrix} 1 & \frac{1}{\tilde{v}-1} \\ 1 & \frac{\tilde{v}}{\tilde{v}-1} \end{pmatrix} \begin{pmatrix} \partial_{\phi} \\ \partial_{z} \end{pmatrix}, \qquad \begin{pmatrix} d\chi \\ d\beta \end{pmatrix} = \begin{pmatrix} \frac{\tilde{v}}{\tilde{v}-1} & -1 \\ -\frac{1}{\tilde{v}-1} & 1 \end{pmatrix} \begin{pmatrix} d\phi \\ dz \end{pmatrix}. \tag{A.3}$$

With this, the metric takes the form

$$ds_{11}^2 = \frac{e^{2\tilde{\lambda}}}{m^2} \left[ds^2 (AdS_5) + \frac{t^2 u^2 e^{-6\tilde{\lambda}}}{4} ds^2 (S^2) + R_{\phi}^2 Dz^2 + R_{\phi}^2 d\phi^2 - \partial_y D \frac{K_1 u^2 + K_2 t^2}{4tu} \left(\frac{dt^2}{K_1} + \frac{du^2}{K_2} \right) \right],$$
(A.4)

where $Dz = dz - Ld\phi$ and we have made the definitions

$$\begin{split} R_z^2 &= \frac{-\partial_y D K_1 K_2}{4tu} + \frac{(v_\beta - 1)^2}{1 - tu\partial_y D} \\ &= \frac{-\sigma^2}{4tu(t_1 t_2 u^2 - u_1 u_2 t^2)} \bigg(ut_1 t_2 (t_1 + t_2) (u - u_1) (u - u_2) \\ &+ t^2 (t_1 + t_2) \bigg(u^3 - u_1 u_2 (3u - u_1 - u_2) \bigg) - tt_1 t_2 \bigg(4u^3 - (u_1 + u_2) (3u^2 - u_1 u_2) \bigg) \\ &+ t^3 \bigg(4u u_1 u_2 - (u_1 + u_2) (u^2 + u_1 u_2) \bigg) \bigg) \ , \\ L &= -\frac{2(u - u_2)}{P} \bigg(tu u_1 \left(t(u t_2 - t u_1) + t_1 (t u - t_2 (2u - u_1)) \right) \\ &- (u - u_1) u_2 (u t_1 t_2 (2t - t_1 - t_2) + t u_1 (t - t_1) (t - t_2) \bigg) \\ &+ t u_1 u_2^2 (t - t_1) (t - t_2) \bigg) \ , \\ R_\phi^2 &= \frac{\sigma(u_1 - u_2)}{P} \bigg(t - t_1 \big) (t - t_2) (u - u_1) (u - u_2) \bigg((t_1 + t_2) u - (u_1 + u_2) t \bigg) \ , \\ P &= \sigma(u_1 - u_2) \bigg(ut_1 t_2 (t_1 + t_2) (u - u_1) (u - u_2) + t^2 (t_1 + t_2) \bigg(u^3 - u_1 u_2 (3u - u_1 - u_2) \bigg) \\ &- t^3 \bigg(u^2 (u_1 + u_2) - u_1 u_2 (4u - u_1 - u_2) \bigg) - tt_1 t_2 \bigg(4u^3 - (u_1 + u_2) (3u^2 - u_1 u_2) \bigg) \bigg) \ . \end{split}$$

From these definitions we can readily read off that the ϕ circle shrinks along the intervals where the K_i vanish, and we can find that the Dz fibration will only vanish at the locations of the monopoles.

In terms of the new angular coordinates, the flux reads

$$\overline{G}_4 = -\frac{G_4}{(2\pi\ell_p)^3} = \frac{\operatorname{vol}_{S^2}}{4\pi} \wedge d\left[Y\frac{d\phi}{2\pi} - W\frac{Dz}{2\pi}\right], \tag{A.6}$$

where the 0-forms Y, W are given by

$$W = t^{3}u^{3}e^{-6\tilde{\lambda}}(v_{\beta} - 1) - tuv_{\beta} - \frac{1}{2}\mathcal{F} ,$$

$$Y + WL = -t^{3}u^{3}e^{-6\tilde{\lambda}}\frac{\tilde{v} - v_{\beta}}{\tilde{v} - 1} - \frac{tuv_{\beta}}{\tilde{v} - 1} - \frac{\mathcal{F}}{2(\tilde{v} - 1)} ,$$
(A.7)

with v_{β} , \mathcal{F} as in (2.16).

Finally, let us record the expression of the calibration 2-form Y' given in (3.14) in terms

of functions appearing in the line element (A.4),

$$Y = \frac{1}{4}(tu)^{3}e^{-9\tilde{\lambda}}\operatorname{vol}_{S^{2}} + \frac{1}{2}tue^{-3\tilde{\lambda}}(1 - (tu)^{2}e^{-6\tilde{\lambda}})(v_{\beta} - 1)d\tau \wedge Dz$$

$$+ \frac{1}{2}tue^{-3\tilde{\lambda}}(1 - (tu)^{2}e^{-6\tilde{\lambda}})\left(\frac{\tilde{v} - v_{\beta}}{\tilde{v} - 1} - (v_{\beta} - 1)L\right)d\tau \wedge d\phi$$

$$+ \left[\frac{1}{2}\tau e^{-3\tilde{\lambda}}u\left(\frac{\tilde{v} - v_{\beta}}{\tilde{v} - 1} - (v_{\beta} - 1)L\right) + \frac{1}{4}\frac{K_{2}tue^{-9\tilde{\lambda}}\tau}{1 - (tu)^{2}e^{-6\tilde{\lambda}}}\left(\frac{1}{\tilde{v} - 1} + L\right)\right]dt \wedge d\phi$$

$$+ \left[\frac{1}{2}\tau e^{-3\tilde{\lambda}}t\left(\frac{\tilde{v} - v_{\beta}}{\tilde{v} - 1} - (v_{\beta} - 1)L\right) - \frac{1}{4}\frac{K_{1}tue^{-9\tilde{\lambda}}\tau}{1 - (tu)^{2}e^{-6\tilde{\lambda}}}\left(\frac{1}{\tilde{v} - 1} + L\right)\right]du \wedge d\phi$$

$$+ \left[\frac{1}{2}\tau e^{-3\tilde{\lambda}}y_{2}(v_{\beta} - 1) - \frac{1}{4}\frac{K_{2}tue^{-9\tilde{\lambda}}\tau}{1 - (tu)^{2}e^{-6\tilde{\lambda}}}\right]dt \wedge Dz$$

$$+ \left[\frac{1}{2}\tau e^{-3\tilde{\lambda}}y_{1}(v_{\beta} - 1) + \frac{1}{4}\frac{K_{1}tue^{-9\tilde{\lambda}}\tau}{1 - (tu)^{2}e^{-6\tilde{\lambda}}}\right]du \wedge Dz, \tag{A.8}$$

A.2 Solutions in Case II in the notation of [15]

Brief review. The AdS_5 solutions discussed in [15] were obtained by uplift from 7d gauged supergravity. The 11d metric and flux are given by

$$m^{2} ds_{11}^{2} = \frac{2 B w^{1/3} \mathcal{H}(w,\mu)^{1/3}}{\sqrt{1-w^{2}}} \left[ds^{2} (AdS_{5}) + \frac{dw^{2}}{2 w h(w) (1-w^{2})^{3/2}} + \frac{\mathcal{C}^{2} h(w) dz^{2}}{B} + \frac{\sqrt{1-w^{2}}}{2 B} \left(\frac{d\mu^{2}}{w (1-\mu^{2})} + \frac{(1-\mu^{2}) D\phi^{2}}{w \mathcal{H}(w,\mu)} + \frac{w \mu^{2} ds^{2}(S^{2})}{\mathcal{H}(w,\mu)} \right) \right].$$
(A.9)

The quantities B, \mathcal{C} are parameters specifying the solution and satisfy

$$0 < B < 1$$
, $C = \frac{1}{\ell \sqrt{1 - B^2}}$, $\ell \in \mathbb{Z}_{>0}$. (A.10)

The coordinates z, ϕ are angles with period 2π , while the coordinates μ , w have ranges

$$0 \le \mu \le 1$$
, $0 \le w \le w_1 := \frac{1}{2} \left(\sqrt{1+B} - \sqrt{1-B} \right)$ (A.11)

We have introduced the shorthand notation

$$\mathcal{H}(w,\mu) = \mu^2 + w^2 (1 - \mu^2), \qquad h(w) = B - 2w\sqrt{1 - w^2}.$$
 (A.12)

The quantity $ds^2(S^2)$ is the metric on the round unit 2-sphere, while the 1-form $D\phi$ reads

$$D\phi = d\phi + \mathcal{C}(2w^2 - 1)dz. \tag{A.13}$$

The expression for G_4 is

$$G_4 = -\frac{1}{m^3} \operatorname{vol}_{S^2} d \left[\frac{\mu^3}{\mu^2 + w^2 (1 - \mu^2)} D\phi \right], \tag{A.14}$$

where vol_{S^2} is the volume form on the 2-sphere of unit radius.

When these solutions are cast in canonical LLM form, the Toda potential D reads

$$e^{D} = \frac{16 B C^{2} (1 - \mu^{2})^{1+1/C} \left[B - 2 w \sqrt{1 - w^{2}} \right]}{(1 - w^{2}) \mathcal{G}(w)^{2}}.$$
 (A.15)

The LLM coordinates r, y are related to the coordinates w, μ by the relations

$$y = \frac{4 B w \mu}{\sqrt{1 - w^2}}, \qquad r = (1 - \mu^2)^{-\frac{1}{2C}} \mathcal{G}(w).$$
 (A.16)

In the previous expressions, the quantity $\mathcal{G}(w)$ is a function of w only, satisfying the ODE

$$\frac{\mathcal{G}'(w)}{\mathcal{G}(w)} = \frac{-B w}{\mathcal{C} (1 - w^2) \left[B - 2 w \sqrt{1 - w^2} \right]} . \tag{A.17}$$

Let us define a new variable \hat{t} via

$$\widehat{t} = \frac{w}{\sqrt{1 - w^2}} \ . \tag{A.18}$$

The above ODE can be written in the form

$$\frac{d}{d\hat{t}}\log \mathcal{G}(\hat{t}) = \frac{\alpha_1}{\hat{t}_1 - \hat{t}} + \frac{\alpha_2}{\hat{t}_2 - \hat{t}}, \qquad (A.19)$$

where

$$\hat{t}_{1,2} = \frac{1 \mp \sqrt{1 - B^2}}{B} , \qquad \alpha_{1,2} = -\frac{B^2}{2\mathcal{C}[1 - B^2 \pm \sqrt{1 - B^2}]} .$$
 (A.20)

The solution can be written as

$$\log \mathcal{G}(\widehat{t}) = -\alpha_1 \log(\widehat{t}_1 - \widehat{t}) - \alpha_2 \log(\widehat{t}_2 - \widehat{t}) + \text{const} . \tag{A.21}$$

Dictionary with Case II solutions. The μ , w coordinates are related to the t, u coordinates of Case II via

$$u = u_2 \mu$$
, $t = \frac{4Bw}{u_2 \sqrt{1 - w^2}} = \frac{4B}{u_2} \hat{t}$. (A.22)

We also record the identifications

$$\sigma = -\mathcal{C} , \qquad \frac{t_2}{t_1} = \frac{1 + \sqrt{1 - B^2}}{1 - \sqrt{1 - B^2}} .$$
 (A.23)

B Formulae for the electrostatic potential

In this appendix we discuss the electrostatic potential generated by a piecewise linear charge density profile with an arbitrary number of monopoles. The electrostatic potential is computed from the charge density using the standard Green's function for the Laplace operator on \mathbb{R}^3 , see (4.26).

We consider a total of n monopoles, located at η_i , i = 1, ..., n. We start by computing the contribution of the linear charge density between two consecutive monopoles, which we parametrize as

$$\lambda(\eta) = m_i \eta + q_i \quad \text{for } \eta_i < \eta < \eta_{i+1} , \quad i = 1, \dots, n-1 .$$
 (B.1)

This segment of charge density gives the electrostatic potential

$$V(\eta_{i}, \eta_{i+1}, m_{i}, q_{i}) = \frac{1}{2} \left[m_{i} \sqrt{\rho^{2} + (\eta - \eta_{i})^{2}} - (m_{i} \eta + q_{i}) \operatorname{arctanh} \left(\frac{\eta - \eta_{i}}{\sqrt{\rho^{2} + (\eta - \eta_{i})^{2}}} \right) - m_{i} \sqrt{\rho^{2} + (\eta - \eta_{i+1})^{2}} + (m_{i} \eta + q_{i}) \operatorname{arctanh} \left(\frac{\eta - \eta_{i+1}}{\sqrt{\rho^{2} + (\eta - \eta_{i+1})^{2}}} \right) \right].$$
(B.2)

Next, we study the semi-infinite line at the right of the last monopole. The charge density is written as

$$\lambda(\eta) = m_n \eta + q_n \quad \text{for } \eta > \eta_n .$$
 (B.3)

This contribution suffers from divergences, which are treated in the same way as for Case I in the main text. We introduce a regulator η_R and we subtract the divergences as $\eta_R \to \infty$, with the result

$$V_{\text{right}} = \lim_{\eta_R \to \infty} \left[V(\eta_n, \eta_R, m_n, q_n) + \frac{m_n \eta + q_n}{2} \log(2\eta_R) + \frac{m_n}{2} \eta_R \right]$$

$$= \frac{1}{2} \left[m_n \sqrt{\rho^2 + (\eta - \eta_n)^2} - (m_n \eta + q_n) \operatorname{arctanh} \left(\frac{\eta - \eta_n}{\sqrt{\rho^2 + (\eta - \eta_n)^2}} \right) + (m_n \eta + q_n) \log \rho + m_n \eta \right]. \tag{B.4}$$

The semi-infinite line at the left of the first monopole is treated in an analogous way. We parametrize the charge density as

$$\lambda(\eta) = m_0 \eta + q_0 \quad \text{for } \eta < \eta_1 .$$
 (B.5)

We then compute

$$V_{\text{left}} = \lim_{\eta_L \to \infty} \left[V(-\eta_L, \eta_1, m_0, q_0) + \frac{m_0 \eta + q_0}{2} \log(2\eta_L) - \frac{m_0}{2} \eta_L \right]$$

$$= \frac{1}{2} \left[-m_0 \sqrt{\rho^2 + (\eta - \eta_1)^2} + (m_0 \eta + q_0) \operatorname{arctanh} \left(\frac{\eta - \eta_1}{\sqrt{\rho^2 + (\eta - \eta_1)^2}} \right) + (m_0 \eta + q_0) \log \rho + m_0 \eta \right].$$
(B.6)

Let us remark that continuity of the charge density imposes the following constraints on the monopole locations η_i , the slope parameters m_i , and the intercept parameters q_i ,

$$m_{i-1}\eta_i + q_{i-1} = m_i\eta_i + q_i , \qquad i = 1, \dots, n .$$
 (B.7)

The total electrostatic potential for the full charge density takes the form

$$V_{\text{tot}} = \sum_{i=1}^{n-1} V(\eta_i, \eta_{i+1}, m_i, q_i) + V_{\text{left}} + V_{\text{right}} .$$
 (B.8)

\mathbf{C} Detailed analysis of generalized Case II

In this appendix we present a more detailed analysis of the generalized Case II solutions discussed in section 5. Before addressing these solutions, however, we describe the electrostatic picture for Case II solutions in the notation of [15].

Electrostatic interpretation of Case II, revisited

Determination of ρ , η , V. The expression of ρ as a function of (w, μ) is obtained directly by combining (4.1), (A.15), and (A.16),

$$\rho = \frac{4C\sqrt{B}\sqrt{1-\mu^2}\sqrt{B-2w\sqrt{1-w^2}}}{\sqrt{1-w^2}}.$$
 (C.1)

The function $\eta = \eta(\mu, w)$ can be determined as follows. Let us regard V as a function of μ , w. Its derivatives with respect to w, μ can be computed from $\partial_{\rho}V$, $\partial_{\eta}V$ with the help of the chain rule, in terms of an unspecified $\eta = \eta(\mu, w)$. The result reads

$$\partial_{\mu}V(\mu, w) = \partial_{\mu}\eta(\mu, w) \log\left[(1 - \mu^{2})^{-\frac{1}{2C}}\mathcal{G}(w)\right] - \frac{4Bw\mu^{2}}{(1 - \mu^{2})\sqrt{1 - w^{2}}}, \tag{C.2}$$

$$\partial_{w}V(\mu, w) = \partial_{w}\eta(\mu, w) \log\left[(1 - \mu^{2})^{-\frac{1}{2C}}\mathcal{G}(w)\right] + \frac{4Bw\mu(2w^{2} - 1)}{(1 - \mu^{2})^{-\frac{1}{2C}}\mathcal{G}(w)} + \frac{4Bw^{2}\mu}{(1 -$$

$$\partial_w V(\mu, w) = \partial_w \eta(\mu, w) \log \left[(1 - \mu^2)^{-\frac{1}{2C}} \mathcal{G}(w) \right] + \frac{4 B w \mu (2w^2 - 1)}{(1 - w^2) \left[B - 2 w \sqrt{1 - w^2} \right]} + \frac{4 B w^2 \mu}{(1 - w^2)^{3/2}}.$$

The integrability condition $\partial_w \partial_\mu V(\mu, w) = \partial_\mu \partial_w V(\mu, w)$ yields

$$0 = B w (1 - \mu^{2}) \partial_{\mu} \eta(\mu, w) + \mu (1 - w^{2}) \left[B - 2 w \sqrt{1 - w^{2}} \right] \partial_{w} \eta(\mu, w)$$
$$- 4 B \mathcal{C} w (1 + \mu^{2}) + \frac{4 B^{2} \mathcal{C} \left[\mu^{2} + w^{2} (1 - \mu^{2}) \right]}{\sqrt{1 - w^{2}}} . \tag{C.3}$$

We have used the expression for $\mathcal{G}'(w)/\mathcal{G}(w)$. On the other hand, the function V must satisfy the Laplace equation (4.5), up to localized sources. In the first term of (4.5), we make use of $\partial_{\rho}(\rho \partial_{\rho}V) = \partial_{\rho}y$, and in the second term we write $\partial_{\eta}^{2}V = \partial_{\eta}\log r$. The quantities $\partial_{\rho}y$,

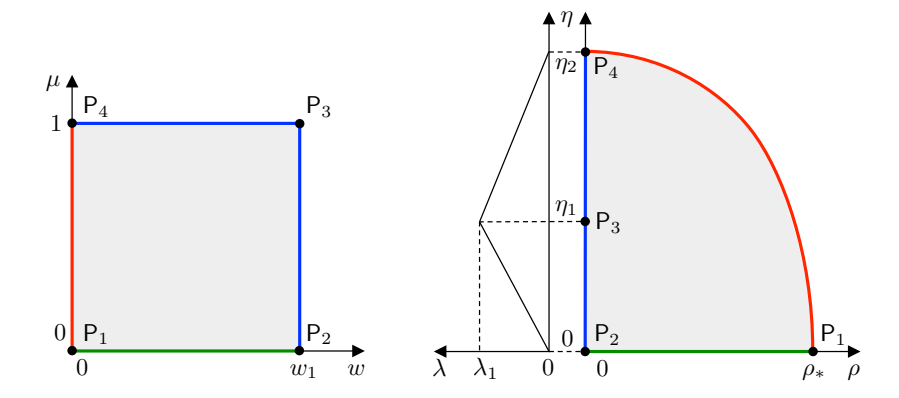


Figure 10: A schematic depiction of the relation between the (w, μ) coordinates and (ρ, η) coordinates. The shaded regions on both sides correspond to the allowed values of the (w, μ) , (ρ, η) coordinates. On the right, we also include the plot of the charge density $\lambda(\eta)$.

 $\partial_{\eta} \log r$ are then expressed as functions of μ , w with the help of the chain rule, in terms of $\eta = \eta(\mu, w)$. We get

$$\mu \,\partial_{\mu} \eta(\mu, w) - w \,(1 - w^2) \,\partial_{w} \eta(\mu, w) - 4 \,\mathcal{C} \,\mu = 0 \,.$$
 (C.4)

Combining (C.3) and (C.4), we have two linear equations in $\partial_{\mu}\eta(\mu, w)$, $\partial_{w}\eta(\mu, w)$, with solution

$$\partial_{\mu}\eta(\mu,\eta) = 4\mathcal{C}\left(1 - \frac{Bw}{\sqrt{1 - w^2}}\right), \qquad \partial_{w}\eta(\mu,\eta) = -\frac{4B\mathcal{C}\mu\sqrt{1 - w^2}}{(1 - w^2)^2}.$$
 (C.5)

We can now solve these PDEs for the function $\eta = \eta(\mu, w)$,

$$\eta = 4 \mathcal{C} \mu \left(1 - \frac{B w}{\sqrt{1 - w^2}} \right) . \tag{C.6}$$

We have fixed an integration constant by requiring $\eta = 0$ for $\mu = 0$.

In Figure 10 we depict schematically the change of coordinates from (w, μ) to (ρ, η) . It is convenient to define

$$\eta_1 = 4C\sqrt{1 - B^2} = \frac{4}{\ell}, \qquad \eta_2 = 4C = \frac{4(N+k)}{N}, \qquad \rho_* = 4BC.$$
(C.7)

The locus w = 0 is mapped to an arc of the ellipse defined by the equation

$$\frac{\rho^2}{16 B^2 C^2} + \frac{\eta^2}{16 C^2} = 1 . {(C.8)}$$

Using (C.6), we can find the explicit solution to the PDEs (C.2). We may start with the equation for $\partial_{\mu}V$ and integrate it in μ . To do so, we do not need the explicit form of $\mathcal{G}(w)$. The resulting expression for V, up to an arbitrary function of w, is then plugged back

in the equation for $\partial_w V$. Making use of the expression for $\mathcal{G}'(w)/\mathcal{G}(w)$, we complete the determination of V, up to an overall constant. The result reads

$$V_{\rm T} = 4 \,\mu - 2 \,\log \frac{1+\mu}{1-\mu} - 2 \left[1 - \frac{B \,w}{\sqrt{1-w^2}} \right] \mu \,\log(1-\mu^2) + 4 \,\mathcal{C} \left[1 - \frac{B \,w}{\sqrt{1-w^2}} \right] \mu \,\log \mathcal{G}(w) \ . \tag{C.9}$$

We have added a subscript 'T' as a reminder that this the electrostatic potential that is inferred from the Toda form of the solution, via the Bäcklund transform. We have fixed an arbitrary additive shift in $V_{\rm T}$ by demanding $V_{\rm T}=0$ for $\mu=0$. We can also extract the charge density along the η axis from $V_{\rm T}$ using (4.6). The result, written as a function of η , takes the form of a continuous piecewise linear function defined on the interval $[0, \eta_2]$,

$$\lambda_{\mathrm{T}}(\eta) = \begin{cases} \frac{\lambda_{1}}{\eta_{1}} \eta & \text{for } 0 \leq \eta \leq \eta_{1} ,\\ -\frac{\lambda_{1}}{\eta_{2} - \eta_{1}} (\eta - \eta_{2}) & \text{for } \eta_{1} < \eta \leq \eta_{2} , \end{cases}$$
(C.10)

where we have introduced

$$\lambda_1 = 4(1 - \sqrt{1 - B^2}) \ . \tag{C.11}$$

Finally, we notice that the function $\mathcal{G}(w)$ is determined only up to a multiplicative constant. This ambiguity, however, translates into an ambiguity in the potential $V_{\rm T}$ of the form (4.7), and therefore has no effect on the metric and flux.

Improved form for V. The expression (C.9) for the electrostatic potential has two draw-backs: it is not given in closed form as a function of ρ , η ; it is only determined in the interior of the shaded region in Figure C.9 in the (ρ, η) plane. Correspondingly, the charge density $\lambda_{\rm T}$ is known on the interval $[0, \eta_2]$, but not on the entire η axis. We now discuss an improved potential V, which is given explicitly as a function on the entire (ρ, η) plane.

To write V, we start by prescribing a charge density along the η axis, which is continuous and piecewise linear, and extends (C.10) beyond the interval $[0, \eta_2]$,

$$\lambda(\eta) = \begin{cases}
\frac{\lambda_1}{\eta_1} \eta & \text{for } -\eta_1 \le \eta \le \eta_1, \\
-\frac{\lambda_1}{\eta_2 - \eta_1} (\eta - \eta_2) & \text{for } \eta > \eta_1, \\
-\frac{\lambda_1}{\eta_2 - \eta_1} (\eta + \eta_2) & \text{for } \eta < -\eta_1.
\end{cases}$$
(C.12)

Given this charge density, the electrostatic potential is determined using the standard Green's function for the Laplacian in \mathbb{R}^3 . The naive expression for V would be

$$-\frac{1}{2} \int_{-\infty}^{+\infty} \frac{\lambda(\eta')}{\sqrt{\rho^2 + (\eta - \eta')^2}} d\eta' , \qquad (C.13)$$

but this quantity suffers from logarithmic divergences from the large $|\eta'|$ region in the domain of integration. We regularize the divergence by integrating in η' in the range $[-\eta_*, \eta_*]$, with η_* large and positive. We perform a "minimal subtraction" of the divergence, and we send the regulator η_* to infinity. This prescription yields

$$V = \lim_{\eta_* \to +\infty} \left[-\frac{\lambda_1}{\eta_2 - \eta_1} \eta \log \eta_* - \frac{1}{2} \int_{-\eta_*}^{+\eta_*} \frac{\lambda(\eta')}{\sqrt{\rho^2 + (\eta - \eta')^2}} d\eta' \right].$$
 (C.14)

The first term implements the minimal subtraction and it corresponds to a shift in the electrostatic potential of the form (4.7). Computing the η' integral and taking the limit, we find

$$V = \frac{\lambda_{1}}{2\eta_{1}(\eta_{1} - \eta_{2})} \left[\eta_{2} \sqrt{(\eta - \eta_{1})^{2} + \rho^{2}} - \eta_{2} \sqrt{(\eta + \eta_{1})^{2} + \rho^{2}} - (\eta - \eta_{1}) \eta_{2} \operatorname{arctanh} \left(\frac{\eta - \eta_{1}}{\sqrt{(\eta - \eta_{1})^{2} + \rho^{2}}} \right) + (\eta + \eta_{1}) \eta_{2} \operatorname{arctanh} \left(\frac{\eta + \eta_{1}}{\sqrt{(\eta + \eta_{1})^{2} + \rho^{2}}} \right) + 2\eta \eta_{1} \log(\rho) + 2\eta \eta_{1} - \eta \eta_{1} \log(4) \right].$$
(C.15)

The charge density (C.12) satisfies $\lambda(-\eta) = -\lambda(\eta)$, implying that V is equal to zero along the ρ axis at $\eta = 0$: this is a standard application of the method of images.

We may now compare V with the potential V_T given in (C.9). The values of η_1 , η_2 , λ_1 in terms of B, C were given in (C.7), (C.11). After a lengthy but straightforward computation, using the expression for G(w) in (A.21), one verifies that

$$V_{\rm T} - V = \frac{\mathcal{K}}{4 \,\mathcal{B} \,\mathcal{C}} \eta \,\,\,\,(\text{C}.16)$$

where \mathcal{K} is a constant, given by

$$\mathcal{K} = 4\mathcal{B} + 4\mathcal{B}\mathcal{C}\log\mathcal{G}_* + 2\operatorname{arctanh}\mathcal{B} + \mathcal{B}\log(16B^2) + 4\mathcal{B}\log\mathcal{C}. \tag{C.17}$$

We see that the difference $V_{\rm T} - V$ is of the form (4.7). It follows that, for the purposes of computing the 11d metric and flux, we can use V in (C.15) instead of $V_{\rm T}$.

C.2 Generalization of the charge density profile

We now turn to the generalization of Case II solutions. The metric and flux are as in (4.9). Our task is to specify \mathcal{C} and V. The main idea is to compute V using the standard Green's function starting from a given charge density profile λ along the η axis. Building on solutions of Case II, we make the following working assumptions. The charge density is taken to be continuous and piecewise linear. Its slope changes at a finite number of points along the η axis. Moreover, we require

$$\lambda(-\eta) = -\lambda(\eta) , \qquad (C.18)$$

so that it is sufficient to specify λ for $\eta \geq 0$.

A generic continuous, piecewise linear profile for λ can be parametrized as follows. Let $0 < w_1 < w_2 < \cdots < w_p$ be the locations on the η axis where the slope of λ changes. We may then write

$$\lambda(\eta) = \begin{cases} m_0 \, \eta & \text{for } 0 \le \eta < w_1 ,\\ m_a \, \eta + y_a & \text{for } w_a \le \eta < w_{a+1}, \, a = 1, 2, \dots, p-1 ,\\ m_p \, \eta + y_p & \text{for } \eta \ge w_p , \end{cases}$$
 (C.19)

where we have introduced the slope parameters m_a (a = 0, 1, ..., p) and the intercepts y_a (a = 1, 2, ..., p). We also define $q_0 := 0$. Continuity of λ imposes

$$(m_a - m_{a-1}) w_a + (y_a - y_{a-1}) = 0, a = 1, 2, \dots, p.$$
 (C.20)

Further constraints on the slope and intercept parameters will be derived below from metric regularity and flux quantization. The outcome of our analysis will be the charge density (5.2) discussed in the main text.

The electrostatic potential determined by the charge density (C.19) can be computed as a sum of various contributions. Firstly, we may consider the interval $[w_a, w_{a+1}]$, $a = 0, 1, \ldots, p-1$, and its mirror image $[-w_{a+1}, -w_a]$. (By definition, $w_0 := 0$.) The corresponding contribution to the electrostatic potential reads

$$V(w_{a}, w_{a+1}, m_{a}, y_{a}) = -\frac{1}{2} \int_{w_{a}}^{w_{a+1}} \frac{m_{a} \eta' + y_{a}}{\sqrt{\rho^{2} + (\eta - \eta')^{2}}} d\eta' - \frac{1}{2} \int_{-w_{a+1}}^{w_{a}} \frac{m_{a} \eta' - y_{a}}{\sqrt{\rho^{2} + (\eta - \eta')^{2}}} d\eta'$$

$$= \frac{1}{2} \left(m_{a} \sqrt{(\eta - w_{a})^{2} + \rho^{2}} - \operatorname{arctanh} \left(\frac{\eta - w_{a}}{\sqrt{(\eta - w_{a})^{2} + \rho^{2}}} \right) (m_{a} \eta + y_{a}) \right)$$

$$+ \frac{1}{2} \left(-m_{a} \sqrt{(\eta + w_{a})^{2} + \rho^{2}} + \operatorname{arctanh} \left(\frac{\eta + w_{a}}{\sqrt{(\eta + w_{a})^{2} + \rho^{2}}} \right) (m_{a} \eta - y_{a}) \right)$$

$$+ \frac{1}{2} \left(-m_{a} \sqrt{(\eta - w_{a+1})^{2} + \rho^{2}} + \operatorname{arctanh} \left(\frac{\eta - w_{a+1}}{\sqrt{(\eta - w_{a+1})^{2} + \rho^{2}}} \right) (m_{a} \eta + y_{a}) \right)$$

$$+ \frac{1}{2} \left(m_{a} \sqrt{(\eta + w_{a+1})^{2} + \rho^{2}} - \operatorname{arctanh} \left(\frac{\eta + w_{a+1}}{\sqrt{(\eta + w_{a+1})^{2} + \rho^{2}}} \right) (m_{a} \eta - y_{a}) \right). \quad (C.21)$$

Next, we have the contribution of the semi-infinite interval $[w_p, +\infty)$ and its mirror image $(-\infty, -w_p]$. In this case, a naïve integration of the charge density against the standard Green's function yields a logarithmic divergence. We regulate and subtract the divergence in the same way as in (C.14). We thus obtain the quantity

$$V(w_p, \infty, m_p, y_p) =$$

$$= \lim_{w_* \to +\infty} \left[-\frac{1}{2} \int_{w_p}^{w_*} \frac{m_p \eta' + y_p}{\sqrt{\rho^2 + (\eta - \eta')^2}} d\eta' - \frac{1}{2} \int_{-w_*}^{-w_p} \frac{m_p \eta' - y_p}{\sqrt{\rho^2 + (\eta - \eta')^2}} d\eta' + m_p \eta \log \eta_* \right]$$

$$= \frac{1}{2} m_p \sqrt{(\eta - w_p)^2 + \rho^2} - \frac{1}{2} m_p \sqrt{(\eta + w_p)^2 + \rho^2} - \frac{1}{2} m_p \eta (-2 \log \rho - 2 + \log 4) \qquad (C.22)$$

$$+ \frac{1}{2} (m_p \eta - y_p) \operatorname{arctanh} \left(\frac{\eta + w_p}{\sqrt{(\eta + w_p)^2 + \rho^2}} \right) - \frac{1}{2} (m_p \eta + y_p) \operatorname{arctanh} \left(\frac{\eta - w_p}{\sqrt{(\eta - w_p)^2 + \rho^2}} \right).$$

The final expression for V is

$$V = \sum_{a=0}^{p-1} V(w_a, w_{a+1}, m_a, y_a) + V(w_p, \infty, m_p, y_p) .$$
 (C.23)

By virtue of the method of images, V is an odd function of η , and thus in particular it is zero at $\eta = 0$.

C.2.1 Metric regularity

Monopole sources. The 11d metric functions entering (4.9) may now be computed in closed form by plugging (C.23) into (4.10). In particular, we observe that

- The quantity R_ϕ^2 vanishes along the η axis in the (ρ,η) plane.
- The quantity R_z^2 has isolated zeros in the (ρ, η) plane, situated along the η axis at the locations w_a (a = 1, 2, ..., p) where the slope in $\lambda(\eta)$ changes.
- The quantity L is piecewise constant along the η axis,

if
$$w_a < \eta < w_{a+1}$$
, $\lim_{\rho \to 0^+} L(\rho, \eta) := \ell_{a+1} = m_a + \frac{1}{\mathcal{C}}$. (C.24)

We infer that the internal geometry admits the following description. The total 6d space is a fibration of S^2 and S_z^1 over a 3d base space, spanned by ρ , η , ϕ . The quantity R_{ϕ} is the radius of S_{ϕ}^1 in the 3d base space. The fact that it vanishes along the η axis implies that S_{ϕ}^1 shrinks smoothly there inside the 3d base space. The locations w_a ($a=1,2,\ldots,p$) on the η axis are monopoles for the S_z^1 fibration over the 3d base space. Indeed, the radius R_z of S_z^1 goes to zero at w_a , and the function L which governs the fibration of S_z^1 over S_{ϕ}^1 jumps at w_a . The discontinuity of L at w_a is identified with the monopole charge k_a of the ath monopole, which must be a positive integer,

$$\ell_a - \ell_{a+1} = k_a \in \mathbb{Z}_{>0}$$
, $a = 1, 2, \dots, p$. (C.25)

It follows that all the slope parameters m_a can be determined recursively in terms of the monopole charges k_a and the outermost slope parameter m_p . Based on analogy with the original solution given by the charge density (C.12), we set

$$m_p = -\frac{1}{\mathcal{C}}$$
, or equivalently $\ell_{p+1} = 0$. (C.26)

All slope parameters are thus fixed,

$$m_a = -\frac{1}{\mathcal{C}} + \sum_{b=a+1}^{p} k_b , \qquad a = 0, 1, \dots, p-1 .$$
 (C.27)

The intercepts y_a are then also fixed, using $y_0 = 0$ and the continuity condition (C.20),

$$y_a = \sum_{b=1}^{a} k_b w_b , \qquad a = 1, \dots, p .$$
 (C.28)

The original solution based on the charge density (C.12) corresponds to the case of one monopole, p = 1. In that case, the value of λ at the location w_1 is positive. By analogy, we now require that the value of λ at the location w_p of the last monopole be positive,

$$\lambda(w_p) = -\frac{w_p}{C} + \sum_{b=1}^p k_b \, w_b > 0 \ . \tag{C.29}$$

It follows that the charge density profile has a zero at a point $w_{\rm m} > w_p$, given by

$$w_{\rm m} = \mathcal{C} \sum_{b=1}^{p} k_b w_b \ .$$
 (C.30)

We observe that the charge density λ is positive and concave in the interval $[0, w_{\rm m}]$.

Allowed region in the (ρ, η) plane. As already explained in the main text, it is determined by the inequalities (5.10). The arc $\partial_{\rho}V = 0$ intersects the η axis at the value $w_{\rm m}$ where the positive zero of λ is located, see (C.30).

C.2.2 Flux quantization

In our normalization conventions, the quantity \overline{G}_4 in (4.9) has integral periods on any 4-cycle in the internal space. The computation of the periods of \overline{G}_4 is facilitated by the following properties of the functions Y, W in (4.9), which can be verified by direct computation using (4.10), (C.23).

• The quantity $Y(\rho, \eta)$ is piecewise constant along the η axis. Its values are determined by the intercepts parameters y_a in the charge density profile,

$$Y(0, \eta) = y_a$$
, for $w_a < \eta < w_{a+1}$, $a = 0, ..., p-1$,
 $Y(0, \eta) = y_p$, for $\eta > w_p$. (C.31)

• The values of the quantity $W(\rho, \eta)$ at the monopole locations are

$$W(0, \eta_a) = w_a , \qquad a = 1, \dots, p .$$
 (C.32)

• Both $Y(\rho, \eta)$ and $W(\rho, \eta)$ vanish for $\eta = 0$, for arbitrary ρ .

We can now list the 4-cycles in the geometry and evaluate the corresponding G_4 -flux parameters. Our discussion follows closely the approach and notation of [33].

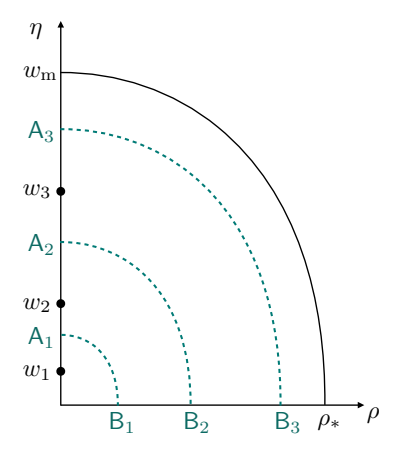


Figure 11: The 4-cycles of type **C** are obtained combining the dashed arcs A_aB_a with the S^2 and the ϕ circle in the base of the Dz fibration. The 4-cycles of type **B** are obtained combining a segment $[w_a, w_{a+1}]$ on the η axis with the S^2 and the Dz circle fiber.

Four-cycles of type C. With reference to Figure 11, let us consider the arc A_aB_a . The S^2 shrinks at B_a . The ϕ circle in the base of the Dz fibration shrinks at A_a , because R_{ϕ}^2 goes to zero there. We then have a four-cycle, which we denote C_a .

To identify the ϕ circle in the base of the Dz fibration, we use that $L = \ell_{a+1}$ and we set $0 = Dz = dz - \ell_{a+1} d\phi$, giving us $dz = \ell_{a+1} d\phi$ along the arc $\mathsf{A}_a \mathsf{B}_a$. As a result, the relevant terms in \overline{G}_4 are

$$\overline{G}_4 = \frac{\text{vol}_{S^2}}{4\pi} d(Y + LW - \ell_{a+1}W) \frac{d\phi}{2\pi}$$
 (C.33)

The integral of this quantity over C_a yields the value of the function Y at the endpoint A_a ,

$$\int_{\mathbf{C}_a} \overline{G}_4 = Y(\mathsf{A}_a) \ . \tag{C.34}$$

But $Y(A_a) = y_a$ from (C.31). We conclude that the intercept parameters y_a are all integrally quantized. (Throughout this appendix, we fix the mass scale m as in (2.7)).

We also notice that the outermost flux quantum y_p (p = 3 in the example of Figure 11) is identified with the number N of M5-branes,

$$y_p = N . (C.35)$$

Four-cycles of type B. We can consider the segment $[w_{a-1}, w_a]$ along the η axis, combined with the S^2 and the Dz circle, to get a four-cycle denoted \mathbf{B}_a . The relevant terms in \overline{G}_4 are

$$\overline{G}_4 \supset \frac{\operatorname{vol}_{S^2}}{4\pi} \left(-dW \right) \frac{Dz}{2\pi} \ . \tag{C.36}$$

The corresponding flux quantization implies that the following are integers.

$$\int_{\mathbf{B}_a} \overline{G}_4 = W(0, w_a) - W(0, w_{a-1}) = w_a - w_{a-1} . \tag{C.37}$$

In the second step we used (C.32). Since $w_0 = 0$, we conclude that

$$\{w_a\}_{a=1}^p$$
 is an increasing sequence of positive integers. (C.38)

We can also extend the arguments of the previous paragraphs to the last segment $[w_p, w_m]$. The interpretation is now different: this is a four-cycle because the warp factor goes to zero along the boundary of the (ρ, η) region. The lesson is that w_m must be also an integer. The flux quantum w_m should be regarded as a property of the smeared M5-brane source located at $\partial_{\rho}V = 0$, which is discussed in greater detail below. We find it convenient to parametrize it in terms of N and another integer parameter k,

$$w_{\rm m} = N + k \;, \qquad k \in \mathbb{Z} \;. \tag{C.39}$$

The zero $w_{\rm m}$ of the charge density is located at the right of the last monopole location, $w_{\rm m} > w_{\rm p}$. It follows that the integer k must satisfy

$$N + k > w_p . (C.40)$$

Regularity of \overline{G}_4 near monopoles. We observed above that Y and L are piecewise constant along the η axis. This might potentially generated delta-function singularities in \overline{G}_4 , due to the presence of the derivatives $\partial_{\eta}Y$, $\partial_{\eta}L$. One can verify, however, that these singularities are absent by virtue of the conditions (C.20), which guarantee the continuity of the charge density profile. The continuity condition implies (C.28), which together with (C.35) gives us

$$N = \sum_{a=1}^{p} w_a k_a . (C.41)$$

We have thus verified the emergence of a partition of N from regularity and flux quantization.

The parameter C is fixed by flux quanta. The slope of the charge density profile for $\eta > w_p$ is given in (C.26) in terms of C. It can be alternatively be computed by connecting the points $(\eta, \lambda) = (w_p, N - w_p/C)$ and $(\eta, \lambda) = (N + k, 0)$. The result is the following relation between C and the flux quanta N, k,

$$C = \frac{N+k}{N} \ . \tag{C.42}$$

C.2.3 M5-brane source

To clarify the behavior of the solution near the arc defined by $\partial_{\rho}V = 0$, let us start from (4.9) and perform two operations:

- We break up Dz and we complete the $d\phi$ square, so that the line element is written in terms of dz and $\mathcal{D}\phi = d\phi \mathcal{L} dz$. (The quantity \mathcal{L} is fixed requiring the absence of cross terms $dz\mathcal{D}\phi$).
- We collect the leading terms in the limit $\dot{V} \to 0$.

All electric sources are localized along the η axis. As a result, at a generic point along the arc $\partial_{\rho}V=0$, the potential V satisfies the Laplace equation. Using this information, we can write the resulting line element in the form

$$\frac{ds_{11}^2}{(4\pi)^{2/3}\ell_p^2} \approx \dot{V}^{1/3} \left[\frac{(\dot{V}')^2 - \ddot{V}\,V''}{2\,V''} \right]^{1/3} \left[ds^2 (AdS_5) + \mathcal{C}^2 \,dz^2 \right]
+ \frac{1}{4} \dot{V}^{-2/3} \left[\frac{(\dot{V}')^2 - \ddot{V}\,V''}{2\,V''} \right]^{-2/3} \left[\dot{V}^2 \,ds^2 (S^2) + \frac{\rho^2}{\mathcal{C}^2} \,\mathcal{D}\phi^2 + \left[(\dot{V}')^2 - \ddot{V}V'' \right] (d\rho^2 + d\eta^2) \right].$$
(C.43)

We observe that, at leading order near the locus $\partial_{\rho}V = 0$, we can write $\mathcal{L} \approx \mathcal{C}$, and hence $\mathcal{D}\phi \approx d\phi - \mathcal{C} dz$. This line element is compatible with an interpretation in terms of smeared M5-branes. Near the arc $\partial_{\rho}V = 0$, we can parametrize the (ρ, η) 2d space in terms of a normal coordinate $n = \dot{V}$, and a tangential coordinate t, which varies along the arc. From the term $\dot{V}^2 ds^2(S^2) = n^2 ds^2(S^2)$ inside the bracket on the second line, we see that, at small n near the arc, n and S^2 combine into a local \mathbb{R}^3 . We also observe the appearance of overall \dot{V} prefactors with powers 1/3, -2/3 in the first and second lines of (C.43), respectively, This structure implies that the M5-branes are: extended in the AdS_5 and z directions; smeared in the t and ϕ directions; localized at the origin of the local \mathbb{R}^3 parametrized by n and S^2 . These findings are directly analogous to the analysis of [15], which applies to the case p = 1.

We can also analyze the form of the G_4 -flux in the vicinity of the arc defined by $\partial_{\rho}V = 0$. Making use of (4.9), (4.10), we verify that, as we approach the locus $\partial_{\rho}V = 0$, we have

$$L \approx \frac{1}{C}, \qquad W \approx \eta , \qquad Y \approx 0 .$$
 (C.44)

It follows that the G_4 is given at leading order by

$$\overline{G}_4 \approx \frac{\text{vol}_{S^2}}{4\pi} \wedge \frac{d\eta}{\mathcal{C}} \wedge \frac{\mathcal{D}\phi}{2\pi}$$
 (C.45)

We can integrate this quantity along the S^2 and $\mathcal{D}\phi$, combined with an arc in the (ρ, η) plane that approaches the boundary component $\partial_{\rho}V = 0$ from the inside of the allowed region. We can use the coordinate η to parametrize this arc, regarding $\rho = \rho(\eta)$ as fixed by $\partial_{\rho}V = \epsilon$, with small positive ϵ . As ϵ goes to zero, the integral of \overline{G}_4 approaches a finite value,

$$\int \overline{G}_4 \approx \frac{w_{\rm m}}{\mathcal{C}} = \frac{N+k}{\mathcal{C}} = N \ . \tag{C.46}$$

We have made use of (C.39) and (C.42). We conclude that the smeared M5-brane source has a total charge equal to N.

C.3 Inflow analysis

In this section we derive the 't Hooft anomaly coefficients quoted in (5.26), (5.28). We first construct E_4 , the equivariant completion of the background flux \overline{G}_4 , and we then compute the integral of E_4^3 on the internal space M_6 .

C.3.1 Construction of E_4

The background flux \overline{G}_4 is presented in (4.9) as the wedge product of vol_{S^2} with the total derivative of a locally defined 1-form. This suggests a naïve candidate for E_4 . Firstly, we replace $\operatorname{vol}_{S^2}/(4\pi)$ with e_2 , which is the standard global angular form of SO(3), normalized to integrate to 1 on S^2 . (For more details, see for instance [33, 36].) Secondly, we consider the local 1-form inside the total derivative, and we perform the replacements

$$d\phi \to d\phi + A_{\phi}$$
, $dz \to dz + A_z$. (C.47)

Here A_{ϕ} , A_z denote the external background gauge fields associated to the isometries ∂_{ϕ} , ∂_z . The E_4 resulting is manifestly closed and gauge invariant. It takes the form

$$E_4^{\text{naive}} = e_2 \left[(dY + W dL) \frac{\mathcal{D}\phi}{2\pi} - dW \frac{\mathcal{D}z}{2\pi} \right] - e_2 W \frac{F_z}{2\pi} + e_2 (Y + W L) \frac{F_\phi}{2\pi} , \qquad (C.48)$$

where we have introduced

$$\mathcal{D}\phi = d\phi + A_{\phi}$$
, $\mathcal{D}z = dz + A_z - L D\phi$, $F_{\phi} = dA_{\phi}$, $F_z = dA_z$. (C.49)

Crucially, however, E_4 is not automatically guaranteed to be globally defined. To clarify this point it is convenient to trade A_z , A_{ϕ} for the external gauge fields A_{β} , A_{χ} , associated to the canonical LLM angular variables, making use of (4.8). We obtain

$$E_4^{\text{naive}} = e_2 \left[(dY + W \, dL) \, \frac{\mathcal{D}\phi}{2\pi} - dW \, \frac{\mathcal{D}z}{2\pi} \right] + e_2 \left[Y + (L - \mathcal{C}^{-1}) \, W \right] \frac{F_\chi}{2\pi} + e_2 \left[Y + (L - \mathcal{C}^{-1} - 1) \, W \right] \frac{F_\beta}{2\pi} \,. \tag{C.50}$$

The coefficients of F_{χ} , F_{β} must be well-defined 2-forms in the internal space M_6 . Recall that the S^2 shrinks both along the ρ axis, and along the arc in the (ρ, η) plane defined by the condition $\partial_{\rho}V = 0$. We have already notices that both Y and W vanish along the ρ axis, so regularity there is guaranteed both for the F_{χ} and the F_{β} term. Along the arc where $\partial_{\rho}V = 0$, on the other hand, we have $W \approx \eta$, $L \approx \mathcal{C}^{-1}$ and $Y \approx 0$. As a result, we observe that the coefficient of F_{χ} goes to zero, but the coefficient of F_{β} does not.

Equivalently, we can observe that the 3-form $\iota_{\chi}\overline{G}_4$ is exact, while the 3-form $\iota_{\beta}\overline{G}_4$ is closed but not exact. This is the same phenomenon encountered in [15] for the solutions of Case II (before generalization). Since $\iota_{\beta}\overline{G}_4$ is cohomologically non-trivial, expansion of the M-theory 3-form on $\iota_{\beta}\overline{G}_4$ yields an axion. The would-be massless gauge field A_{β} participates to a Stückelberg coupling with this axion, and is thus massive. It does not correspond to a continuous U(1) global symmetry on the field theory side. We refer the reader to [15] for further details about this Stückelberg mechanism.

Since we are interested in studying anomalies for continuous symmetries, we proceed setting $A_{\beta} = 0$. We can then write

$$E_{4} = e_{2} \left[(dY + W dL) \frac{\mathcal{D}\phi}{2\pi} - dW \frac{\mathcal{D}z}{2\pi} \right] + e_{2} \left[Y + (L - \mathcal{C}^{-1}) W \right] \frac{F_{\chi}}{2\pi} + \sum_{a=1}^{p} \sum_{I=1}^{k_{a}-1} \frac{\widehat{F}_{a,I}}{2\pi} \widehat{\omega}_{a,I} .$$
 (C.51)

On the second line we have introduced the contributions originating from the Cartan generators of the non-Abelian $\mathfrak{su}(k_a)$ flavor algebra associated to the ath monopole, of charge k_a . The 2-forms $\widehat{\omega}_{a,I}$ are dual to the resolutions 2-cycles in the local $\mathbb{C}^2/\mathbb{Z}_{k_a}$.

C.3.2 Integration of E_4^3

Let us start from the contributions that do not involve the $\mathfrak{su}(k_a)$ flavor symmetries. By a standard application of the Bott-Cattaneo formula [41], we arrive at

$$-I_6^{\text{inflow}} = \int_{M_6} \frac{1}{6} E_4^3 \supset -\frac{1}{8} c_1(U(1)_{\chi}) p_1(SO(3)) \int_{\mathcal{B}_2} dW \wedge d \left[Y + W \left(L - \mathcal{C}^{-1} \right) \right]^2. \quad (C.52)$$

Here $c_1(U(1)_{\chi}) = F_{\chi}/(2\pi)$ and $p_1(SO(3))$ is the first Pontryagin class of the SO(3) background gauge field associated to the isometries of the S^2 in the geometry. We have assigned positive orientation to $\mathcal{D}z \wedge \mathcal{D}\phi$. The symbol \mathcal{B}_2 denotes the domain in the first (ρ, η) quadrant, see Figure 7. The integral over \mathcal{B}_2 can be written as

$$\int_{\mathcal{B}_2} dW \wedge d\left[Y + W\left(L - \mathcal{C}^{-1}\right)\right]^2 = \int_{\partial \mathcal{B}_2} W d\left[Y + W\left(L - \mathcal{C}^{-1}\right)\right]^2. \tag{C.53}$$

Let us analyze in turn the components of $\partial \mathcal{B}_2$:

- Along the ρ axis, W=0, hence we get zero.
- Along the arc defined by $\partial_{\rho}V = 0$, we know that $W = \eta$, Y = 0, $L = \mathcal{C}^{-1}$, hence we get zero.
- Since L and Y are piecewise constant along the η axis, it is convenient to treat each segment in turn. On a segment of the form $[w_a, w_{a+1}]$, with $a = 0, \ldots, p-1$, we know that $L = \ell_{a+1} = m_a + \mathcal{C}^{-1}$. We also have $Y = y_a$. We thus get a contribution

$$\int_{\partial \mathcal{B}_{2}} W d \Big[Y + W (L - \mathcal{C}^{-1}) \Big]^{2} \supset - \int_{[w_{a}, w_{a+1}]} W d \Big[y_{a} + W m_{a} \Big]^{2}
= - \int_{[w_{a}, w_{a+1}]} W d \Big[y_{a}^{2} + 2 m_{a} y_{a} W + m_{a}^{2} W^{2} \Big]
= - \int_{[w_{a}, w_{a+1}]} d \Big[\frac{2}{3} m_{a}^{2} W^{3} + m_{a} y_{a} W^{2} \Big]
= - \frac{2}{3} m_{a}^{2} (w_{a+1}^{3} - w_{a}^{3}) - m_{a} y_{a} (w_{a+1}^{2} - w_{a}^{2}) .$$
(C.54)

We have used $W(0, w_a) = w_a$. The minus sign in front comes from the fact that we are taking $\partial \mathcal{B}_2$ with a counterclockwise orientation in the (ρ, η) plane. Finally, we have the final segment $[w_p, w_m]$. It gives a contribution of the same form, formally obtained taking a = p with the convention $w_{p+1} = N + k$, $\ell_{p+1} = 0$.

Making use of (C.52) and (C.54), as well as (5.24), we recover the expression (5.26) for $\mathcal{A}_{r,R}$ quoted in the main text. The comparison between (5.26) and (5.22) relies on the following identity,

$$\sum_{a=0}^{p} \left[\frac{1}{3} m_a^2 \left(w_{a+1}^3 - w_a^3 \right) + m_a y_a \left(w_{a+1}^2 - w_a^2 \right) + y_a^2 \left(w_{a+1} - w_a \right) \right]
= -\sum_{a=0}^{p} \left[\frac{2}{3} m_a^2 \left(w_{a+1}^3 - w_a^3 \right) + m_a y_a \left(w_{a+1}^2 - w_a^2 \right) \right].$$
(C.55)

Let us now turn to the contributions associated to the $\mathfrak{su}(k_a)$ factor of the symmetry associated to the regular puncture. The relevant terms in the inflow anomaly polynomial are

$$-I_{6}^{\text{inflow}} \supset \frac{1}{2} \frac{F_{\chi}}{2\pi} \sum_{a=1}^{p} \sum_{I,I=1}^{k_{a}-1} \frac{\widehat{F}_{a,I}}{2\pi} \frac{\widehat{F}_{a,J}}{2\pi} \int \widehat{\omega}_{a,I} \widehat{\omega}_{a,J} \left[Y + (L - C^{-1}) W \right]. \tag{C.56}$$

The 2-forms dual to the resolution cycles are localized at the monopole locations. Even though Y and L have jumps at the monopoles, the quantity $Y + (L - C^{-1})W$ is continuous at each monopole location, as may be verified using the continuity conditions (C.20) for the charge density profile λ . We can write

$$\left[Y + (L - C^{-1})W\right]_{(\rho,\eta)=(0,w_a)} = y_a + m_a w_a.$$
 (C.57)

It follows that the relevant term in the inflow anomaly polynomial reads

$$-I_{6}^{\text{inflow}} \supset \frac{1}{2} \frac{F_{\chi}}{2\pi} \sum_{a=1}^{p} \sum_{I,I=1}^{k_{a}-1} \frac{\widehat{F}_{a,I}}{2\pi} \frac{\widehat{F}_{a,J}}{2\pi} (y_{a} + m_{a} w_{a}) (-C_{IJ}^{\mathfrak{su}(k_{a})}) . \tag{C.58}$$

We have used the fact that the intersection pairing among the 2-forms $\widehat{\omega}_{a,I}$ reproduces minus the Cartan matrix $C_{IJ}^{\mathfrak{su}(k_a)}$ of $\mathfrak{su}(k_a)$. This result implies the expression (5.28) for the flavor central charge quoted in the main text.

References

- [1] D. Gaiotto, "N=2 dualities," JHEP 08 (2012) 034, arXiv:0904.2715 [hep-th].
- [2] D. Gaiotto, G. W. Moore, and A. Neitzke, "Wall-crossing, Hitchin Systems, and the WKB Approximation," arXiv:0907.3987 [hep-th].
- [3] K. Maruyoshi, M. Taki, S. Terashima, and F. Yagi, "New Seiberg Dualities from N=2 Dualities," *JHEP* **09** (2009) 086, arXiv:0907.2625 [hep-th].

- [4] F. Benini, Y. Tachikawa, and B. Wecht, "Sicilian gauge theories and N=1 dualities," *JHEP* **01** (2010) 088, arXiv:0909.1327 [hep-th].
- [5] I. Bah and B. Wecht, "New N=1 Superconformal Field Theories In Four Dimensions," *JHEP* 07 (2013) 107, arXiv:1111.3402 [hep-th].
- [6] I. Bah, C. Beem, N. Bobev, and B. Wecht, "AdS/CFT Dual Pairs from M5-Branes on Riemann Surfaces," Phys. Rev. D85 (2012) 121901, arXiv:1112.5487 [hep-th].
- [7] I. Bah, C. Beem, N. Bobev, and B. Wecht, "Four-Dimensional SCFTs from M5-Branes," *JHEP* **06** (2012) 005, arXiv:1203.0303 [hep-th].
- [8] G. Bonelli, K. Maruyoshi, and A. Tanzini, "Wild Quiver Gauge Theories," JHEP 02 (2012) 031, arXiv:1112.1691 [hep-th].
- [9] D. Xie, "General Argyres-Douglas Theory," JHEP 01 (2013) 100, arXiv:1204.2270 [hep-th].
- [10] Y. Wang and D. Xie, "Classification of Argyres-Douglas theories from M5 branes," Phys. Rev. D 94 no. 6, (2016) 065012, arXiv:1509.00847 [hep-th].
- [11] P. C. Argyres and M. R. Douglas, "New phenomena in SU(3) supersymmetric gauge theory," Nucl. Phys. B 448 (1995) 93–126, arXiv:hep-th/9505062.
- [12] J. M. Maldacena and C. Nunez, "Supergravity description of field theories on curved manifolds and a no go theorem," *Int. J. Mod. Phys. A* **16** (2001) 822–855, arXiv:hep-th/0007018.
- [13] D. Gaiotto and J. Maldacena, "The Gravity duals of N=2 superconformal field theories," *JHEP* **10** (2012) 189, arXiv:0904.4466 [hep-th].
- [14] I. Bah, F. Bonetti, R. Minasian, and E. Nardoni, "Holographic Duals of Argyres-Douglas Theories," *Phys. Rev. Lett.* **127** no. 21, (2021) 211601, arXiv:2105.11567 [hep-th].
- [15] I. Bah, F. Bonetti, R. Minasian, and E. Nardoni, "M5-brane sources, holography, and Argyres-Douglas theories," *JHEP* 11 (2021) 140, arXiv:2106.01322 [hep-th].
- [16] C. Couzens, H. Kim, N. Kim, and Y. Lee, "Holographic duals of M5-branes on an irregularly punctured sphere," arXiv:2204.13537 [hep-th].
- [17] A. Brandhuber and Y. Oz, "The D-4 D-8 brane system and five-dimensional fixed points," *Phys. Lett. B* **460** (1999) 307–312, arXiv:hep-th/9905148.
- [18] F. Apruzzi, M. Fazzi, D. Rosa, and A. Tomasiello, "All AdS₇ solutions of type II supergravity," *JHEP* **04** (2014) 064, arXiv:1309.2949 [hep-th].
- [19] D. Gaiotto and A. Tomasiello, "Holography for (1,0) theories in six dimensions," *JHEP* 12 (2014) 003, arXiv:1404.0711 [hep-th].
- [20] F. Apruzzi, M. Fazzi, A. Passias, A. Rota, and A. Tomasiello, "Six-Dimensional Superconformal Theories and their Compactifications from Type IIA Supergravity," *Phys. Rev. Lett.* **115** no. 6, (2015) 061601, arXiv:1502.06616 [hep-th].
- [21] E. D'Hoker, M. Gutperle, A. Karch, and C. F. Uhlemann, "Warped $AdS_6 \times S^2$ in Type IIB supergravity I: Local solutions," *JHEP* **08** (2016) 046, arXiv:1606.01254 [hep-th].
- [22] E. D'Hoker, M. Gutperle, and C. F. Uhlemann, "Warped $AdS_6 \times S^2$ in Type IIB supergravity II: Global solutions and five-brane webs," *JHEP* **05** (2017) 131, arXiv:1703.08186 [hep-th].

- [23] I. Bah, A. Passias, and A. Tomasiello, "AdS₅ compactifications with punctures in massive IIA supergravity," *JHEP* 11 (2017) 050, arXiv:1704.07389 [hep-th].
- [24] I. Bah, A. Passias, and P. Weck, "Holographic duals of five-dimensional SCFTs on a Riemann surface," *JHEP* **01** (2019) 058, arXiv:1807.06031 [hep-th].
- [25] H. Lin, O. Lunin, and J. M. Maldacena, "Bubbling AdS space and 1/2 BPS geometries," *JHEP* 10 (2004) 025, arXiv:hep-th/0409174.
- [26] A. D. Shapere and Y. Tachikawa, "Central charges of N=2 superconformal field theories in four dimensions," *JHEP* **09** (2008) 109, arXiv:0804.1957 [hep-th].
- [27] D. Xie and P. Zhao, "Central charges and RG flow of strongly-coupled N=2 theory," *JHEP* 03 (2013) 006, arXiv:1301.0210 [hep-th].
- [28] S. Cecotti, M. Del Zotto, and S. Giacomelli, "More on the N=2 superconformal systems of type $D_p(G)$," *JHEP* **04** (2013) 153, arXiv:1303.3149 [hep-th].
- [29] S. Giacomelli, N. Mekareeya, and M. Sacchi, "New aspects of Argyres–Douglas theories and their dimensional reduction," *JHEP* 03 (2021) 242, arXiv:2012.12852 [hep-th].
- [30] P. Agarwal, A. Sciarappa, and J. Song, " $\mathcal{N}=1$ Lagrangians for generalized Argyres-Douglas theories," *JHEP* 10 (2017) 211, arXiv:1707.04751 [hep-th].
- [31] S. Benvenuti and S. Giacomelli, "Lagrangians for generalized Argyres-Douglas theories," *JHEP* **10** (2017) 106, arXiv:1707.05113 [hep-th].
- [32] J. P. Gauntlett, E. O Colgain, and O. Varela, "Properties of some conformal field theories with M-theory duals," *JHEP* **02** (2007) 049, arXiv:hep-th/0611219.
- [33] I. Bah, F. Bonetti, R. Minasian, and E. Nardoni, "Anomaly Inflow for M5-branes on Punctured Riemann Surfaces," *JHEP* **06** (2019) 123, arXiv:1904.07250 [hep-th].
- [34] I. Bah, F. Bonetti, R. Minasian, and E. Nardoni, "Anomalies of QFTs from M-theory and Holography," *JHEP* 01 (2020) 125, arXiv:1910.04166 [hep-th].
- [35] D. Freed, J. A. Harvey, R. Minasian, and G. W. Moore, "Gravitational anomaly cancellation for M theory five-branes," Adv. Theor. Math. Phys. 2 (1998) 601–618, arXiv:hep-th/9803205.
- [36] J. A. Harvey, R. Minasian, and G. W. Moore, "NonAbelian tensor multiplet anomalies," *JHEP* **09** (1998) 004, arXiv:hep-th/9808060 [hep-th].
- [37] I. Bah, "AdS5 solutions from M5-branes on Riemann surface and D6-branes sources," *JHEP* **09** (2015) 163, arXiv:1501.06072 [hep-th].
- [38] P. M. Petropoulos, K. Sfetsos, and K. Siampos, "Gravity duals of $\mathcal{N}=2$ SCFTs and asymptotic emergence of the electrostatic description," *JHEP* **09** (2014) 057, arXiv:1406.0853 [hep-th].
- [39] G. Bonelli, O. Lisovyy, K. Maruyoshi, A. Sciarappa, and A. Tanzini, "On Painlevé/gauge theory correspondence," *Lett. Math. Phys.* **107** (2017) pages 2359–2413, arXiv:1612.06235 [hep-th].
- [40] S. Giacomelli, "RG flows with supersymmetry enhancement and geometric engineering," *JHEP* **06** (2018) 156, arXiv:1710.06469 [hep-th].
- [41] R. Bott and A. S. Cattaneo, "Integral invariants of 3-manifolds," J. Differential Geom 48 no. 1, (1998) 91–133, arXiv:dg-ga/9710001 [dg-ga].